2003

Synthesis and Characterization of a Polypyridyl Ru(II)-Alloxazine Complex for Adsorption on TiO2-coated ITO Electrodes

Manisha A. Patel
Eastern Illinois University

Recommended Citation

Patel, Manisha A., "Synthesis and Characterization of a Polypyridyl Ru(II)-Alloxazine Complex for Adsorption on TiO2-coated ITO Electrodes" (2003). *Masters Theses*. 1422.
https://thekeep.eiu.edu/theses/1422

THESIS/FIELD EXPERIENCE PAPER
REPRODUCTION CERTIFICATE

TO: Graduate Degree Candidates (who have written formal theses)

SUBJECT: Permission to Reproduce Theses

The University Library is receiving a number of request from other institutions asking permission to reproduce dissertations for inclusion in their library holdings. Although no copyright laws are involved, we feel that professional courtesy demands that permission be obtained from the author before we allow these to be copied.

PLEASE SIGN ONE OF THE FOLLOWING STATEMENTS:

Booth Library of Eastern Illinois University has my permission to lend my thesis to a reputable college or university for the purpose of copying it for inclusion in that institution's library or research holdings.

[redacted] [redacted]

Author's Signature Date

I respectfully request Booth Library of Eastern Illinois University **NOT** allow my thesis to be reproduced because:

Author's Signature Date

thesis4.form

Synthesis and Characterization of a Polypyridyl Ru(II)-Alloxazine Complex for Adsorption on TiO_2-coated ITO Electrodes.

TITLE

BY

Manisha A. Patel

THESIS

SUBMITTED IN PARTIAL FULFILLMENT OF THE REQUIREMENTS FOR THE DEGREE OF

Master of Science in Chemistry

IN THE GRADUATE SCHOOL, EASTERN ILLINOIS UNIVERSITY
CHARLESTON, ILLINOIS

2003

YEAR

I HEREBY RECOMMEND THIS THESIS BE ACCEPTED AS FULFILLING
THIS PART OF THE GRADUATE DEGREE CITED ABOVE

[redacted]
DATE

[redacted]
ADVISOR

[redacted]
DATE

[redacted]
DEPARTMENT CHAIR

Synthesis and Characterization of a Polypyridyl Ru(II)-Alloxazine Complex for Adsorption on TiO_2-coated ITO Electrodes.

Thesis Approved By:

[redacted]
Dr. Mark E. McGuire

[redacted]
Date

[redacted]
Dr. Douglas G. Klarup

[redacted]
Date

[redacted]
Dr. Richard L. Keiter

[redacted]
Date

[redacted]
Dr. Edward M. Treadwell

[redacted]
Date

I wish to thank my husband Jignesh for his patience and support. I would also like to thank Ken and Maria for their help with finding the things I needed. I would also like to thank Dr. Edward Treadwell for useful discussion on the synthesis of my complex. Finally I would like to thank Dr. Mark E. McGuire for the time and effort invested in this project, I could have never done it without you. Thank you once again.

Abstract

TiO_2-coated conducting glass electrodes can be modified by attachment of redox-active molecules to the TiO_2 surface. This thesis describes the synthesis and characterization of a polypyridyl Ru(II) complex that can be covalently bound to a TiO_2 surface through the carboxylate groups of 2,2'-bipyridine-4,4'-dicarboxylic acid, H_2dcbpy. In addition, the bound complex contains a redox-active alloxazine derivative, pptd, which is capable of $2e^-/2H^+$ transfers. Thus the TiO_2-coated electrode is modified with a transition metal complex capable of shuttling H-atoms to substrates in solution.

Synthesis of the PF_6^- salt of this complex, $[Ru^{II}(H_2dcbpy)_2pptd](PF_6)_2$, proved challenging due to the difficulties in obtaining starting materials of sufficient purity. Details of the efforts to purify these materials are included.

UV-Vis, ^{1}H-NMR, and electrochemical characterization of $[Ru^{II}(H_2dcbpy)_2pptd](PF_6)_2$, and its adsorption to TiO_2 electrodes, are included in the thesis. In addition, several well-known reference compounds have been characterized for comparison purposes.

Table of Contents

List of Figures

Lists of Schemes

List of Tables

1. INTRODUCTION

Scientists have always been interested in the idea of converting freely available solar energy into electric power or into the production of chemical fuels such as hydrogen gas.[1] The natural process of photosynthesis in green plants is a good example of a system that efficiently harvests solar energy. It is therefore logical to try and mimic the natural process of photosynthesis in order to build devices that would convert sunlight into electrical or chemical energy. However, the design of efficient systems based on plant photosynthesis has been slow due to the lack of knowledge on how to organize molecules on a nanometric scale. Another problem has been that the efficiency of conversion of light energy to chemical energy stored in charge separated products is severely hindered by thermodynamically favored back reactions between the photo-products. Nature, on the other hand, uses highly organized assemblies of chromophores and electron donors and acceptors to separate the photo-produced redox products spatially and further enhances the charge separation through a cascade of energetically downhill electron transfer reactions.[2]

The first pioneering efforts to build a device that harvests solar energy and converts it to electrical or chemical energy were made by Becquerel in 1839. Becquerel's photoelectric experiments were done on liquid devices, unlike solid state devices used today. The experiments involved the illumination of an electrolyte solution containing a metal halide salt and two platinum electrodes. Becquerel's experiments were motivated by photography. The first photographic images were made by Daquerre in 1837.

The developments of new types of devices that harvest solar energy and convert it to electrical or chemical energy have always been on the minds of scientists; however, lately there has been an increase in such developments due to the increasing public awareness that the earth's oil reserves could run out during this century. Concern is also rising over the disastrous environmental pollution caused by oil spills and the effect on the environment of greenhouse gases produced by fossil fuel combustion.[1]

Up until recently, the science of harvesting solar energy was dominated by solid state photovoltaic devices. Photovoltaic devices are those that convert sunlight into electrical power. Solid state photovoltaic devices are mostly made of inorganic materials, such as n- or p-doped forms of crystalline or amorphous silicon.[1] The silicon used in these solar cells must have certain properties in order to work well. First of all, it must absorb sunlight and convert photons into negative and positive charge carriers (electrons and holes). At the same time, the electrons and holes must then be separated and conducted to the current collectors. In order to efficiently achieve all this, the material must be of high purity. Therefore, the electricity produced by solid state devices is more expensive than that from conventional methods of producing electricity.[3, 4]

In recent years, the dominance of silicon based photovoltaic devices has been challenged by increasing emergence of a new generation of photovoltaic cells based on nanocrystalline materials and conducting polymer films. Photovoltaics take advantage of the fact that photons falling on a semiconductor can create electron-hole pairs which can set up an electrical potential difference across the interface between two different materials. The materials can also be shaped or tinted to suit various devices for either architectural or decorative purposes. It is now possible to depart completely from the classical solid-state devices by simply replacing the phase in contact with the semiconductor by an electrolyte (liquid, gel or organic solid), hence forming a new type of photo-electrochemical device.[1]

The foundation of modern photoelectrochemistry was worked out by Brattain and Garret[5] followed by Gerischer[6] who undertook the first detailed electrochemical and photoelectrochemical studies of the semiconductor-electrolyte interface.[1] Much of the current research on photoelectrochemical solar cells is focused on two particular types of cells. The first type is the regenerative cell, which converts light to electric power without any net chemical change. In the early versions of this type of cell, photons of energy exceeding that of the semiconductor band gap (energy gap between valence band and conduction band) generate electron-hole pairs. The electrons then move through the semiconductor, collect at the back electrode and travel through the external circuit. The second type of cell is the photosynthetic cell which operates on similar principles as the regenerative cell except that there are two redox systems: one reacting with the holes at the surface of the semiconductor electrode and the second reacting with the electrons entering the counter-electrode. One example of an application of a photosynthetic cell would be the cleavage of water by visible light. In this case oxidation of water to oxygen occurs at the semiconductor photoanode and reduction to hydrogen occurs at the counter electrode cathode.

The ideal semiconductor used in solar cells must be stable under illumination and these are typically oxides of metals such as TiO_2, ZnO, ZrO_2, Nb_2O_5, WO_3 and many more.[7] However, the most prevalent semiconductor used in solar cells is titanium dioxide since it had been used by Fujishima and Honda for water photolysis.[8] Many metal oxide semiconductors have a wide band gap (TiO_2 band gap 3-3.2 eV) with an absorption edge towards the ultraviolet part of the solar emission and consequently are insensitive to the visible solar spectrum. Hence using these semiconductors as solar cell sensitizers leads to very low conversion efficiencies.[1] On the other hand, it is critical to use a wide band gap semiconductor in photoelectrochemical cells because using narrow band gap semiconductors leads to absorption of visible light. The absorption of visible light leads to excitation of the band gap, which results in the generation of holes in the valence band and electrons in conduction band. The holes in the valence band can lead to photocorrosion of the semiconductor. Photocorrosion of the semiconductor occurs when holes generated in the valence band act as very strong oxidants and destroy the chemical integrity of the molecules surrounding the semiconductor surface (such as chromophores and redox mediators). Photocorrosion of the semiconductor can also occur if the holes in the valence band undergo redox reactions with components of the semiconductor itself. This often occurs with non-oxide semiconductors. Since metal oxides are exceptionally stable against photocorrosion on optical excitation in the band gap, they are commonly used as semiconductors.[2]

In order to solve the above dilemma, researchers came up with the idea of separating the light absorption function from the charge carrier transport function by introducing an electron transfer sensitizer which absorbs in the visible region of the solar spectrum and then injects charge carriers across the semiconductor-electrolyte junction into a wide band gap semiconductor substrate.[8] These devices are known as the dye-sensitized photoelectrochemical cells.

An example of a photoelectrochemical cell that separates the function of light absorption from the function of charge carrier transport is the Grätzel-type solar cell, developed by O'Regan and Grätzel.[9] In the Grätzel-type solar cell, the phase in contact with the semiconductor is an electrolyte rather than a solid state junction as in conventional photovoltaic cells that use doped forms of silicon. The typical Grätzel-type solar cell is created from materials of low to medium purity. The device is based on a 10-μm thick, transparent film of n-type semiconductor titanium dioxide (TiO_2) particles which are a few nanometers in size. These particles are coated with a monolayer of a charge transfer dye to sensitize the film for light harvesting (see Figure 1). Dye sensitized cells, unlike conventional semiconductor devices; separate the function of light absorption from charge-carrier transport. Current is generated when a photon absorbed by a dye molecule gives rise to electron injection into the conduction band of the semiconductor. The dye molecule is regenerated by electron transfer from a redox species in solution which is then reduced at the counter electrode (see Figure 2). The ideal spectral characteristics of the dyes used and the high surface area of the semiconductor film enable the device to have exceptionally high efficiencies for the conversion of incident photons to electrical current.[9]

1.1 Construction of a Grätzel-type solar cell [7, 8]

A Grätzel-type solar cell consists of two conducting glass electrodes separated by a redox-active electrolyte. The glass electrodes are conducting because one side of the glass plate is coated with F-doped indium tin oxide (ITO - Indium Tin Oxide)[10]. One of the two glass electrodes is coated with a thin layer of TiO_2. The TiO_2 is deposited onto the conducting side of the glass electrode by applying a colloidal preparation of monodispersed TiO_2 particles, followed by heat treatment to reduce the resistivity of the film. The TiO_2 layer is porous and has a high surface area. Dye molecules are deposited by simply immersing the TiO_2-coated electrode in a dye solution for several hours. The oxide layer behaves like a sticky material and immediately adsorbs the dye from the solution, which results in the coloration of the white TiO_2 oxide layer. The dye-coated electrode is then sandwiched with another conducting glass electrode and the space in between is filled with an organic solvent such as glutaronitrile ($NCCH_2CH_2CH_2CN$) containing a redox electrolyte (I^-/I_3^-). A small amount of Pt (5-10 $\mu g/cm^2$) is deposited to the counter electrode to catalyze the cathodic reduction of triiodide to iodide. The schematic of a Grätzel-type solar cell is shown below.

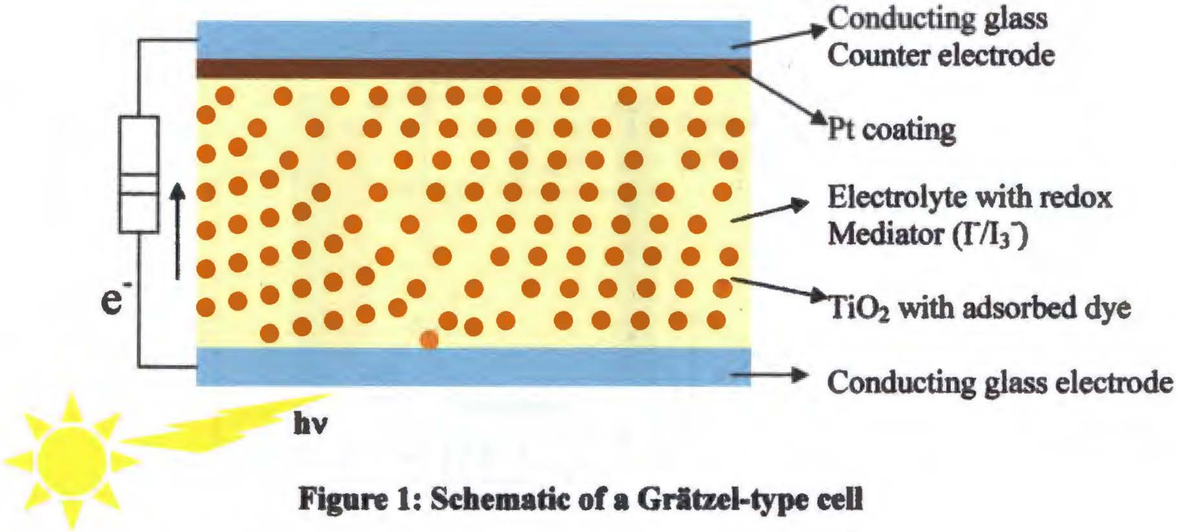

Figure 1: Schematic of a Grätzel-type cell

1.2 Principles of operation of a Grätzel-type cell [1, 6]

Figure 2 is an energy diagram depicting electron flow in a Grätzel-type cell. Light is absorbed by the monolayer of dye (S) which is chemically adsorbed onto the TiO_2 surface. Optical excitation of the dye with visible light leads to excitation of the dye to an excited electronic state (S*) that undergoes electron transfer quenching, injecting electrons into the conduction band of TiO_2:

$$S^* \longrightarrow S^+ + e^-$$

The oxidized dye is reduced back to the ground state (S) by the electron donor (I^-) present in the electrolyte filling the pores:

$$2S^+ + 3I^- \longrightarrow 2S + I_3^-$$

The electrons in the conduction band pass through the external circuit, perform work and arrive at the counter electrode, where the I_3^- is reduced back to I^-.

$$I_3^- + 2e^- \longrightarrow 3I^- \text{ (at the counter electrode)}$$

The photovoltage ΔV in Figure 2, generated by the cell, corresponds to the difference between the Fermi level in the semiconductor under illumination and the reduction potential of the I_3^-.

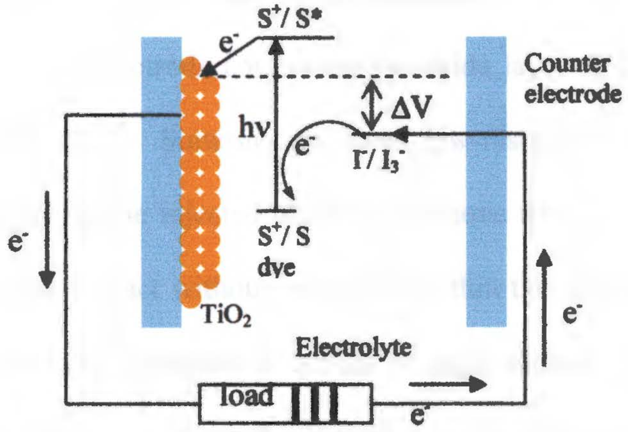

Figure 2: Energy diagram for a Grätzel-type cell; adapted from reference 2

1.3 Properties of the TiO_2 nanocrystalline layer[2, 7]

As mentioned earlier, TiO_2 is the most prevalent nanocrystalline material used in solar cells. Along with meeting the requirements for use in solar cells, it is also an inert and non-toxic material. The chemical composition, structure, and morphology of the nanocrystalline TiO_2 is of critical importance to the performance of the solar cell. First of all, for efficient dye distribution, the surface area of the film must be large. It is well known that the smaller the particle size the larger the surface area of the film.[2] Therefore, a large surface area can be simply obtained by using highly porous nanotextured films. Highly porous materials also allow the fast regeneration of the reduced dye and efficient charge transport since the redox electrolyte can penetrate the pores efficiently and occupy places where the dye penetrates. The second critical consideration in obtaining an efficient TiO_2 layer is sintering. Sintering of the particles forming the film results in electron percolation within the film and reduces dark currents. Electron percolation refers to the process by which the injected electrons hop through the colloidal oxide particles and arrive at the collector conducting glass electrode.[2] Dark currents result from the reduction of the redox mediator ($2e^- + I_3^- \rightarrow 3I^-$) by the glass electrode containing the oxide layer or it can actually happen at any bare TiO_2 surface.[2] Sintering produces low-resistance ohmic contacts between the particles enabling the injected electrons to move through the network of particles and reach the back contact without being lost within the oxide layer. Thirdly, the injected electrons must be transported across a large number of colloidal particles. The probability of recombination (back reaction of injected electrons with the oxidized dye molecules) increases with increased film thickness. It is therefore critical to obtain an optimal film thickness for maximum photocurrents. Large film thickness can also lead to resistance loss, which decreases the photovoltage.[2]

1.4 Properties of the photosensitizer/dye[2]

The efficient operation of a photoelectrochemical device is also dependent on the type of photosensitizer used. In particular, a dye complex must have the following five characteristics in order to function as an efficient photosensitizer. First of all, the dye must be able to absorb the maximum amount of solar energy incident upon the Earth (i.e. optimally, it must have an intensity and spectral range of coverage in the visible, near IR, and IR regions). Secondly, the dye must have a tunable (changeable) absorption band (discussed later). Thirdly, it must have certain photophysical properties such as an appropriately long excited state lifetime. The lifetime of the excited state is critical for injection kinetics into the conduction band of the semiconductor. The fourth important characteristic of a photosensitizer involves its redox properties in the ground state and excited state. Charge injection and regeneration of the dye are two key electron transfer steps that must occur rapidly in order for solar cells to have high quantum efficiency and long term stability. Efficient charge injection from the electronically excited state of the dye to the conduction band of the semiconductor depends on the redox potential of the excited state dye $E(S^+/S^*)$. Rapid regeneration of the dye depends on the redox potential of the ground state of the oxidized dye. Finally, the oxidized and reduced forms of the redox sensitizers or mediators that make up the electrolyte must be reversible and stable.

Transition metal complexes of polypyridine, porphines, or phthalocyanines seem to have many of the characteristics of ideal photosensitizers. The ligands in these types of complexes are nitrogen heterocycles with delocalized π ring systems capable of complexing with a variety of metal ions. Complexes of these ligands have been found to have reasonable solubility in many solvents and they also have a variety of low lying excited states ($\pi \rightarrow \pi^*$, $d \rightarrow d^*$, $d \rightarrow \pi^*$/ charge transfer). Many of these complexes have long-lived luminescent excited states which readily undergo electron-transfer reactions. The variety of complexes available gives researchers the flexibility to "tune" the redox and photophysical properties of the photosensitizers.

Most systems today are in fact based on mono or polynuclear polypyridine complexes of Ru(II). Polypyridine complexes of Ru(II) have metal to ligand charge transfer (MLCT) transitions that can account for all the visible light absorption. The MLCT transition occurs when an electron from a largely Ru(II) based (filled t_{2g} level) molecular orbital is promoted to a molecular orbital that is largely ligand based (empty π^* orbitals of the bipyridine ligand).

As mentioned earlier, one of the key characteristics of an efficient photosensitizer is the tunability of its absorption band. Polypyridine complexes of Ru(II) have tunable t_{2g} and π^* levels. For example, attachment of electron withdrawing groups to metal-complexed polypyridine ligands generally lowers the π^* levels of the ligand more than the t_{2g} metal orbitals. Hence, the MLCT energy decreases and the observed wavelength of the transition increase.

1.5 Attachment of dye molecules onto the TiO_2 nanocrystalline layer[2]

Once the ideal dye molecule has been synthesized, it is critical to adsorb the dye onto the TiO_2 layer. There are several different methods of attachment such as covalent attachment, electrostatic interaction, hydrogen bonding, hydrophobic interactions and van der Waals forces. However, covalent attachment is the most appropriate for adsorption onto the TiO_2 layer of solar cells. Covalent attachment can be achieved through various functional groups such as silanyl (-OSi), amide (-CONH), carboxyl (-COOH) or phosphonato (-PO_3H_2). These functional groups spontaneously react with surface hydroxyl groups of the oxide layer surface to form stable linkages. Carboxyl and phosphonato groups attached to polypyridine ligands have been found to have good affinities for TiO_2. In fact, the 4,4'-dicarboxy-2,2'- bipyridine (H_2-dcbpy) and 6-phosphonato terpyridine have shown high affinities toward TiO_2 surfaces. Carboxylic acid groups in particular not only promote efficient adsorption of the dye on the TiO_2 surface, but also promote electronic coupling between the donor levels of the excited dye (a ligand-based π^* molecular orbital) and the acceptor levels of the semiconductor (3d level/conduction band of TiO_2). The stability of the carboxy ester linkage formed on the TiO_2 surface in aqueous solution is dependent on the pH. Solutions of pH $\leq$ 4.5 are acceptable, but above this pH range hydrolysis and de-chelation of the anchoring group from the TiO_2 surface is possible.[2]

Although there are many different types of semiconductors and photosensitizers available for use in solar cells, it is important to select a complimentary semiconductor-photosensitizer pair. For example, Moser et al.[11] examined the wavelength dependence of charge injection from the excited state dye $Ru(H_2dcbpy)_2(NCS)_2$ into the conduction bands of two different oxide surfaces (TiO_2 and Nb_2O_5). Nb_2O_5 has the same band gap energy as TiO_2 (3.2 eV), but its conduction band is located 0.2-0.3 eV more negative than that of TiO_2. Therefore, if the dye is illuminated with 650 nm photons, photo-induced charge injection from the dye complex can occur on TiO_2, since E_{cb} of TiO_2 is located at a favorable location with respect to $E(S^*)$, but charge injection can not occur into the Nb_2O_5 conduction band. On the other hand, if 450 nm photons are used, charge injection can take place on both oxide semiconductors. See Figure 3 for an illustration.

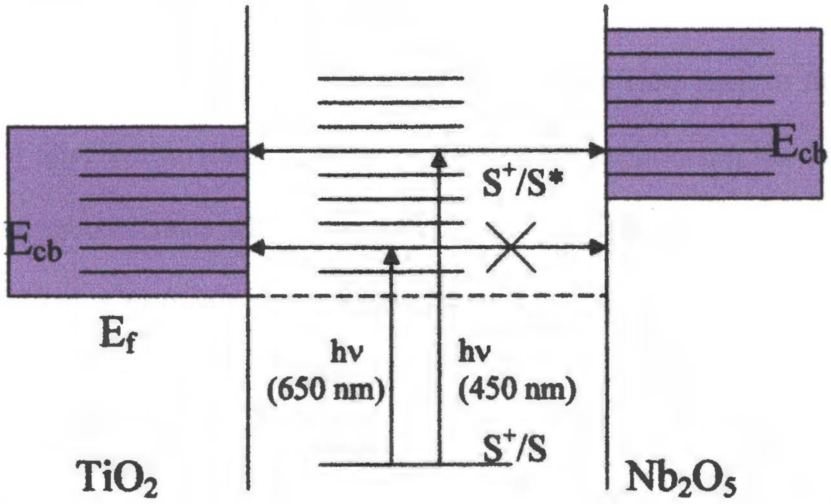

Figure 3: Charge injection from excited state of anchored dye into TiO_2 and Nb_2O_5 (adapted from reference 2)

Grätzel et al.[7] have developed a solar cell based on TiO_2 sensitized with ruthenium polypyridyl complexes. This solar cell shows an overall photon to electron conversion efficiency of 10%, which is considered significant. The ruthenium polypyridyl complex used by Grätzel et al.[7] was $Ru^{II}(H_2dcbpy)_2(NCS)_2$ (Figure 4), which was the same dye used by Moser et al. for their wavelength dependence studies.

Figure 4: $Ru^{II}(H_2dcbpy)_2(NCS)_2$

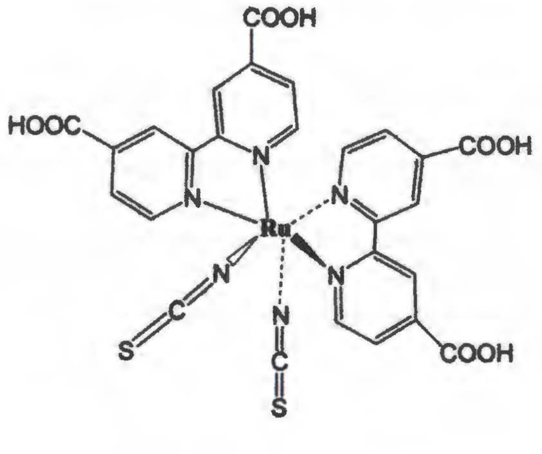

One of the reasons for the efficiency of nanocrystalline TiO_2 solar cells with Ru-carboxy bipyridine based sensitizers is the relatively slow ($\geq$ 100 ns) back electron transfer (i.e., electron transfer from the conduction band of TiO_2 back to the oxidized dye molecules) after the forward injection.[2] This difference between the forward and reverse electron transfer rates allows for the efficient processing (i.e., the reduction of oxidized dye by redox mediators and the percolation of the injected charges through the TiO_2 layer to the back collector electrode) of the charge separated products. For Ru-bpy complexes, with $E(Ru^{3+}/Ru^{2+})$ located between 0.8 and 1.2 V and an $E_{cb}(TiO_2/TiO_2^-)$ of approximately –0.8 V, the driving force for the back electron transfer is $\geq$ 1.6 eV. Such a large driving force should make the reaction kinetics fall in the classical Marcus inverted region. Hence the back reaction is very slow. Another reason for the slow back reaction is that it involves d-orbitals localized on the Ru-metal whose electronic overlap with the TiO_2 orbitals of the conduction band is small. With no favorable interactions for the back reaction to occur, the Grätzel-type solar cell is an efficient photoelectrochemical device.

A significant amount of progress has been made towards building efficient devices that harvest solar energy since the initial attempts by Becquerel in 1839. Grätzel's solar cell is an example. This progress has prompted researchers to design and build systems that carry out functions other than pure light-induced generation of electrical current. In fact, Meyer et al.[10] have recently used the basic Grätzel-type cell design to construct a photoelectrosynthetic cell where a photooxidized metal complex assembly is recycled via the oxidation of a target substrate in solution rather than by iodide reducing equivalents from the electrolyte. The sensitizing dye is a bimetallic Ru complex (Figure 5) where light absorption is followed by internal metal-to-metal electron transfer. This produces a catalytic site on the outer edge of the complex.

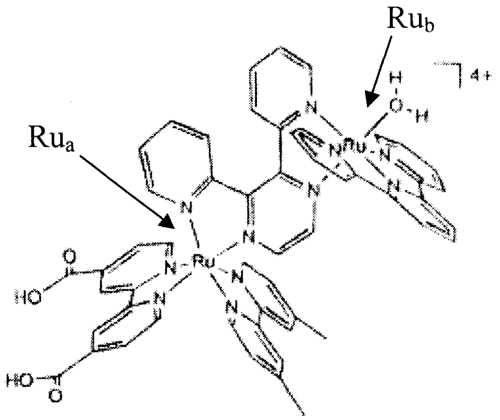

Figure 5: Sensitizer-catalyst assembly for photosynthetic cell (adapted from ref. 10)

Just as in the Grätzel-type solar cell, the carboxylate groups of the above dye are used as attachment points to nanocrystalline TiO_2 particles coated on the conducting glass electrode. Photooxidation of Ru_a attached to the 2,2'-bipyridine-4,4'-dicarboxylic acid eventually leads (through a two-step process) to the conversion of $Ru_b(II)\text{-}OH_2$ to the powerful oxidant Ru_b (IV)=O. This powerful oxidant can then oxidize substrates in solution. In this instance, 2-propanol was photooxidized to acetone at the surface of the electrode (at photogenerated Ru^{IV}=O sites).

The photoelectrosynthetic cell described by Meyer et. al.[10a] was actually a two compartment cell with photoinjected electrons from TiO_2 being used to reduce hydrogen ions to hydrogen in a separate compartment. If the bimetallic complex is represented as $[Ru_a^{II}\text{-}Ru_b^{II}\text{-}OH_2]^{4+}$, with Ru_a^{II} being the dicarboxybipyridine complex portion directly attached to TiO_2, the series of photoinduced reactions can be summarized in Scheme 1.[10a]

$$\text{i) } TiO_2|\text{-}[Ru_a^{II}\text{-}Ru_b^{II}\text{-}OH_2]^{4+} + H^+(Pt) \overset{h\nu}{\rightarrow\rightarrow} TiO_2|\text{-}[Ru_a^{II}\text{-}Ru_b^{III}\text{-}OH]^{4+} + H^+ + \tfrac{1}{2}H_2(Pt)$$

$$\text{ii) } TiO_2|\text{-}[Ru_a^{II}\text{-}Ru_b^{III}\text{-}OH]^{4+} + H^+(Pt) \overset{h\nu}{\rightarrow\rightarrow} TiO_2|\text{-}[Ru_a^{III}\text{-}Ru_b^{III}\text{-}OH]^{5+} + \tfrac{1}{2}H_2(Pt)$$

$$\text{iii) } TiO_2|\text{-}[Ru_a^{III}\text{-}Ru_b^{III}\text{-}OH]^{5+} \rightarrow TiO_2|\text{-}[Ru_a^{II}\text{-}Ru_b^{IV}{=}O]^{4+} + H^+$$

$$\text{iv) } TiO_2|\text{-}[Ru_a^{II}\text{-}Ru_b^{IV}{=}O]^{4+} + H^+(Pt) \overset{h\nu}{\rightarrow\rightarrow} TiO_2|\text{-}[Ru_a^{III}\text{-}Ru_b^{IV}{=}O]^{5+} + \tfrac{1}{2}H_2(Pt)$$

Scheme 1: Photooxidation of Meyer et.al. bimetallic complex

(adapted from reference 10a)

The utility of modifying electrode surfaces with metal complexes attached through dicarboxybipyridine linkages can be generalized. For example, one might envision adsorption of metal complexes onto TiO_2-coated electrodes where the adsorbed molecule simply acts as an electron transfer mediator between the solid electrode surface and substrates dissolved in solution. If the electrode-adsorbed molecule assembly can be configured to deliver reducing equivalents in the form of H-atoms, useful transformations such as the pH dependent reduction of CO_2 might be possible. Moreover, light-sensitive adsorbed mediators may allow such reductions to be photon-assisted.

Studies on the electrochemical reduction of CO_2 on a metallic cathode were begun as early as the nineteenth century.[12] The transformation of CO_2 into useable organic substances has been a long term objective, since it allows for the preparation of fuels or chemicals from a cheap and abundant carbon source.[12] In general, the electrochemical reduction of CO_2 on metallic cathodes requires highly negative potentials (typically below -2.0 V (NHE)). This problem might be resolved by adsorbing molecular catalysts onto the electrode. The advantage of using molecular electrocatalysts is that they can be very selective and efficient and at the same time their selectivity can be altered by simply changing their structures or by fine control of the transition metal center environment.[12] Figure 6 illustrates the above concept.

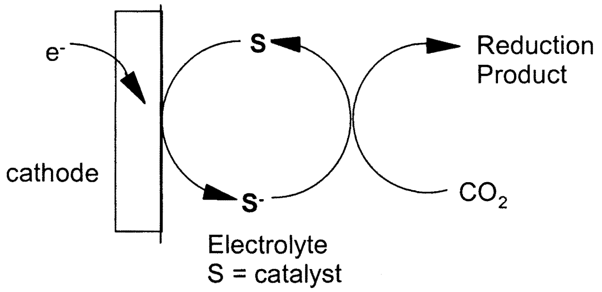

Figure 6: Schematic of CO_2 reduction via an electrocatalyst

Scheme 2 lists thermodynamic potentials for various CO_2 reduction pathways. As mentioned previously, direct reduction of CO_2 (at a bare electrode surface) is mechanistically simple but energetically costly (-2.0 V). If a metal complex adsorbed onto an electrode (e.g. Ru-dicarboxy bipyridine complex on TiO_2-coated electrodes) can be designed to provide reducing equivalents in the form of H-atoms, other low energy pathways for CO_2 reductions might become accessible, ultimately leading to useful products such as methanol.

$$CO_2 + 2H^+ + 2e^- \rightarrow CO + H_2O \qquad E^{\circ\prime} = -0.52\ V$$

$$CO_2 + 2H^+ + 2e^- \rightarrow HCOOH \qquad E^{\circ\prime} = -0.61\ V$$

$$CO_2 + 4H^+ + 4e^- \rightarrow HCHO + H_2O \qquad E^{\circ\prime} = -0.48\ V$$

$$CO_2 + 6H^+ + 6e^- \rightarrow CH_3OH + H_2O \qquad E^{\circ\prime} = -0.38\ V$$

$$CO_2 + 8H^+ + 8e^- \rightarrow CH_4 + 2H_2O \qquad E^{\circ\prime} = -0.24\ V$$

Scheme 2: Electrochemical reduction of CO_2 to various products (from reference 12)

The reduction of CO_2 is used here for mostly illustrative purposes. In general, it would be useful to synthesize and characterize a molecular catalyst that would adsorb onto TiO_2 coated electrodes and function as an oxidizing or reducing agent (H-atom transfer reagent) under positive or negative bias (dark reactions), under illumination by photons (light reactions), or under a combination of electrode bias and photons (photoassisted reactions). In particular, this project will focus on the synthesis and characterization of $[Ru^{II}(H_2dcbpy)_2\,pptd]^{2+}$ where pptd = 10, 12-dimethylpteridino[6,7-][1,10]phenanthroline-11,13 (10*H*,12*H*)-dione (Figure 7).

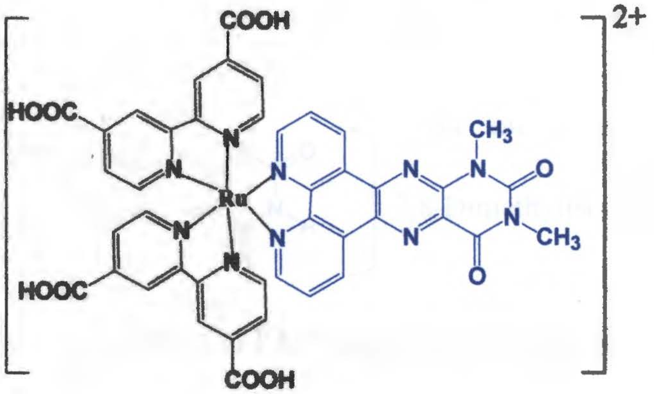

Figure 7: Structure of $[Ru^{II}(H_2dcbpy)_2pptd]^{2+}$

The first goal of this project was to synthesize and characterize this new complex. The second was to attach this complex onto a TiO_2-coated conducting electrode and begin initial electrochemical characterization of the Ru-TiO_2-electrode assembly in aqueous and/or organic/aqueous solutions.

The ruthenium polypyridyl complex, $[Ru^{II}(H_2dcbpy)_2pptd]^{2+}$, contains a coordinated flavin isomer (pptd). Flavins (isoalloxazines) are tricyclic molecules capable of reversible proton-coupled electron transfer reactions (H-atom transfers).[13] Flavin ring systems are generally associated with important biological molecules. For example the enzyme glutathione reductase contains the electron-transfer prosthetic group flavin adenine dinucleotide (FAD, Figure 8).[14] The flavin portion of FAD, 7,8-dimethylisoalloxazine, is capable of undergoing either two sequential one-electron transfers or simultaneous two electron transfer. Both processes are coupled to H^+ transfer and thus the flavin redox potentials are pH-dependent. Figure 9 illustrates this concept for isolated 7,8-dimethylisoalloxazine.[13]

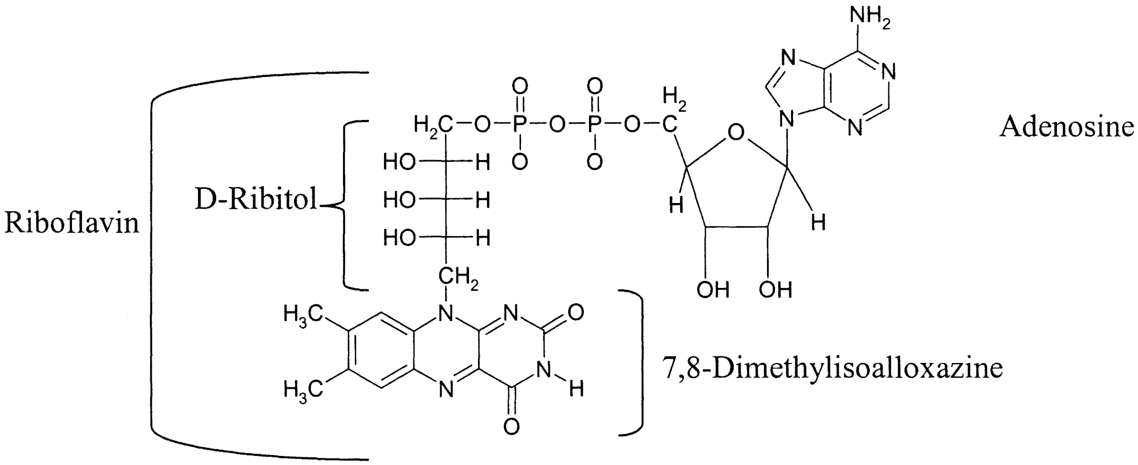

Figure 8: Structure of FAD (adapted from reference 13)

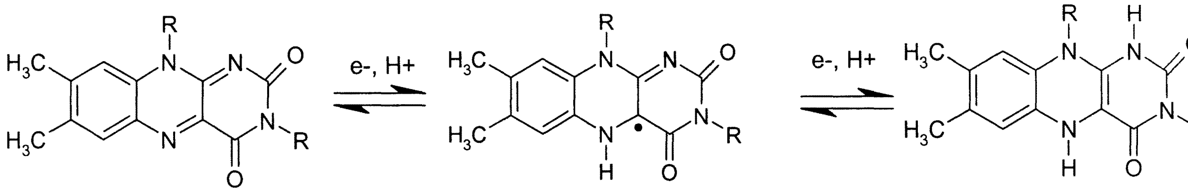

Figure 9: Reversible, pH-dependent reductions of flavin (adapted from reference 16)

Alloxazines, which are simply structural isomers of flavins, have an analogous set of pH-dependent reductions (Figure 10).

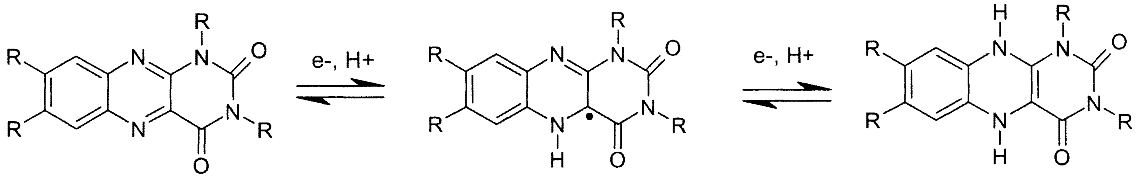

Figure 10: Reversible reductions of an alloxazine

The pptd functionality of $[Ru^{II}(H_2dcbpy)_2\ pptd]^{2+}$ is essentially an alloxazine moiety fused with a bipyridine ligand. This ligand (pptd) was originally synthesized by McGuire et. al.[14] and it coordinates to the Ru(II) through a stable bidentate *N,N* linkage. The pptd was obtained from a condensation reaction between 1,10-phenanthroline-5,6-dione and 5,6-diamino-1,3-dimethyl uracil (Figure 11).

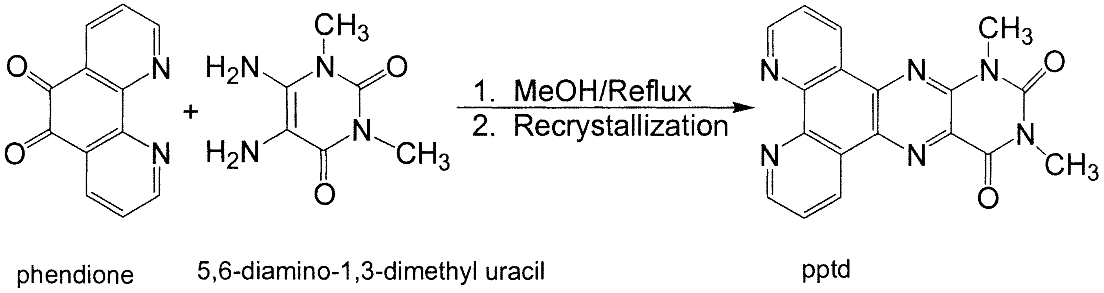

Figure 11: Synthesis of pptd (adapted from reference 14)

For comparison purposes, two reference compounds were also synthesized: $[Ru^{II}(H_2dcbpy)_2\ phen]^{2+}$ and $[Ru^{II}(bpy)_2\ pptd]^{2+}$ (Figure 12).

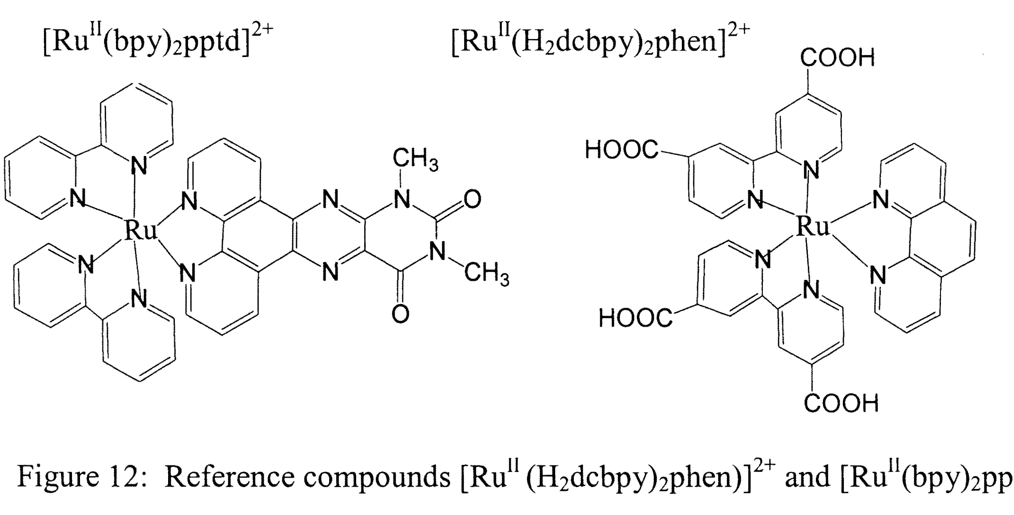

Figure 12: Reference compounds $[Ru^{II}(H_2dcbpy)_2phen)]^{2+}$ and $[Ru^{II}(bpy)_2pptd]^{2+}$

The complex $[Ru^{II}(bpy)_2\ pptd]^{2+}$ is known to show pH-dependent electron transfer in aqueous solutions,[14] but should, in principle, not be able to adsorb onto a TiO_2-coated electrode. On the other hand, $[Ru^{II}(H_2dcbpy)_2\ phen)]^{2+}$ should be able to be adsorbed onto TiO_2 but should not show pH-dependent behavior.

As stated previously, the second goal of this project was to attach the $[Ru^{II}(H_2dcbpy)_2\ pptd)]^{2+}$ complex onto a TiO_2-coated conducting glass electrode and study its electrochemical properties. In practical terms this means that the TiO_2-coated glass electrode with adsorbed Ru-complex would simply be used as the working electrode in an electrochemical cell. In the presence of various aqueous buffer electrolytes, the reduction potential(s) of the pptd ligand should show significant pH-dependence. Cyclic voltammograms would be expected to reveal two sequential 1 ē reductions or a single 2 ē reduction with both processes coupled to H^+ uptake from the aqueous buffer.

$$\begin{tikzcd}
Ru^{II}\text{-pptd}^{2+} \arrow[r, "\bar{e}"] & Ru^{II}\text{-pptdH}^{2+} \arrow[r, "\bar{e}"] & Ru^{II}\text{-pptdH}_2^{2+} \\
H^+ \text{ (from buffer)} \arrow[ur] & H^+ \text{ (from buffer)} \arrow[ur] &
\end{tikzcd}$$

OR

$$\begin{tikzcd}
Ru^{II}\text{-pptd}^{2+} \arrow[r, "2\bar{e}"] & Ru^{II}\text{-pptdH}_2^{2+} \\
2H^+ \text{ (from buffer)} \arrow[ur] &
\end{tikzcd}$$

Reduction of the Ru(II)-pptd complex in aqueous buffers should provide numerous H-atom donating sites throughout the channeled structure of the TiO_2. These H-atom donating sites could be accessed by substrate molecules in solution (i.e. CO_2 (aq)).

In previous descriptions, the Ru(II)-pptd complex would be reduced under a negative electrode bias (dark reaction). However, it is possible, to "photoassist" this reduction. The well-known metal to ligand charge transfer (MLCT) absorption of Ru(II) complexes could be used to assist in the reduction of the attached pptd. Figure 13 illustrates this photoassisted reduction of the pptd.

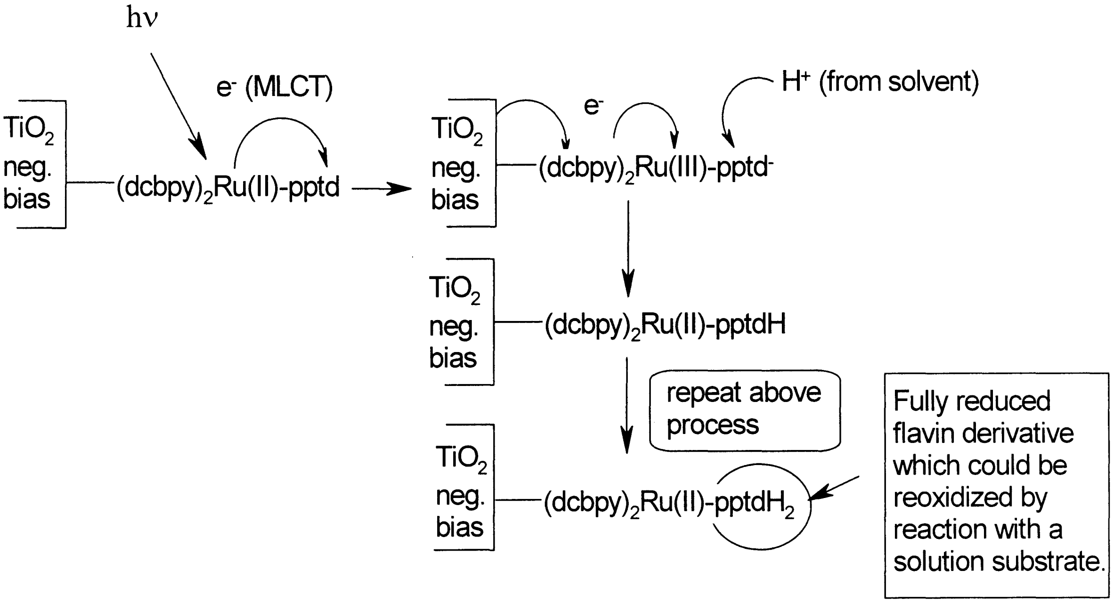

Figure 13: Photoassisted reduction of attached flavin derivatives

The first step in Figure 13 involves the excitation of an electron from the metal center by a photon of light. The excited metal electron then hops onto the ligand (pptd) making it negatively charged. Once the ligand is negatively charged, it can pick-up a proton from solution and this process can be repeated once more resulting in two H-atom transfers giving the fully reduced form of pptd.

In summary, the immediate goals of this research are to synthesize and characterize a molecular catalyst that would adsorb onto TiO_2-coated electrodes and function as an oxidizing or reducing agent. However, it is hoped that this research will contribute to the long term goal of converting freely available solar energy into electrical power or chemical fuels such as hydrogen gas and methanol.

References

[1] Grätzel, M. *Nature*, **2001**, *414*, 338-344.

[2] Kalyanasundaram, K.; Grätzel, M. *Coord. Chem. Rev.*, **1998**, *77*, 347-414.

[3] Grätzel, M. *Nature*, **2003,** *421*, 586-587.

[4] Internet source http://dcwww.epfl.ch/icp/icp-2/solarcellE.html accessed August, 2003

[5] Brattain, W. H.; Garrett, C. G. B. *Bell Syst. Tech. J.* **1995**, *34,* 129-176.

[6] Gerischer, H. *J. Electrochem. Soc.* **1966,** *113*, 1174-1182.

[7] Kalyanasundaram, K.; Grätzel, M. *In Optoelectronic Properties of Inorganic Compounds,* Roundhill, M., Fackler, P. Jr., Eds.; Plenum: New York, 1999; pp 169-194.

[8] Fujishima, A.; Honda, K. *Nature*, **1972**, *238*, 37-38.

[9] O' Regan, B.; Grätzel, M. *Nature*, **1991**, *353*, 737-739.

[10] a. Treadway, J.A.; Moss, J.A.; Meyer, T.J. *Inorg. Chem.* **1999**, *38*, 4386.

b. Thompson, M.S.; De Giovanni, W.F.; Moyer, B. A.; Meyer, T. J. *J. Org. Chem.* **1984**, *49*, 4972.

[11] Moser, J. E.; Grätzel, M. *Chimia* **1998,** *52*, 160.

[12] Collin, T.P.; Sauvage, J. P. *Coord. Chem. Rev.* **1989**, *93,* 245-268.

[13] a. Zubay, G. *Biochemistry*; W.M.C. Brown: Dubuque, IA, 1993; 289.

b. Muller, F. In *Topics in Current Chemistry*, Bosche F.L., Ed.; Springer-Verlag: Berlin, 1983; 108, pp 71-107.

[14] Voet, D.; Voet, J. *Biochemistry*; John Wiley and Sons: New York, 1995; p 401.

2. EXPERIMENTAL

2.1. Instrumentation and Methods

All ^{1}H-NMR spectra were obtained using a General Electric QE-300 MHz FT-NMR spectrometer. UV-Vis spectra were taken on a Shimadzu UV-3100 UV-Vis-NIR recording spectrometer or a Shimadzu UV-160 UV-Vis spectrophotometer. IR spectra were taken on a Nicolet Avatar 360 FT-IR E.S.P. instrument.

All electrochemical experiments were performed using an EG&G PAR model 263A potentiostat/galvanostat. The reference electrode used was either a saturated sodium chloride calomel electrode (SSCE) or a Ag wire (with ferrocene as an internal reference). The auxially (counter) electrode in all cases was a Pt wire.

A Corning 320 pH meter and/or an Orion 230 digital pH meter were used for all pH measurements. The furnace used for preparation of the TiO_2-coated electrodes was a Fisher Scientific (Model 650-58) Isotemp programmable muffle furnace. Water used in reactions and for solution preparations was obtained by running house deionized water through a Millipore "Milli-Q" system.

2.2 Reagents and Solvents

The following were purchased from Aldrich Chemical Co. and used as received: ammonium hexafluorophosphate (NH_4PF_6, Lot # 00127TY); TBAH (Bioanalytical systems); ruthenium (III) chloride hydrate ($Ru^{III}Cl_3.xH_2O$, Lot # 02103MV); 4,4'-dicarboxy-2,2'-bipyridine (H_2-dcbpy, Lot # 08311BI); *N,N*-dimethylformamide (DMF, Lot # 01616TT); trifluoromethanesulfonic acid (CF_3SO_3H, 98%, Lot # 05525PY); Triton X-100 (Lot # 03508CA); tetrabutylammonium hexafluorophosphate (BAS). The following reagents and solvents were obtained from the EIU stockroom: 6 M sodium hydroxide (NaOH, made from ACS-certified NaOH pellets); 3 M hydrochloric acid (HCl); concentrated sulfuric acid (H_2SO_4); reagent grade methanol (CH_3OH); copper wire and ethylene glycol. The following reagents and solvents were obtained from various sources: absolute ethanol (CH_3CH_2OH, McCormick Distilling Co Inc.); diethyl ether ($C_2H_5OC_2H_5$, Fisher Scientific, Lot # 01130013); 2,4-pentanedione ($C_5H_8O_2$, Spectrum Quality Products Inc., Lot # H1289); d_6-dimethyl sulfoxide (d_6-DMSO, Cambridge Isotope Laboratories Inc., Lot # DLM-10); deuterated sodium hydroxide (NaOD, Cambridge Isotope Laboratories Inc., Lot # BJ-1055); d_1-chloroform ($CDCl_3$, ACROS, Lot # 130700959) and d_3-acetonitrile (CD_3CN, Cambridge Isotope Laboratories Inc., Lot # DLM-21). Acetonitrile used for UV-Vis experiments was purchased from OmniSolv (HPLC grade, Lot # AX0142-3). Phosphate buffers for UV-Vis experiments were made from various combinations of 0.1 M pH 4.36 (NaH_2PO_4), 9.17 (Na_2HPO_4) and 12.13 (Na_3PO_4) buffers which were made from reagents obtained from the EIU stockroom. Titanium dioxide for the electrodes was purchased from Degussa Corporation (TiO_2, P-25, Lot # P1S1-18C1). Conducting glass electrodes were purchased from the Hartford Glass Company.

The pptd ligand was prepared previously in the McGuire lab. The $Ru(bpy)_2Cl_2 \cdot 2H_2O$ complex was also prepared previously in the McGuire lab[1].

2.3 Synthesis of 2,2'-bipyridine-4,4'-diethylcarboxyl (Et_2dcbpy)

This compound was synthesized according to a method outlined in the supporting material from Wolfbauer et. al.[2] A 1000 mg (0.005 moles) sample of 4,4'-dicarboxy-2,2'-bipyridine (H_2dcbpy) and 1.0 mL of concentrated H_2SO_4 (6M) were refluxed in 60 mL of absolute ethanol for 4-5 days. The reaction started off as a cloudy mixture and after the first day of refluxing the mixture showed a pink color. After 4 days the mixture cleared to become a pink solution at which point the reaction was complete. As the solution cooled to room temperature, white needle-like crystals of product started to form. The product was filtered through a 15-mL fine frit and washed with cold absolute ethanol and diethyl ether. It was dried under vacuum for several hours and the yield of Et_2-dcbpy obtained was 0.855 g (70.4% based on H_2-dcbpy).

2.4 Synthesis of bis (2,2'-bipyridine-4,4'-diethyldicarboxy)dichlororuthenium (II): $[Ru^{II}(Et_2dcbpy)_2Cl_2]$

This compound was also synthesized according to the protocol provided in the supporting material by Wolfbauer et. al.[1] Approximately 35 mL of DMF was placed in a round bottom flask under N_2 flow and heated to 125 °C. Once the DMF had reached a constant 125 °C, 507.0 mg (1.690×10^{-3} mol) of Et_2-dcbpy and 218.6 mg (9.690×10^{-4} mol) of $RuCl_3 \cdot H_2O$ (assume one water of hydration) were added to the DMF and the mixture was refluxed for 2.5 h with a constant N_2 flow and stirring.[a] The solvent was then removed by rotary evaporation. Methanol (100 mL) was added to the solid residue and the mixture was stirred overnight. The solid product, collected the next day by filtration through a 15-mL fine frit, was washed with cold methanol. After vacuum drying, 369.0 mg of product was obtained (49.3% based on $RuCl_3 \cdot H_2O$)

2.5 Synthesis of bis (2,2'-bipyridine-4,4'-dicarboxy)dichlororuthenium (II): $Ru^{II}(H_2dcbpy)_2Cl_2$

---

[a] The mole ratio of Et_2-dcbpy to $RuCl_3 \cdot H_2O$ was less than ideal due to experimental error. The ideal mole ratio of Et_2-dcbpy to $RuCl_3 \cdot H_2O$ should be 2:1

This complex was made by hydrolysis of $Ru^{II}(Et_2dcbpy)_2Cl_2$ according to the method reported by Keene et. al.[3] A 107.2 mg (1.390 x 10^{-4} mol) sample of $Ru^{II}(Et_2dcbpy)_2Cl_2$ was refluxed in 13 mL of 0.1 M NaOH (1.3 x 10^{-3} mol) at 65 °C with constant stirring in a round bottom flask for 3 h. At this point heat was removed and stirring was continued. Upon cooling, the NaOH was neutralized by adding a slight excess (1.5 mL) of 1 M HCl (1.5 x 10^{-3} mol) and a rotary evaporator was used to remove the solvent. The solid was collected and dried in a vacuum dessicator. The weight of the $Ru^{II}(H_2dcbpy)_2Cl_2$ obtained was 63.6g mg after accounting for the NaCl formed due to the neutralization reaction (see Discussion section). This represented a 70.7% yield based on $Ru^{II}(Et_2dcbpy)_2Cl_2$.

2.6 Synthesis of bis(2,2'-bipyridine-4,4'-dicarboxy)10,12-dimethylpteridino[6,7-][1,10]phenanthroline-11,13-(10*H*,12*H*)-dione ruthenium(II)hexafluorophosphate: [$Ru^{II}(H_2dcbpy)_2pptd](PF_6)_2$

DMF (25 mL) was heated to 135 °C with stirring under N_2 flow. When it was clear that the temperature of the DMF would remain constant at 135 °C, 0.1396 g of the $Ru^{II}(H_2dcbpy)_2Cl_2/NaCl$ mixture from the previous step ($\cong$ 9.810 x 10^{-5} mol of $Ru^{II}(H_2dcbpy)_2Cl_2$) and 0.0769 g (2.23 x 10^{-4} mol) of pptd were added to the reaction flask. The reaction was monitored every hour by simply taking a UV-Vis spectrum of a drop of the reaction mixture added to pH 9.17 phosphate buffer. Over time the 520-530 nm absorption characteristic of $[Ru^{II}(dcpby)_2Cl_2]^{4-}$ decreased and an absorption at about 460 nm due to $[Ru^{II}(dcbpy)_2pptd]^{4-}$ increased.[b] The next morning the reaction was halted

---

[b] The charge on the Ru-complex is assumed to be 4-, since all four dcbpy ligands are expected to be deprotonated in pH 9.17 phosphate buffer

when it became apparent that the 460 nm to 530 nm spectral window had stopped changing (460 nm absorption maximized, only residual absorption at 520-530 nm). The DMF was removed by rotary evaporation and the orange-red powder that remained was collected (0.1976 g). The solid was then dissolved in approximately 10 mL of water and the pH of the mixture was measured to be approximately 2.5. The pH of the mixture was then raised to ~10 using 1 M NaOH and this mixture was filtered through a 30 mL fine frit to remove undissolved material. The pH of the filtrate was reduced to ~2.5 with 0.1 M triflic acid (CF_3SO_3H) and at this point solid started to precipitate. After stirring overnight at this pH, the mixture was filtered and the collected solid was dried under vacuum (0.0822 g). The solid was then resuspended in water and the pH was adjusted to ~10 with 0.1 M NaOH. Approximately 0.0995 g (6.10×10^{-4} mol) of NH_4PF_6 was added to the solution and the pH decreased to 7.16. The pH of the solution was further reduced to ~2.5 by adding 0.1 M HCl dropwise at which point solid started to precipitate out of solution. The solid was then filtered and vacuum dried. The dried product, formulated as $[Ru^{II}(H_2dcbpy)_2pptd](PF_6)_2$[c], weighed 0.0752 g (62.7% yield based on $Ru^{II}(H_2dcbpy)_2Cl_2$).

2.7 Synthesis of bis (2,2'-bipyridine)10,12-dimethylpteridino[6,7-][1,10]phenanthroline-11,13-(10*H*,12*H*)-dioneruthenium(II) hexafluorophosphate: $[Ru^{II}(bpy)_2pptd](PF_6)_2$

A 0.110 g (2.12×10^{-4} moles) sample of $Ru^{II}(bpy)_2Cl_2 \cdot 2H_2O$ and 0.0876 g (2.54×10^{-4} mol) of pptd, both synthesized previously in the McGuire lab, were added to a 3-neck round bottom flask containing approximately 20 mL of ethylene glycol under Ar

---

[c] See discussion section A-1 v (p. 44)

flow. Stirring and heating were begun simultaneously. A UV-Vis spectrum of a drop of the reaction mixture in CH_3CN after the first hour of heating indicated the disappearance of the $Ru^{II}(bpy)_2Cl_2$ peak at 500 nm and the appearance of the expected $[Ru^{II}(bpy)_2pptd]^{2+}$ peaks at 440 nm and 420 nm. The reaction was stopped once the bis-Ru complex peaks had almost disappeared by removing the heat, but stirring and Ar flow were continued until the mixture cooled. Approximately 95% of the solvent (ethylene glycol) was then removed by rotary evaporation and 30 mL of 1.0 M HCl was added to the flask. In order to precipitate the product, an excess (0.387 g, 2.37×10^{-3} mol) of NH_4PF_6 was also added to the reaction flask. The reaction mixture was then filtered through a 15-mL fine frit and the solid product was washed with diethyl ether and then dried in a vacuum dessicator for several hours. The yield of solid product was 0.2308 g (104.0% yield based on $Ru^{II}(bpy)_2Cl_2.2H_2O$) The yield is greater than 100% and this could be due to excess NH_4PF_6 that may have been carried with the solid. Recrystallization of this solid from water would probably result in a lower yield. The solid was characterized by ^1H-NMR (Figure 40) and UV-Vis (Figure 41).

2.8 Synthesis of bis (2,2'-bipyridine-4,4'-dicarboxy)1,10-phenanthrolineruthenium (II) hexafluorophosphate: $[Ru^{II}(H_2dcbpy)_2phen](PF_6)_2$

A 0.0460 g (7.096×10^{-5} mol) sample of $Ru^{II}(H_2dcbpy)_2Cl_2$ and 0.0157 g (8.71×10^{-5} mol) of 1,10-phenanthroline were added to 20 mL of ethylene glycol in a 50-mL round bottom flask under Ar flow. A UV-Vis spectrum of the reaction mixture after approximately two hours of refluxing indicated the disappearance of the $Ru^{II}(H_2dcbpy)_2Cl_2$ peak at 520 nm and the appearance of the expected $[Ru^{II}(H_2dcbpy)_2phen]^{2+}$ peaks at 480 and 438 nm. At this point the heating was stopped and the mixture was allowed to stir while cooling under Ar. Approximately 95% of the ethylene glycol was removed by rotary evaporation and 15 mL of 1.0 M HCl was added to the reaction flask. Addition of a ten-fold excess (0.1157 g, 7.090 x 10^{-4} mol) of NH_4PF_6 produced a solid that was isolated by filtration through a 15-mL fine frit and then dried in a vacuum dessicator for several hours. The dried product weighed 0.0213 g (44.3% yield based on $Ru^{II}(H_2dcbpy)_2Cl_2$). The solid was characterized by ^{1}H-NMR (Figure 42) and UV-Vis (Figure 43).

2.9 Construction of TiO_2-coated glass electrode[3]

The TiO_2-coated glass electrodes were constructed according to "method B" described by Gratzel et. al.[4] An approximately 1-g sample of TiO_2 powder was ground to a fine paste in a glass mortar using 0.33 mL of water containing 0.033 mL of acetylacetone (2,4-pentanedione). The acetylacetone was added in order to prevent re-aggregation of the particles. After the powder had been ground into a paste, it was diluted by slow addition of water (1.33 mL) while constantly grinding. Once all the water was added, 0.0167 mL of Triton X-100 (detergent) was added to the mixture in order to facilitate spreading on the glass electrode. The conducting glass electrodes were each covered with scotch tape on all four sides, leaving rectangles in the middle of each piece. This was done to control the thickness of the TiO_2 film and to provide non-coated areas for electrical contact. Approximately 10 μL of the colloidal mixture was obtained using a micro pipette and placed on one edge of the rectangle on each electrode and it was distributed with a glass rod sliding over the tape-covered glass. After air drying for 5 min, the glass electrodes were placed in the muffle furnace at 450 °C for 30 min. At this point, the setting on the muffle furnace controller was lowered to 80 °C and the electrodes were left in the furnace (as the temperature slowly decreased) for another 30 min. The (still quite warm) electrodes were then removed from the furnace and stored in a dessicator to prevent water absorption.

2.10 Dye-coating of the TiO_2 coated conducting glass electrodes[3]

Coating of the TiO_2 surface with dye was carried out by soaking the TiO_2-coated electrode for a day in an absolute ethanol solution of $[Ru^{II}(H_2dcbpy)_2pptd](PF_6)_2$. Prior to placing the electrode in the ethanol solution, it was heated to about 60 °C in order to remove any water adsorbed on the film. The coating of the TiO_2 was dependent on the thickness of the film (i.e. the thicker the TiO_2 film[d], the longer it took to coat it with dye). The thickness of the film was determined by visual inspection (a thick film would be one that is opaque; on the other hand an ideal film thickness would be if the film was transparent).

2.11 Preparation of 0.01 M NaOD/D_2O

A 100.0 g (90.33 mL) bottle of D_2O was obtained from Aldrich Chemicals. Exactly 0.084 mL of 30% NaOD in D_2O (by weight) was added to this bottle in order to make 0.01 M NaOD.

2.12 Preparation of pH 4.9 phthalate buffer

A 0.1 M solution of potassium hydrogen phthalate was made by combining 2.042 g of potassium hydrogen phthalate in enough water to make 100 mL of solution. A 50-mL sample of this 0.1 M potassium hydrogen phthalate solution was combined with 19.4 mL

---

[d] The thickness of the TiO_2 film was determined by visual inspection. The film thickness is ideal if it is slightly transparent. An opaque film would be considered too thick.

of 0.1 M NaOH (obtained from EIU stock room) in order to produce a pH 4.90 phthalate buffer.

2.13 Preparation of pH 3.5, pH 4.0 and pH 7.0 acetate buffers

The three different pH acetate buffers were prepared from two pre-made solutions of 0.1 M acetic acid and 0.1 M sodium acetate solution. The 0.1 M acetic acid was made by mixing 10 mL of 6 M acetic acid with 590 mL of Millipore water. The 0.1 M sodium acetate solution was prepared by dissolving approximately 6.65 g of sodium acetate in 500 mL of Millipore water. The pH 3.5, pH 4.0 and pH 7.0 acetate buffers were made by combining the appropriate amounts of 0.1 M acetic acid 0.1 M sodium acetate solutions and measuring the pH with a pH meter.

2.14 Preparation of 0.1 M TBAH/DMF

A 0.1 M sample of tetrabutylammonium hexafluorophosphate/dimethyl formamide solution was made by combining 0.3875 g of TBAH with DMF in a 10 mL volumetric flask. The solution was mixed until all the TBAH had dissolved.

References

[1] Black, K. J.; Huang, H.; High, S.; Starks, L.; Olson, M.; McGuire, M.E. *Inorg. Chem.* **1993**, *32*, 5591-5596

[2] Wolfbauer, G.; Bond, A.; MacFarlane, D.R. *Inorg. Chem.* **1999,** *38*, 3836-3846.

[3] Keene, F. R.; Patterson, B. T. *Aust. J. Chem.* **1998,** *51,* 999-1002.

[4] Nazeeruddin, M.K.; Kay, A.; Rodicio, I.; Humphrey-Baker, R.; Mueller E.; Liska, P.; Vaichopoulos, N.; Grätzel, M. *J. Am. Chem. Soc.* **1993***,* *115*, 6382-6390.

3. Results and Discussion

A) Synthesis and characterization of Ru-complexes

The scheme below (Scheme 3) presents the general synthetic outline for the synthesis of the target complex $[Ru^{II}(H_2dcbpy)_2pptd](PF_6)_2$. Each of the synthetic steps leading toward the target complex will be discussed and the results will be presented in this section.

Scheme 3: Outline of synthesis of target complex $[Ru^{II}(H_2dcbpy)_2pptd](PF_6)_2$

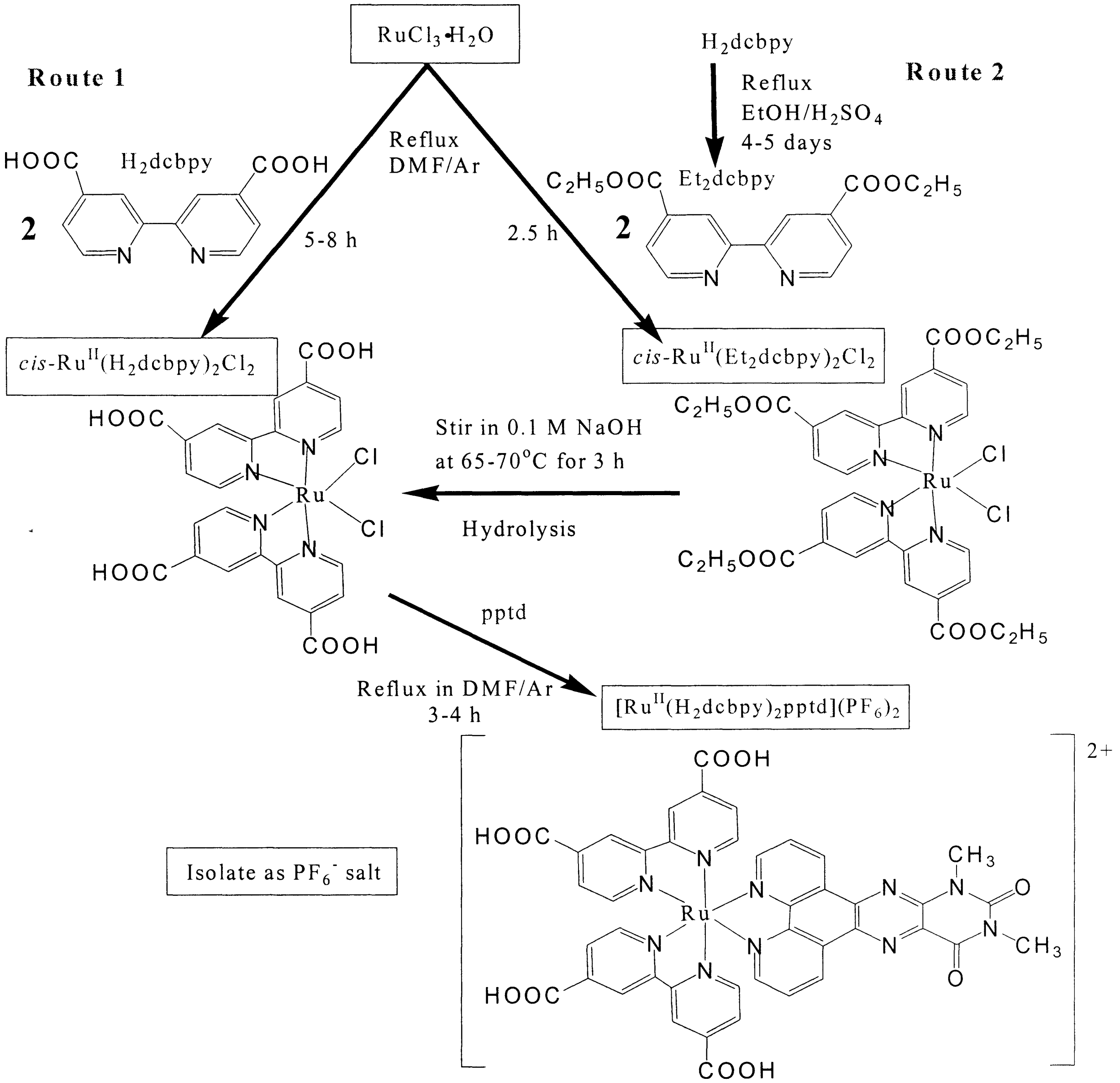

A-1) Synthesis and/or characterization of starting materials

i) Characterization of 2,2'-bipyridine-4,4'-dicarboxylic acid (H_2dcbpy)

The ligand H_2dcbpy was purchased from Aldrich and used as received. However, the analysis on the bottle claimed that the sample was 10% monomethylester, which prompted us to characterize the ligand. The H_2dcbpy ligand was characterized by two methods: ^{1}H-NMR and FT-IR. Characterization by FT-IR was done using KBr and compared to the FT-IR data (KBr) provided by Nelissen et. al.[1] The observed C=O stretch was at 1722 cm^{-1} and Nelissen et. al. reported a C=O stretch at 1720 cm^{-1}. The Aldrich website provided an FT-IR spectrum in KBr; their spectrum showed a very broad absorption at 1720 cm^{-1}.

Characterization by ^{1}H-NMR was fairly challenging due to solubility problems. The H_2dcbpy ligand was not soluble enough in d_4-MeOD to get a ^{1}H-NMR spectrum, but it was slightly soluble in d_6-DMSO (Figure 14a). The assignment of peaks is based on previous literature assignments by Yanagida et. al.[2] A broad peak at 13.85 ppm was assigned to the carboxylic acid protons. A doublet centered at 8.92 ppm was assigned to the 6,6' hydrogen atoms of the bipyridine ring since they are attached to carbons adjacent to nitrogen atoms. The singlet at 8.85 ppm was assigned to the 3,3' hydrogen atoms and another doublet centered at 7.92 ppm was assigned to the 5,5' hydrogen atoms. The doublets in this and other ^{1}H-NMR spectra are not necessarily true doublets; however, structural analysis based on straight chain systems would predict that the hydrogen atoms on carbon atoms 5, 5' and 6, 6' of the bipyridine rings should split each other giving two distinct doublets. The two doublets and the singlet peak each integrate to 2 H each, which gives a total of 6 H for the bipyridine ring system. The broad peak at 13.85

integrates to 1.38, which is less than the 2H expected for the carboxylic acid protons. This integration could be at least partially explained by the presence of monomethyl esters. Assuming that the methyl resonance does not shift much in different solvents, it is expected to be at approximately 3.9 ppm (in $CDCl_3$) based on the model complex methyl benzoate[3]. Figure 14a shows no peak in this area; therefore, if we assume that any such signal is not coincidentally at 3.336 ppm (H_2O peak in DMSO), the sample should be considered to be mostly H_2dcbpy and the less than ideal integration of the broad peak at 13.85 ppm remains unexplained.

The solubility of the H_2dcbpy ligand was greatly improved in 0.01 M NaOD/D_2O presumably due to deprotonation of the carboxylic acid groups in H_2dcbpy (pKa_1, ≅ 4.0; pKa_2 ≅ 2.0)[4] and the spectrum is shown in Figure 14b. The large peak at 4.75 ppm belongs to the solvent D_2O (HOD). Signals in the aromatic region are similar to those observed in d_6-DMSO, with doublets centered at 7.76 ppm (*J* 4.93) and 8.68 ppm (*J* 5.04) assigned to hydrogen atoms on carbon atoms 5, 5' and 6, 6', respectively, and a singlet at 8.30 ppm assigned to the hydrogen atoms on carbon atoms 3 and 3'. The integration worked out to the expected 2: 2: 2 ratios. Literature peak assignments vary somewhat, depending on the source. For example, Nelissen et. al.[1] report the following ^{1}H-NMR signals in D_2O/NaOD: δ 8.65 (d, *J*(H,H)= 5.1 Hz, 2H; bpy-*H*-6,6'), 8.27 (s, 2H; bpy-*H*-3,3'), 7.74 (dd, *J*(H,H) = 1.4 Hz, *J*(H,H) = 5.1 Hz, 2H; bpy-*H*-5,5'). On the other hand, Yanagida et.al.[2] reported the following ^{1}H-NMR signals in D_2O: 8.76 (d), 8.36(s) and 7.94 (d). As in d_6-DMSO, the ^{1}H-NMR spectrum of H_2dcbpy in 0.01 M NaOD/D_2O showed no evidence of any monomethylester.

ii) Synthesis and characterization of bis(2,2'-bipyridine-4,4'-dicarboxy) dichlororuthenium (II): $Ru^{II}(H_2dcbpy)_2Cl_2$

The first major step towards synthesizing the target complex $[Ru^{II}(H_2dcbpy)_2pptd](PF_6)_2$ was the synthesis of $Ru^{II}(H_2dcbpy)_2Cl_2$. This complex was synthesized by two different methods (see Scheme 3). The first method, which was adapted from Grätzel et. al.[5], involved refluxing the appropriate amount of H_2dcbpy and $RuCl_3.H_2O$ in DMF under Ar for approximately 5-8 h (details in Scheme 4). Upon completion of the reaction, two separate solids were isolated. The first solid (020102-A) was isolated by filtration of the reaction mixture and the second solid (020102-B) was isolated after removing most of the DMF by rotary evaporation and precipitating with acetone. The two solids were then dried in a vacuum dessicator. An attempt was made to characterize solid A by ^{1}H-NMR in d_6-DMSO (Figure 15). The solid was only partially soluble in DMSO, but it still gave a readable spectrum. The ^{1}H-NMR spectrum of $Ru^{II}(H_2dcbpy)_2Cl_2$ was expected to be similar to the spectrum of $Ru^{II}(H_2dcbpy)_2(NCS)_2$ which was synthesized and characterized (in D_2O) by Yanagida et. al.[2] They reported two doublets at 9.49 ppm (H-6) and 7.75 ppm (H-6'), two doublet of doublets centered at 8.15 ppm (H-5) and 7.45 ppm (H-5'), and two singlets at 8.87 ppm (H-3) and 8.71 ppm (H-3'). The ^{1}H-NMR spectrum of solid 020102-A (Figure 15) showed signals that looked like doublets centered at approximately 9.99 ppm (*J* 5.4), 8.12 ppm (*J* 5.94) and 7.39 ppm (*J* 5.68), but the exact assignment of peaks to specific hydrogen atoms on the bipyridine rings was difficult since the peaks were not well-resolved and there were only three doublets instead of the expected four. The spectrum also showed two signals that looked like singlets at 8.95 ppm and 8.76 ppm which could be assigned to hydrogen atoms on carbon atoms 3'and 3, respectively.[2] The singlet at approximately 7.95 ppm belonged to residual DMF in the sample. There was a considerable amount of DMF in the sample and this was due to the fact that the sample was isolated directly from the reaction mixture. The other DMF signals appeared as singlets at 2.89 and 2.73 ppm. One of the problems with the spectrum was that the integration of the peaks in the aromatic region did not coincide with the number of hydrogen atoms (12) on the bipyridine rings. The integration was calculated by manually setting the integration of the peak at 9.96 ppm to 2H, and the rest of the peaks were integrated in relation to this peak. The total integration of the aromatic regions gave a total of 19.49 protons. The singlet at 8.95 ppm appears to have an abnormally broad base (impurities). If much of this broad base was eliminated from the integration, it would help bring the total integration down closer to the theoretical value of 12.

A second ^{1}H-NMR of solid 020102-A was taken in d_4-MeOD in which the solid appeared to be more soluble (Figure 16). The peaks of importance were as follows: four multiplets centered at 10.08 ppm, 8.20 ppm, 7.76 ppm, and 7.53 ppm and two singlets at 9.00 ppm and 8.83 ppm, which is somewhat more consistent with the data reported by Yanagida et. al.[2] for $Ru^{II}(H_2dcbpy)_2(NCS)_2$. Peaks from residual DMF are also noted in Figure 16. The total integration in the aromatic region was approximately 15.6 H.

Grätzel et. al.[5] filtered the DMF mixture in order to remove traces of tris ruthenium complex RuL_3, implying that the desired bis complex stayed in solution. Our experience differed in that solid 020102-A, isolated directly from DMF, showed no evidence of tris complex formation (not a red complex, nor had UV-Vis peaks at around 450-470 nm). Noting these discrepancies and the fact that we refluxed for 5 h instead of the recommended 8 h, it was decided that the solids (020102-A and B) would be combined and refluxed again in DMF. Also it was hoped that subsequent recrystallization from acetone would remove residual DMF from the solid sample. The two solids were combined in 125 mL of DMF and refluxed for an additional 4 h. A final solid product (021802-F) was isolated after several filtrations and recrystallization steps (Scheme 4).

Scheme 4: Direct synthesis of $Ru^{II}(H_2dcbpy)_2Cl_2$

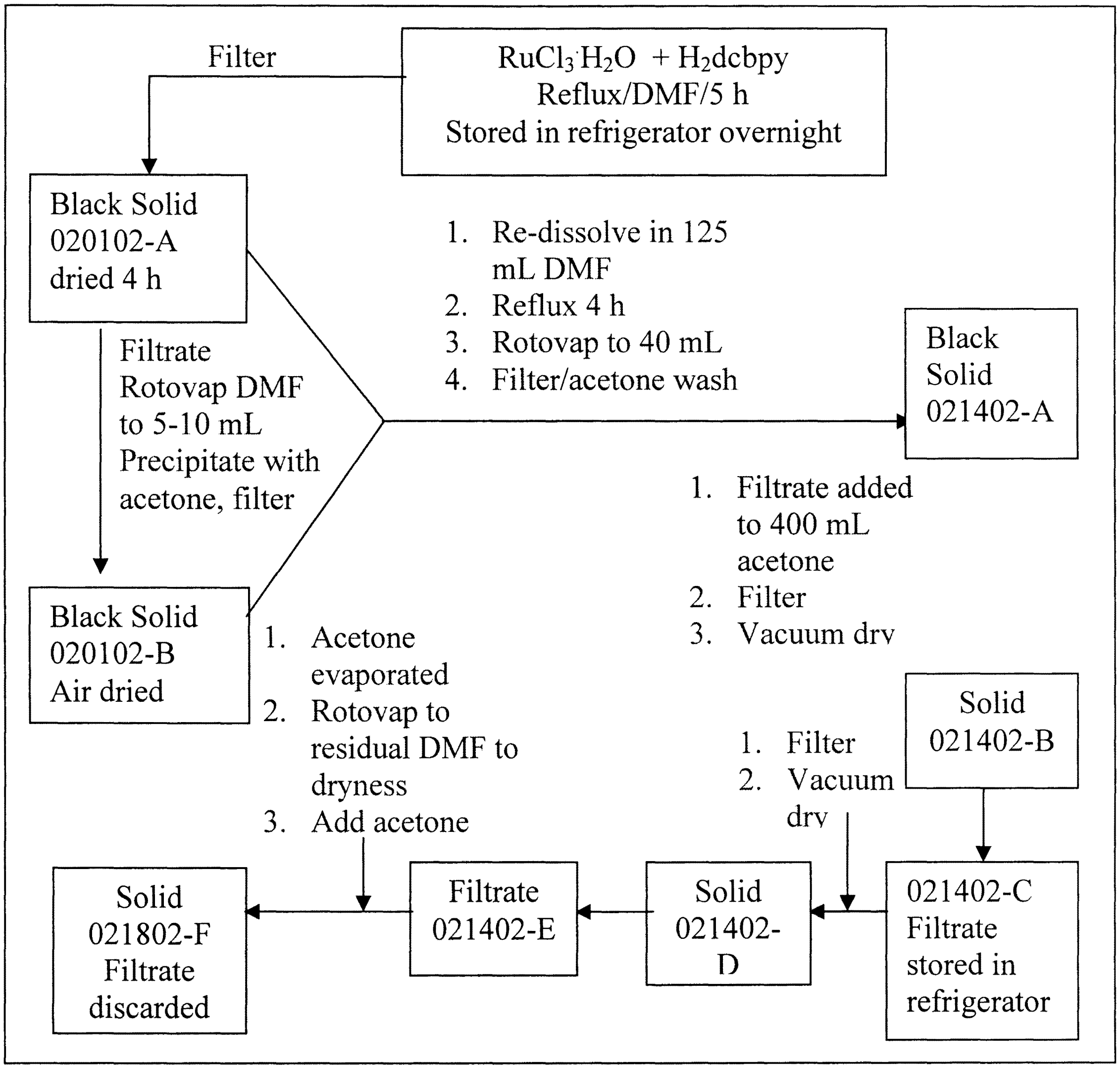

Part of the difficulty in isolating the solid was its extreme solubility in DMF. The synthetic preparation reported by Grätzel et. al.[5] calls for evaporating most of the DMF under vacuum and then precipitating with acetone. However, they do not mention the exact amount of DMF evaporated, which made it very difficult to reproduce their results. It was finally discovered through numerous filtrations and recrystallization steps that in order for the solid to precipitate out of acetone, the DMF had to be removed almost completely. Scheme 4 shows a solid (021802-F) that was finally isolated after effectively removing all DMF before isolating the solid from acetone. This solid was characterized by UV-Vis in pH 4.9 phthalate buffer (Figure 17) and by ^{1}H-NMR in 0.01 M NaOD/D_2O (Figure 18). The UV-Vis spectrum showed two important characteristic peaks, one at 512 nm and the other at 376 nm. These peaks are common to almost all bis ruthenium complexes and are the result of metal to ligand charge transfer (MLCT). For example, $Ru^{II}(bpy)_2Cl_2 \cdot 2H_2O$, which was previously synthesized in McGuire's laboratory[6] showed two absorption bands at 551 nm and 377 nm in acetonitrile. Another very similar compound, synthesized by Grätzel et. al.[5], $[Ru^{II}(H_2dcbpy)_2(H_2O)_2]^{2-}$, also shows two absorption bands at 500 nm and 370 nm in pH 4.85 buffer. The characteristic UV-Vis bands in this region are consistent with isolation of the bis complex.

The ^{1}H-NMR (Figure 18) in 0.01 M NaOD/D_2O showed the expected four signals that look like multiplets and two signals that look like singlets in the aromatic region. The residual DMF peaks were no longer present, probably due to recrystallization and washing efforts aimed at removing as much DMF as possible. However, the peaks in the aromatic region were still not well-resolved, there was a considerable amount of noise as well as an additional signal centered at 9.8 ppm, and the total integration was > 17 H.

The synthesis of $Ru^{II}(H_2dcbpy)_2Cl_2$ using the Grätzel preparation was attempted four more times in the hopes of getting a cleaner product. The final two synthetic preparations were the most successful of the six trials. Refluxing time was kept to exactly that recommended by Grätzel (8 h) and the DMF was removed completely prior to precipitation with acetone. The solid isolated from the fifth synthesis was labeled (062702-B) and it was characterized by UV-Vis and ^1H-NMR. The UV-Vis spectrum (Figure 19) was taken in pH 4.8 phthalate buffer and the peaks of importance were at 378 and 518 nm, which compares well with the UV-Vis spectrum in Figure 17. The ^1H-NMR spectrum was taken in d_4-MeOD (Figure 20). There was still noticeable impurities evident in the aromatic region, but the integration seemed to be closer to that expected for *cis*-$Ru^{II}(H_2dcbpy)_2Cl_2$ (11.76 protons), although in this sample the integration of several peaks seemed too low.

The solid isolated from the sixth synthesis (071602-B) appeared to be the most successful of all the attempts. The ^1H-NMR spectrum was taken in d_4-MeOD (Figure 21). The peaks in the aromatic region seemed fairly well-resolved and impurity levels appeared to be relatively low. The total integration in the aromatic region came to about 13.5 H, still somewhat off from the expected 12 H.

The fact that it took so many filtration and recrystallization steps and six synthetic trials to get a final complex that was at least "partially acceptable" prompted us to use an alternate route for synthesizing $Ru^{II}(H_2dcbpy)_2Cl_2$. This alternate route involved using an ethyl ester derivative of H_2dcbpy, which will be designated as Et_2dcbpy (see Scheme 3). Synthesis of Et_2dcbpy and *cis*-$Ru^{II}(Et_2dcbpy)_2Cl_2$ were carried out according to a method outlined by Wolfbauer et. al.[7], which was then followed by hydrolysis to give cis-$Ru^{II}(H_2dcbpy)_2Cl_2$. These steps are outlined below.

iii) Synthesis and characterization of 2,2'-bipyridine-4,4'-bis(ethoxycarbonyl): (Et_2dcbpy)

The Et_2dcbpy was synthesized by simply refluxing H_2dcbpy in an ethanol/sulfuric acid mixture for 4-5 days. White needle-like crystals of Et_2dcbpy were isolated by cooling the reaction mixture to room temperature and then filtering. The solid was characterized by ^1H-NMR in $CDCl_3$ (Figure 22). The major peaks were assigned from the work of Patterson and Keene:[8] a multiplet centered at 8.95 ppm (3,3'); a doublet of doublets centered at 8.86 ppm (6,6' J 5.08); a doublet of doublets centered at 7.91 ppm (5,5'); a quartet centered at 4.45 ppm (**CH_2**CH_3, J 7.16) and a triplet centered at 1.44 ppm (CH_2**CH_3**, J 7.03). The multiplet centered at 8.95 ppm was supposed to be a singlet according to Patterson and Keene.[8] Their reported peaks in $CDCl_3$ were: δ 1.44 (t, J 7.15 Hz, 6H), 4.45 (q, J 7.15 Hz, 4H), 7.91 (m, 2H), 8.86 (d, J 4.95 Hz, 2H), 8.95 (s, 2H). Total integration in the aromatic region in Figure 22 was ~ 5.5 H, with some unexplained broadness and asymmetry in the signals. However, the solid was used in the next step without further purification.

iv) Synthesis and characterization of bis(2,2'-bipyridine-4,4'-diethoxycarboxy) dichloro ruthenium (II): $Ru^{II}(Et_2dcbpy)_2Cl_2$

According to Wolfbauer et. al.[7], the reaction temperature and time are crucial for the synthesis of the dichloro ruthenium complex. They had noted in their supporting material that below 120 °C there was no noticeable reaction occurring and above 130 °C the reaction proceeded much faster but also led to a significant amount of decomposition.

As a result of this observation by Wolfbauer et. al.,[7] it was decided that DMF would be heated to a constant temperature of 125 °C prior to addition of the two reactants and once the reactants were added the temperature would be kept at approximately 125 °C throughout the reflux. The solid obtained was characterized by UV-Vis in CH_3CN (Figure 23) and by ^{1}H-NMR in d_6-DMSO (Figure 24). The UV-Vis spectrum shows characteristic absorptions at 430 nm and 575 nm. Wolfbauer et. al.[7] reported these peaks to be at 435 nm and 591 nm in DMF. The ^{1}H-NMR shown in Figure 24 indicated that the sample was fairly pure. The peaks of importance were as follows: four signals that look like doublets centered at 10.05 ppm (*J* 5.7), 8.21 ppm (*J* 5.9), 7.70 ppm (*J* 6.26) and 7.43 ppm (*J* 6.24), which can be assigned to H-atoms on carbon atoms 6, 5, 6' and 5', respectively, according to literature assignments.[7] There were two singlets centered at 9.07 ppm and 8.89 ppm assigned to H-atoms on carbon atoms 3 and 3' respectively . There were two signals that look like quartets centered at 4.47 ppm (*J* 7.02) and 4.32 ppm (*J* 7.07) that could be assigned to the CH_2 protons of the ethyl group and two signals that look like triplets centered at 1.39 ppm (*J* 7.01) and 1.25 ppm (*J* 7.05) that could be assigned to the CH_3 protons of the ethyl group. Adjusting the total integration of the quartet at 4.47 ppm and 4.32 ppm to 8H revealed a total integration for the aromatic region to be approximately 11.4H which is close to the expected 12H for pure $Ru^{II}(Et_2dcbpy)_2Cl_2$. The assignments of signals to protons on specific carbons were made according to literature assignments made by Wolfbauer et. al.[7]. The peaks reported by Wolfbauer et. al.[7] in d_6-DMSO were as follows: δ 10.11 (d, *J* 5.7 Hz, C6), δ 7.77 (d, *J* 5.7 Hz, C6'), δ 8.27 (d, *J* 5.9 Hz, C5), δ 7.50 (d, *J* 5.7 Hz, C5'), δ 9.14 (s, C3), δ 8.96 (s, C3'), δ 4.53 (q, *J* 6.9 Hz, **CH_2**-CH_3), δ 4.36 (q, *J* 6.9 Hz, **CH_2**-CH_3'), δ 1.45 (t, *J* 6.9 Hz,CH_2-**CH_3**), δ 1.31 (t, *J* 6.9 Hz, CH_2-**CH_3**').

v) Synthesis and characterization of bis(2,2'-bipyridine-4,4'-dicarboxy)dichloro ruthenium(II): $Ru^{II}(H_2dcbpy)_2Cl_2$

The complex $Ru^{II}(H_2dcbpy)_2Cl_2$ was obtained by simply hydrolyzing the $Ru^{II}(Et_2dcbpy)_2Cl_2$ synthesized above. The hydrolysis of the ethyl ester complex was done according to the protocol provided by Patterson and Keene[8] and involved stirring the complex in warm dilute NaOH. Once the reaction was complete, the NaOH was neutralized with the appropriate amount of 1 M HCl. The solvent was removed by rotary evaporation and 0.1396 g of solid sample was collected. This however, was not the actual weight of $Ru^{II}(H_2dcbpy)_2Cl_2$ produced because the neutralization of NaOH with HCl led to the production of NaCl. Theoretically, there were 1.3×10^{-3} moles of NaOH which would have reacted with 1.3×10^{-3} moles of HCl producing 1.3×10^{-3} moles of NaCl. Hence the actual weight of $Ru^{II}(H_2dcbpy)_2Cl_2$ obtained was $[0.1396 \text{ g} - (1.3 \times 10^{-3} * 58.45)] = 0.0636$ g. This sample weight was used in the calculation of the percent yield in Section 2.5 of the Experimental section. The product was characterized by UV-Vis in pH 5.0 phosphate buffer (Figure 25) and by ^{1}H-NMR in d_6-DMSO (Figure 26). The UV-Vis once again showed the characteristic peaks due to MLCT transitions at 377 and 512 nm, and compares well with the UV-Vis of earlier preparations of $Ru^{II}(H_2dcbpy)_2Cl_2$ (see Figure 19). The ^{1}H-NMR in d_6-DMSO (Figure 26) showed four signals that look like doublets; these are centered at 9.79 ppm (*J* 5.33), 7.93 ppm (*J* 6.10), 7.39 ppm (*J* 5.9), and 7.26 ppm (*J 6.17*), which could be assigned to H-atoms on carbon atoms 6, 6', 5 and 5' based on assignments of $Ru^{II}(H_2dcbpy)_2(NCS)_2$ made by Yanagida et. al.[2] There were also two signals that looked like singlets at 8.65 ppm and 8.48 ppm, which could be assigned to H-atoms on carbon atoms 3 and 3' respectively[2]. The solvent peaks are also indicated in Figure 26.

Although the total integration in the aromatic region is approximately 14 H, the impurity levels appear to be at least as low as those shown in Figure 21, which was previously the "best" preparation of $Ru^{II}(H_2dcbpy)_2Cl_2$ (Route 1 of Scheme 3). Moreover, the exceptional quality of the $Ru^{II}(Et_2dcbpy)_2Cl_2$ starting material (Figure 24) seems to point to the ethyl ester route as the preferred method for producing $Ru^{II}(H_2dcbpy)_2Cl_2$.

A-2) Synthesis and Characterization of bis(2,2'-bipyridine-4,4'-dicarboxy) 10,12-dimethyl pteridino[6,7][1,10]phenanthroline-11,13-(10H,12H)-dione ruthenium (II) hexafluorophosphate: $[Ru^{II}(H_2dcbpy)_2pptd](PF_6)_2$

The synthesis of the target complex $[Ru^{II}(H_2dcbpy)_2pptd](PF_6)_2$ was approached from four different directions using the starting materials $Ru^{II}(H_2dcbpy)_2Cl_2$, $Ru^{II}(Et_2dcbpy)_2Cl_2$, and pptd.

i) Synthetic Route #1

This first attempt at synthesizing $[Ru^{II}(H_2dcbpy)_2pptd](PF_6)_2$ involved using $Ru^{II}(H_2dcbpy)_2Cl_2$ (solid 021802-F, Scheme 4, Figure 18) and pptd which had been previously synthesized in McGuire's lab. The synthetic process is outlined in Scheme 5. The reaction was initiated by dissolving the starting materials in a mixture of 0.1 M triflic acid and ethylene glycol; this was done for two reasons. First of all, the triflic acid was supposed to keep the reaction mixture acidic, thus keeping the H_2dcbpy ligands protonated. Secondly, the high boiling ethylene glycol was used to aid in dissolution of the starting materials and provide a reducing atmosphere to keep the ruthenium in the +2 oxidation state. The reaction was monitored by UV-Vis since the UV-Vis spectra would show the disappearance of the $Ru^{II}(H_2dcbpy)_2Cl_2$ peaks at 376 nm and 512 nm (Figure 17) and the appearance of the characteristic tris-complex absorption (MLCT) of $[Ru^{II}(H_2dcbpy)pptd]^{2+}$ in the 450-470 nm range as well as the peaks of pptd at approximately 373 nm and 390 nm. The ^{1}H-NMR (d_6-DMSO) of the initial product (033002-A) is shown in Figure 27. The exact assignment of all the peaks was not attempted; however, it was possible to analyze the integration of the spectrum. The aromatic region of the spectrum was expected to integrate to a total of 18 H. From previous work[9], it was known that the spectrum should also show two slightly different pptd-methyl signals in the 3-4 ppm region. In fact, these $-CH_3$ signals appeared as

Scheme 5: First synthetic route for the synthesis of $[Ru^{II}(H_2dcbpy)_2pptd](PF_6)_2$

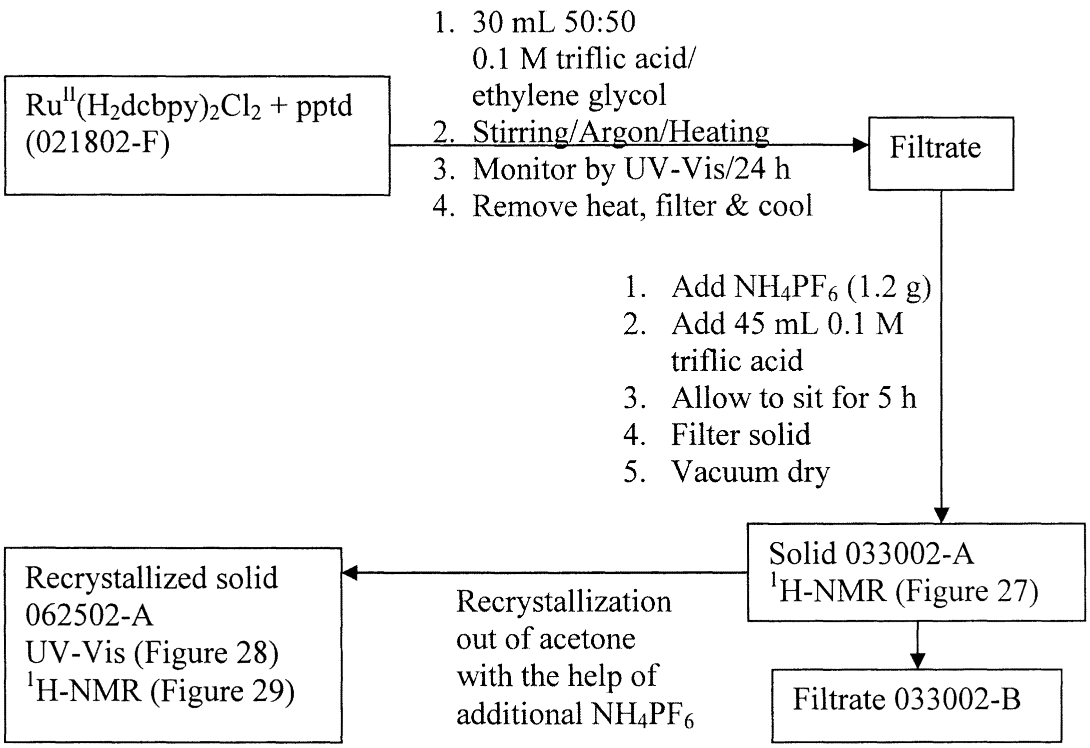

singlets in Figure 27 at 3.86 ppm and 3.48 ppm, with the latter singlet showing significant overlap with a broad absorption assigned to H_2O. If the singlet at 3.86 ppm is set to 3H, the signals in the aromatic region integrate to less than 18 H (~ 11 H). The broad peak centered at 14.33 most likely belongs to the hydroxyl proton of the acid group (COOH). The ^{1}H-NMR also showed signals (singlet) centered at 7 ppm which could not be identified (In hindsight, these signals seemed to be associated with isolation of the product from an acid-containing solution.) As a result of the low integration in the aromatic region and the unknown signals at 7 ppm, it was decided that the solid would be recrystallized from acetone in the presence of NH_4PF_6. The ^{1}H-NMR spectrum of the recrystallized solid is given in Figure 29. This ^{1}H-NMR was taken in CD_3CN, since it was expected that the H_2O signal in CD_3CN (~ 2.5 ppm) would be clear of the $-CH_3$ signals of pptd. These $-CH_3$ signals turned out to be centered at 3.53 ppm and 3.91 ppm. The methyl peak centered at 3.53 ppm was manually integrated to 3 H, and once again the other peaks were integrated in reference to this peak. The peaks in the aromatic region (7-12 ppm) integrated to a total of 14.45 H, which was still less than the expected 18 H, but was an improvement over Figure 27. The –COOH peak was not visible in CD_3CN. The signals previously seen centered around 7 ppm were gone. The peaks that look like multiplets centered at 3.85 ppm and 4.45 ppm were unknowns that will be discussed a little later in this section.

The UV-Vis spectrum of solid 033002-A is shown in Figure 28 and it was taken in CH_3CN. The MLCT absorption appears at about 466 nm with a high energy shoulder at about 430 nm and the pptd absorptions peak appears at about 368 nm with a low energy shoulder at approximately 390 nm. The UV-Vis of this solid (033002-A) can be compared with a similar complex $[Ru^{II}(bpy)_2(pptd)](PF_6)_2 \cdot H_2O$ synthesized previously in McGuire's lab[9]. McGuire et. al.[9] report the characteristic MLCT absorption for the tris-chelated polypyridyl species in CH_3CN around 450 nm and a shoulder at 429 nm. They also report the higher energy pptd peaks at about 374 nm and 389 nm. The red-shift of the MLCT band for $[Ru^{II}(H_2dcbpy)_2(pptd)](PF_6)_2$ (466 nm) compared to $[Ru^{II}(bpy)_2(pptd)](PF_6)_2$ (450 nm) is consistent with the electron withdrawing capability of the H_2dcbpy compared to that of the unsubstituted bpy.

Even though the UV-Vis spectrum of solid 033002-A in CH_3CN showed the characteristic peaks of a tris-chelated complex, the unsatisfactory nature of the ^{1}H-NMR spectra prompted exploration of alternate synthetic routes.

ii) Synthetic Route #2

The second synthetic route, outlined in Scheme 6, involved combining the two starting materials in 30 mL of ethylene glycol without any 0.1 M triflic acid. The reaction was allowed to reflux for a total of 3 h and UV-Vis spectra indicated that the reaction was complete. At this point the solvent ethylene glycol was completely removed by rotary evaporation (a challenging task) and approximately 20 mL of 1.0 M HCl was added to the reaction flask. The target complex was then precipitated by adding excess NH_4PF_6. The solid obtained from this step (070102-A) was characterized by UV-Vis in CH_3CN (Figure 30) and ^{1}H-NMR in CD_3CN (Figure 31).

The UV-Vis spectrum contains a characteristic bound pptd peak at approximately 370 nm with a shoulder at approximately 390 nm and the MLCT absorption at 466 nm with a higher energy shoulder at approximately 430 nm. In fact, this spectrum was very similar to that obtained from synthetic route #1 (Figure 28).

Scheme 6: Second synthetic route for the synthesis of $[Ru^{II}(H_2dcbpy)_2pptd](PF_6)_2$

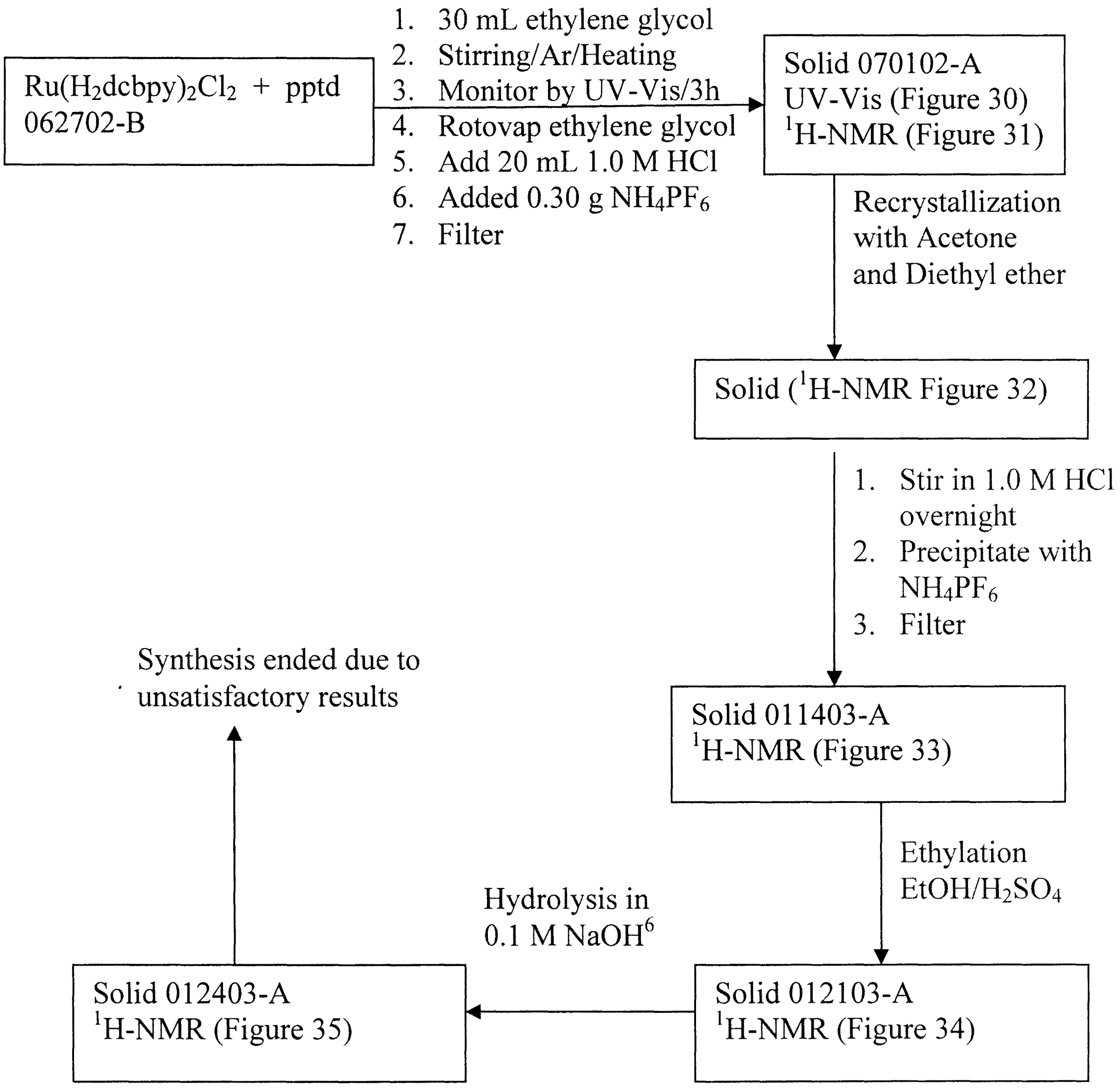

The ^{1}H-NMR spectrum (Figure 31) of this solid was complicated with the aromatic region containing many signals that could not be identified. There were three singlets centered on 6 ppm, and a set of multiplets centered at 3.82 ppm and 4.43 ppm, all of which were puzzling and also appeared in the initially isolated product in the previous synthesis. (Although the singlets were shifted ~ 1 ppm downfield in d_6-DMSO compared to CD_3CN.) Two singlets around 2.7-2.8 ppm were identified as residual DMF peaks. Recrystallization using acetone and diethyl ether yielded a solid that was once again characterized by ^{1}H-NMR in CD_3CN (Figure 32). This simplified the aromatic region (which integrated to ~ 15.5 H) and also eliminated the singlets centered at 6 ppm. However, the multiplets at 3.82 ppm and 4.43 ppm were still present. One explanation that was considered for these peaks was that ethylene glycol (under the reaction conditions) actually bridged the two carboxyl groups in H_2dcbpy through hydrogen bonding (see Illustration a below). However, the integration of these multiplet peaks in Figure 32 give a total of approximately 14.94 H (subtracting 3H for the methyl group at 3.89 ppm), which would indicate that instead of one bridging ethylene glycol, there could be one ethylene glycol molecule H-bonded to each carboxyl group (Illustration b).

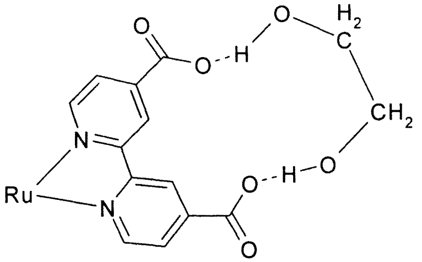

Illustration a

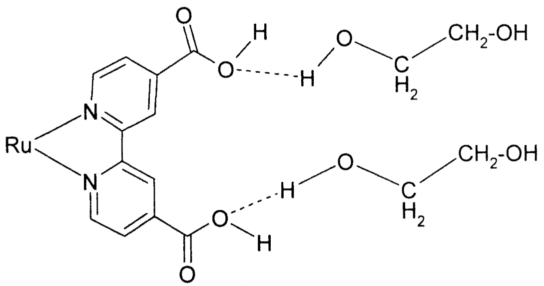

Illustration b

Working on the assumption that the signals at 3.8 ppm and 4.4 ppm originated from some interaction of H_2dcbpy ligands with ethylene glycol, the solid was stirred in 1.0 M HCl and then precipitated with NH_4PF_6 in an attempt to break this interaction. The solid (011403-A) isolated after this step was characterized by ^{1}H-NMR in CD_3CN. The ^{1}H-NMR (Figure 33) showed a slightly better integration in the aromatic region compared to Figure 32 (16.03 vs. 15.54), however the multiplets at 3.82 ppm and 4.43 ppm were still present (with significant intensity; 13.5 H). Consistent with exposure of the solid to acid, the three singlets (centered at 6 ppm in CD_3CN) re-appeared, but at a reduced intensity compared to Figure 31. Since stirring in acid did not remove the supposed "ethylene glycol" peaks, an attempt was made to ethylate the carboxyl groups. Hence the solid was stirred in an ethanol/H_2SO_4 mixture for 3 days according to the protocol reported by Wolbauer et. al.[7]. The solid isolated from this step was once again characterized by ^{1}H-NMR in CD_3CN (Figure 34). The ^{1}H-NMR spectrum did not show a very successful ethylation; however the multiplets now centered at 3.85 ppm and 4.45 ppm seemed to be simplified and the 3.85 ppm peaks were reduced in intensity. Since the "ethylene glycol" peaks were somewhat changed and there was a slight indication of ethylation, we decided to stir the solid in 0.1 M NaOH[8] in order to hydrolyze the ethyl groups. The solid that was isolated after hydrolysis was characterized by ^{1}H-NMR in CD_3CN (Figure 35). The hydrolysis process did not produce the expected results, and in fact the ^{1}H-NMR (Figure 35) showed no methyl peaks from the pptd ligand and the aromatic region showed considerable noise. It was assumed that pptd did not tolerate extended exposure to warm hydroxide solution. Therefore, further work with this product was abandoned.

iii) Synthetic Route #3

The third synthetic attempt was made using starting materials $Ru^{II}(Et_2dcbpy)_2Cl_2$ and pptd. It was thought that there would be several advantages to using the ethylated ruthenium complex. First, $Ru^{II}(Et_2dcbpy)_2Cl_2$ was considered to be a "cleaner" starting material than $Ru^{II}(H_2dcbpy)_2Cl_2$. Secondly, if the interaction of the solvent ethylene glycol with the –COOH groups of H_2dcbpy was indeed a significant problem, the use of the ethylated starting material would hopefully prevent this. Finally, it was hoped that $[Ru^{II}(Et_2dcbpy)_2pptd]^{2+}$ would have a more convenient purification scheme than the weak acid $[Ru^{II}(H_2dcbpy)_2pptd]^{2+}$. The synthetic route is given in Scheme 7.

Scheme 7: Third synthetic route for the synthesis of $[Ru^{II}(H_2dcbpy)_2pptd](PF_6)_2$

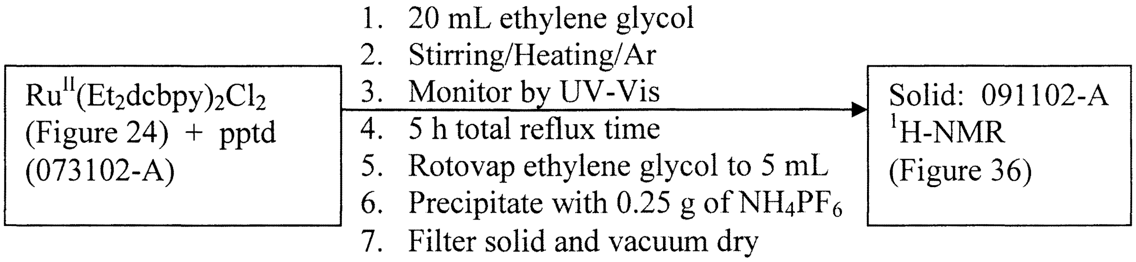

$Ru^{II}(Et_2dcbpy)_2Cl_2$ (Figure 24) + pptd (073102-A)

1. 20 mL ethylene glycol
2. Stirring/Heating/Ar
3. Monitor by UV-Vis
4. 5 h total reflux time
5. Rotovap ethylene glycol to 5 mL
6. Precipitate with 0.25 g of NH_4PF_6
7. Filter solid and vacuum dry

Solid: 091102-A
^{1}H-NMR
(Figure 36)

The ^{1}H-NMR spectrum in CD_3CN of the solid isolated in the above reaction is given in Figure 36. There are several important things to note from Figure 36. First of all, since the ethyl ester ruthenium complex was used as starting material, it was expected that the ^{1}H-NMR would show the ethyl peaks from the Et_2dcbpy ligand; however, these peaks (or at least the $–CH_3$ peaks) were absent from the spectrum. Moreover, the "ethylene glycol peaks" once again appeared around 4.45 ppm and 3.85 ppm. The sample was then recrystallized to remove some of the impurities and then, in an effort to reintroduce ethyl ester groups, it was stirred in a mixture of ethanol and sulfuric acid. Unsatisfactory results lead to the abandonment of this synthetic route. At this point, the following seemed to be clear: 1) ethylene glycol did not appear to be an appropriate solvent for this synthesis and 2) if $Ru^{II}(Et_2dcbpy)_2Cl_2$ was to be used as a starting material, hydrolysis of the ethyl ester had to occur prior to attachment of the pptd ligand since the ligand pptd appeared to be intolerant to treatment with warm 0.1 M NaOH (Scheme 6, Figure 35).

iv) Synthetic Route #4

The synthetic scheme is presented in Scheme 8 below. $Ru^{II}(Et_2dcbpy)_2Cl_2$ was hydrolyzed according to the procedure given in section 2.5 of the Experimental section. The resulting $Ru^{II}(H_2dcbpy)_2Cl_2$ was refluxed with pptd in DMF (instead of ethylene glycol) in the synthesis of $[Ru^{II}(H_2dcbpy)_2pptd](PF_6)_2$.

Scheme 8: Fourth synthetic route for the synthesis of $[Ru^{II}(H_2dcbpy)_2pptd](PF_6)_2$

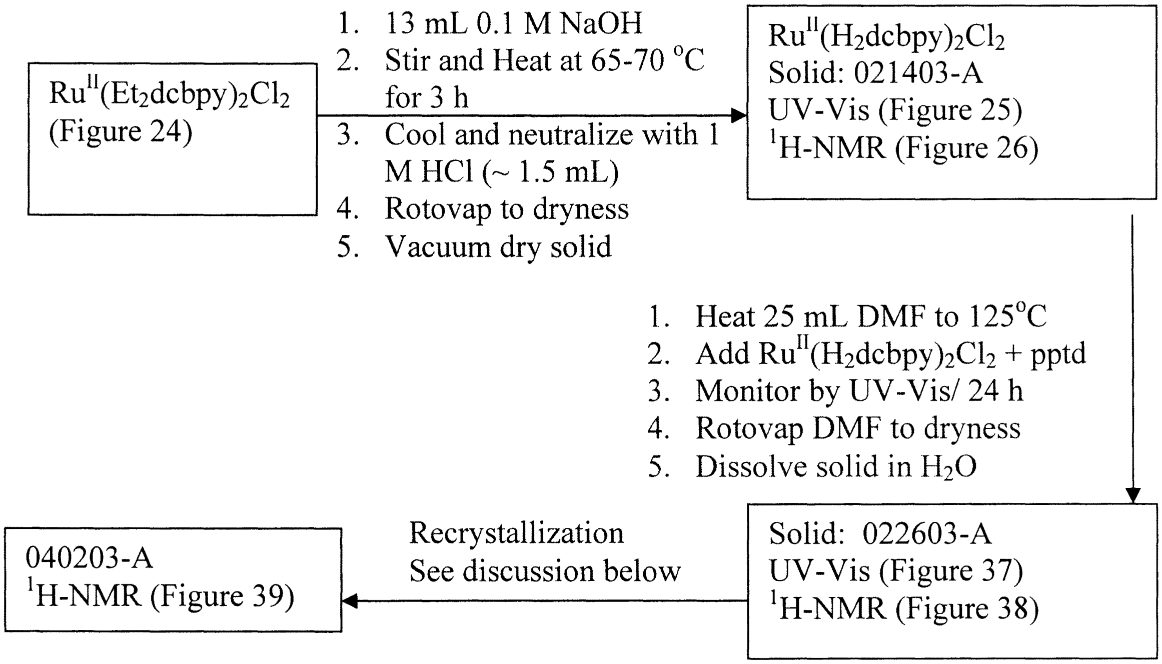

$Ru^{II}(Et_2dcbpy)_2Cl_2$
(Figure 24)

1. 13 mL 0.1 M NaOH
2. Stir and Heat at 65-70 °C for 3 h
3. Cool and neutralize with 1 M HCl (~ 1.5 mL)
4. Rotovap to dryness
5. Vacuum dry solid

$Ru^{II}(H_2dcbpy)_2Cl_2$
Solid: 021403-A
UV-Vis (Figure 25)
^{1}H-NMR (Figure 26)

1. Heat 25 mL DMF to 125°C
2. Add $Ru^{II}(H_2dcbpy)_2Cl_2$ + pptd
3. Monitor by UV-Vis/ 24 h
4. Rotovap DMF to dryness
5. Dissolve solid in H_2O

Solid: 022603-A
UV-Vis (Figure 37)
^{1}H-NMR (Figure 38)

Recrystallization
See discussion below

040203-A
^{1}H-NMR (Figure 39)

The reaction took approximately 24 h and it was monitored by UV-Vis. The UV-Vis spectrum at the beginning of the reaction showed two peaks at approximately 377 nm and 512 nm (Figure 25 in pH 5.0 phosphate buffer). Upon completion of the reaction these peaks were absent, and two peaks were present at approximately 373 nm and 462 nm (Figure 37). The ^{1}H-NMR (Figure 38) spectrum in d_6-DMSO showed very few impurities.

The methyl peaks of pptd were centered at 3.84 and 3.46 ppm. The aromatic region (7-10 ppm) showed two signals that looked like doublets centered around 9.50 ppm and two other signals that looked like singlets at 8.88 ppm and 8.83 ppm. It also showed several signals that looked like multiplets centered between 8.3-7.5 ppm. The assignment of peaks in the aromatic region to specific protons on the complex was not attempted; however, the total integration of these signals came to 19 H which was very close to the expected 18 H.

In order to further purify the sample obtained after evaporating the DMF, the solid was suspended in Millipore™ water. The pH of this solution was approximately 2.5, which probably was the result of partial deprotonation of the weak-acid H_2dcbpy ligand. The pH of the solution was slowly raised to 10 for two reasons. First of all, complete deprotonation of the H_2dcbpy ligand would make the product (which should contain two dcbpy^{2-} ligands) quite soluble in H_2O. Any undissolved solid at this pH would most likely be unwanted side-products which could be filtered. After filtration, the pH of the filtrate was reduced back to approximately 2.5 using 0.1 M triflic acid. Addition of 0.1 M triflic acid was supposed to fully protonate the carboxylate groups of bipyridine. In hindsight, lowering the pH to 2.5 was probably not sufficient since the measured pK_a values for bound H_2dcbpy ligand in the model complex $[Ru^{II}(H_2dcbpy)_2(bpy)]^{2+}$ have been reported to be 2.50 and 1.80 respectively.

In any event, precipitation did occur at a pH $\cong$ 2.5, and the red solid was collected. The intent was to recover the triflate salt of the complex, $[Ru^{II}(H_2dcbpy)_2(pptd)](CF_3SO_3)_2$; however it is possible that the red solid contained a significant amount of neutral complex precipitated at it's isoelectronic point; $[Ru^{II}(Hdcbpy)_2(pptd)]$.

In the literature, adsorption of dyes on to TiO_2-coated glass electrodes occurs from ethanol solutions of the dye. Unfortunately, the red solid isolated at pH 2.5 did not show sufficient solubility in absolute ethanol. It was thought that the hexafluorophosphate salt of the complex might be more soluble since previous attempts at dissolving the PF_6^- salts of previous samples of the complex seemed more successful. Therefore, the red solid was re-suspended in H_2O and the pH of the solution was raised from 2 to 9 using 0.1 M NaOH. This pH 9 solution was then filtered and, in order to precipitate the complex as a PF_6^- salt, excess NH_4PF_6 was added to the pH 9.0 dye solution which brought the pH of the solution down to approximately 7. In order to further reduce the pH and precipitate the complex, 1.0 M HCl was added dropwise until the pH was about 2.5. At this point, solid started to precipitate out of solution. A ^1H-NMR of this solid was taken in d_6-DMSO (Figure 39), however the peaks were not resolved very well, which could be the result of poor solubility of the solid. Once again, the solubility of the dye was tested in ethanol and it turned out to be more soluble compared to the first isolation; however it was still not as soluble as the previous isolations of (impure) $[Ru^{II}(H_2dcbpy)_2pptd](PF_6)_2$. Once again, in hindsight, this slight improvement might have been due to isolation of $[Ru^{II}(Hdcbpy)_2(pptd)]$ with some $[Ru^{II}(H_2dcbpy)_2(pptd)](PF_6)_2$ or even $[Ru^{II}(H_2dcbpy)(Hdcbpy)(pptd)](PF_6)$ present.

In summary, out of all the attempts made at the synthesis of $[Ru^{II}(H_2dcbpy)_2pptd](PF_6)_2$, synthetic route # 4 appeared the most successful based on simplicity of the method and the ^1H-NMR spectrum. The ^1H-NMR of the crude product (Figure 38) looks pretty good and the ^1H-NMR of the recrystallized product seemed to show poor resolution but this could be the result of poor solubility. This last solid, which may contain a mixture of neutral, +1 and +2 forms, was the solid used in the electrochemical experiments described in Section B of the results and discussion.

B) Electrochemistry

This section will focus mainly on the electrochemical behavior of the target complex $[Ru^{II}(H_2dcbpy)_2pptd](PF_6)_2$ in solution and on a TiO_2-coated conducting glass electrode as well as on the solution electrochemical behavior of three reference complexes: $[Ru^{II}(H_2dcbpy)_2phen](PF_6)_2$, $[Ru^{II}(bpy)_2pptd](PF_6)_2$, and $[Ru^{II}(bpy)_2phen](PF_6)_2$. It was noted earlier in the Introduction that the ligand pptd is a flavin isomer capable of reversible pH-dependent H-atom transfers. In fact, the reference complex $[Ru^{II}(bpy)_2pptd](PF_6)_2$ has shown pH-dependent pptd-centered electron transfer in previous solution electrochemical experiments.[9] Therefore, we hoped to gain some preliminary insight into the behavior of metal-bound pptd adsorbed on TiO_2-coated electrodes.

The electrochemical analysis involves cyclic voltammetry (CV) where the potential of a small stationary working electrode is changed linearly with time starting from a potential where no electrode reaction occurs and moving to potentials where reduction or oxidation of a solute in solution or on the electrode surface occurs.[10] The direction of the linear sweep is reversed once the forward sweep is completed in order to observe the electrode reactions of intermediates and products of the forward reaction. The basic concepts of electrochemistry are still applicable here; i.e. reduction occurs at the cathode and oxidation occurs at the anode.

B-1) Basic structure of the electrochemical cell

Figure 44 illustrates the basic structure of the electrochemical cell used in the CV experiments. For experiments involving the TiO_2-coated glass electrode in aqueous buffer solution, the configuration used is shown.

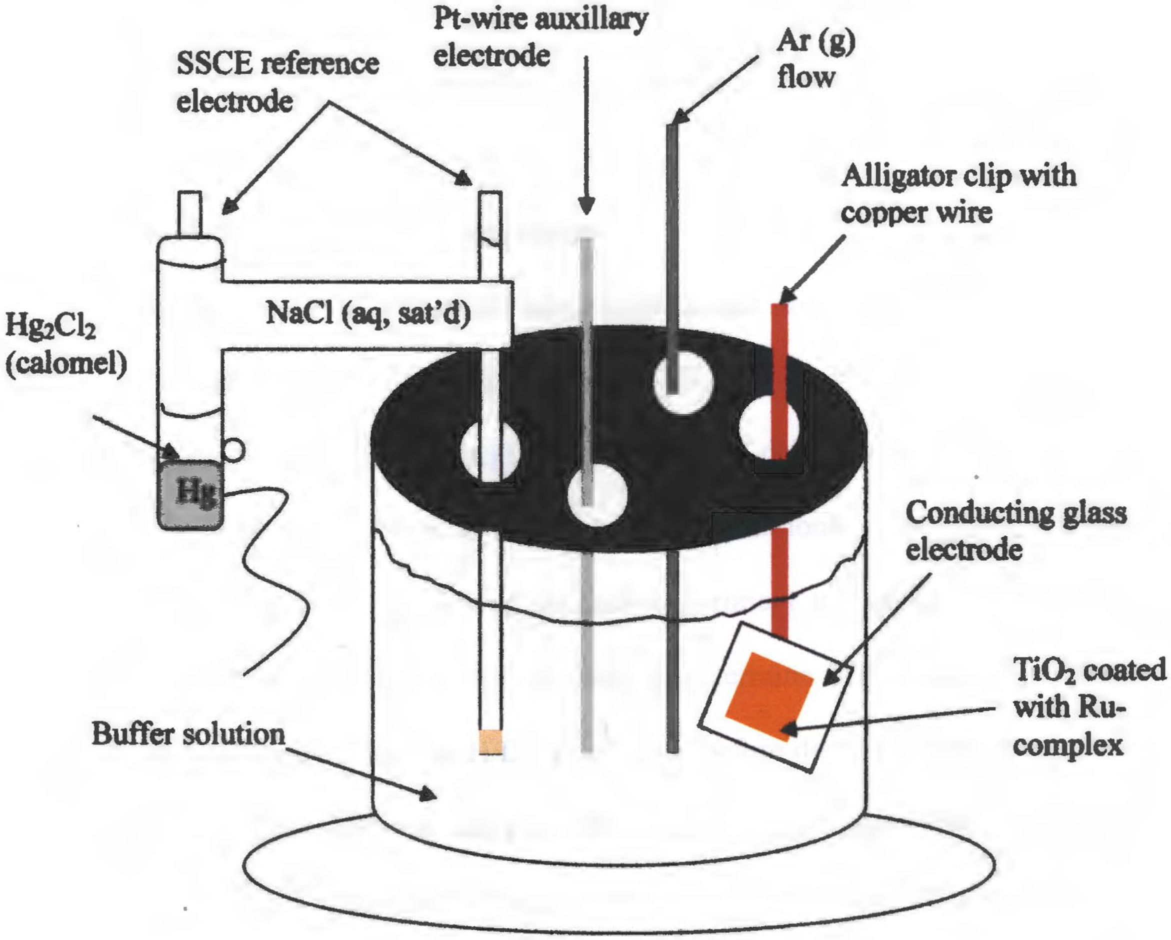

Figure 44: Basic structure of the electrochemical cell

For aqueous solution electrochemistry, the working electrode was switched to glassy carbon electrode. For <u>non</u>-aqueous solution electrochemistry, the working electrode remained glassy carbon, the reference electrode (SSCE[a]) in Figure 44 was replaced with a silver wire, and the aqueous buffer solution was replaced with a 0.1 M TBAH[b]/DMF electrolyte solution containing ferrocene as the internal standard.

B-2) Solution electrochemistry

Solution electrochemistry experiments were performed in both non-aqueous and aqueous solvents. As stated previously, the non-aqueous solvent used was 0.1 M TBAH/DMF. The preparation of this solvent is given in the Experimental section (2.14). The solvents used for aqueous solution electrochemistry were pH 4.0 and pH 7.0 acetate buffers (See Experimental section 2.13).

a) Non-aqueous solution electrochemistry

Non-aqueous solution electrochemistry experiments were carried out for three reference compounds, ($[Ru^{II}(bpy)_2phen](PF_6)_2$, $[Ru^{II}(bpy)_2pptd](PF_6)_2$, $[Ru^{II}(H_2dcbpy)_2phen](PF_6)_2$) and the target complex $[Ru^{II}(H_2dcbpy)_2pptd](PF_6)_2$. Each of the four experiments was conducted under identical conditions. The glassy carbon electrode was polished at the beginning of each experiment in order to remove any absorbed materials from previous scans. In order to determine where the oxygen peak was located, a CV of the 0.1 M TBAH/DMF solution (before deoxygenating) was taken prior to addition of the ruthenium complex (for example, see Figure 45a). Once the oxygen peak was located, the solution was bubbled with Ar for 15-20 min in order to remove as much oxygen as possible. After bubbling with Ar, a second CV (for example, see Figure 45b) was taken to determine if sufficient oxygen had been removed. Residual O_2 peaks were often observed even after extensive bubbling. For example, Figure 45b

---

[a] SSCE = Saturated sodium chloride calomel electrode
[b] TBAH = Tetra butyl ammonium hexafluorophosphate

appears to show residual O_2 activity although its presence has been significantly reduced as can be seen by the smaller peaks and the more sensitive current scale as compared to Figure 45a. It should be noted that the peaks assigned to oxygen in both Figures 45a and 45b are at very similar potentials when referenced against the F_c^+/F_c internal standard. This process of checking for residual O_2 activity was carried out for all electrochemistry experiments.

i) $[Ru^{II}(bpy)_2phen](PF_6)_2$

The CVs for $[Ru^{II}(bpy)_2phen](PF_6)_2$ are given in Figures 45c-e and the results are summarized in Table 1. All the $E_{½}$ values are reported versus the measured $E_{½}$ value of ferrocene (F_c^+/F_c). Figure 45c shows the chemically reversible oxidation of the ferrocene internal reference and it also shows three quasi-reversible $1e^-$ ligand-based reductions which most likely correspond to the two bipyridine ligands (-1.91 V and -2.18 V) and the one phenanthroline ligand (-1.74 V).

Figures 45d and 45e show the metal-centered oxidation of $[Ru^{II}(bpy)_2phen](PF_6)_2$ ($E_{½}$ = +0.83 V vs. F_c^+/F_c). This is known to be a 1 ē process; the ΔE_p value was expected to have been ~ 57 mV. The reported ΔE_p value of 30 mV may well be a reflection of the error inherent in estimating some of these potentials in these experiments, especially when the peaks have low signals, as in Figures 45d and 45e.

ii) $[Ru^{II}(bpy)_2pptd](PF_6)_2$

The CV's of this compound (Figures 46a-c) were more complicated which was expected from the substitution of pptd for phen. Figure 46a shows five ligand-based reductions although they were not all chemically[c] or electrochemically[d] reversible. From

---

[c] chemically reversible when the current in both directions is the same

[d] electrochemically reversible when ΔE_p = 57 mV

the $E_{½}$ values listed in Table 1, it appears that the second reduction wave has a ΔE_p value of 50 mV, which is within the definition for a electrochemically reversible reduction wave. However, the reverse wave is small, and this makes estimating its potential somewhat uncertain. In addition, even if the reduction was electrochemically reversible, the low intensity of the reverse wave rules out chemical reversibility.

From previous published results on this compound,[9] it was expected that the pteridinedione portion of the pptd ligand would be more easily reduced than the bipyridines so the first two $E_{½}$ values (-1.27 V and -1.47 V) are assigned to pteridinedione reductions. Figure 46b shows that the first two reduction waves remain essentially unchanged from Figure 46a even when the scan is reversed before the final three reductions. The last three reduction waves in Figure 46a can be assigned to the phenanthroline portion of pptd and the two bipyridine ligands based on similar reductions in $[Ru^{II}(bpy)_2phen](PF_6)_2$ under the same conditions (Figures 45c). These three reductions are all cathodically shifted (~ 0.6 to 0.16 V) from the same reduction in $[Ru^{II}(bpy)_2phen](PF_6)_2$ which would be expected from the previous reductions of pptd.

Figure 46c shows the metal-centered oxidation of $[Ru^{II}(bpy)_2pptd](PF_6)_2$ in 0.1 M TBAH/DMF. The $E_{½}$ value was calculated to be +0.86 V (Table 1) which is very close to that measured for the similar complex $[Ru^{II}(bpy)_2(phen)](PF_6)_2$ in Figures 45d-e. The large ΔE_p value for $[Ru^{II}(bpy)_2pptd](PF_6)_2$ is difficult to take too seriously here considering the small signals.

iii) *$[Ru^{II}(H_2dcbpy)_2phen](PF_6)_2$*

The CV's of this complex are shown in Figures 47a-d. Figure 47a shows three ligand-based reduction waves which could be attributed to the two H_2dcbpy ligands and one phenanthroline ligand. These reductions do not show appreciable return waves, so that values reported in Table 1 are not $E_{1/2}$ values, but E_{pc} values. The electron withdrawing acid groups of the H_2dcbpy ligands should make them easier to reduce than 2,2'-bpy. The data bears this out. Table 1 shows that bpy reductions are at -1.74 V and -1.91 V in $[Ru^{II}(bpy)_2(phen)](PF_6)_2$ whereas the H_2dcbpy reductions in $[Ru^{II}(H_2dcbpy)_2phen](PF_6)_2$ are at -1.4 V and -1.6 V. Reductions of 1,10-phen appears slightly easier in the H_2dcbpy complex. Figure 47b is simply an expansion of Figure 47a.

Figure 47c shows an oxidative scan and Figure 47d is simply a contraction of Figure 47c in order to better visualize the oxidation. The signal for the oxidation of $[Ru^{II}(H_2dcbpy)_2phen](PF_6)_2$ is very weak and the apparent peaks around + 0.58 V are not likely to be due to the complex since it would be expected to be more difficult to oxidize than $[Ru^{II}(bpy)_2phen](PF_6)_2$. The identity of these peaks is unknown.

iv) $[Ru^{II}(H_2dcbpy)_2pptd](PF_6)_2$

The CVs of $[Ru^{II}(H_2dcbpy)_2pptd](PF_6)_2$ are shown in Figures 48b-d. Figure 48a is a reference scan of 0.1 M TBAH/DMF after it was deoxygenated with Ar. Figure 48b and an expansion in Figure 48c show the reductive scan. There appear to be four reductions with all but the first requiring some estimating due to low signals. Regardless, all the reductions are reported as $E_{½}$ values in Table 1. Some interesting comparisons can be made between the $E_{½}$ values of $[Ru^{II}(H_2dcbpy)_2pptd](PF_6)_2$ and the $E_{½}$ values of the reference compound $[Ru^{II}(bpy)_2pptd](PF_6)_2$. For example, the reference compound shows two reduction waves with $E_{½}$ values of –1.27 V and –1.47 V respectively. These waves were assigned to the pptd portion of the molecule since it is expected to be the most easily reduced. On the other hand, $[Ru^{II}(H_2dcbpy)_2pptd](PF_6)_2$ shows one large reduction wave with a $E_{½}$ value of –1.29 V. It is possible that the broad forward reduction contains two closely spaced overlapping reductions and the reverse wave is one re-oxidation with the other re-oxidation having very low intensity (see same re-oxidation in $[Ru^{II}(bpy)_2pptd](PF_6)_2$ in Figure 46a).

A straight comparison of the reductions assigned to the bpy ligands in $[Ru^{II}(bpy)_2pptd](PF_6)_2$ (-1.8 V, -2.0 V) and those assigned to the H_2dcbpy ligand in $[Ru^{II}(H_2dcbpy)_2pptd](PF_6)_2$ (-2.00 V, -2.19 V) make it appear that coordinated H_2dcbpy is harder to reduce than coordinated bpy. This seemed surprising, especially since reductions of H_2dcbpy ligands in $[Ru^{II}(H_2dcbpy)_2phen](PF_6)_2$ (-1.4 V, -1.6 V) were clearly at less negative potentials than reductions of bpy ligands in $[Ru^{II}(bpy)_2phen](PF_6)_2$ (-1.8 V, -2.0 V). One possibility could be the presence of enough water in the DMF/0.1 M TBAH electrolyte to partially deprotonate the bound H_2dcbpy ligands, causing their reduction to shift in the cathodic direction.

Figure 48d shows barely visible oxidative waves for $[Ru^{II}(H_2dcbpy)_2pptd](PF_6)_2$. An estimation of the $E_{1/2}$ value puts the oxidation at around + 0.84 V, the same as for the previous Ru^{II} model complexes with 1,10-phenanthroline and/or 2,2'-bipyridine.

b) Aqueous Solution Electrochemistry

$[Ru^{II}(H_2dcbpy)_2pptd](PF_6)_2$ in pH 4.0 and pH 7.0 acetate buffers

The goal of these experiments was mainly to observe the effect of pH on the electrochemical behavior of the target complex $[Ru^{II}(H_2dcbpy)_2pptd](PF_6)_2$ in aqueous solution. Two sets of CVs were obtained; one in pH 4.0 acetate buffer and the other in pH 7.0 acetate buffer. Since reduction of bound pptd ligand has been shown to be pH-dependent (easier to reduce at lower pHs), it was expected that pptd-centered reductions for $[Ru^{II}(H_2dcbpy)_2pptd](PF_6)_2$ would be easier by approximately 0.178 V at pH 4.0 than at pH 7.0 (See Appendix A).

Both pH 4.0 and pH 7.0 acetate buffers were made according to the method described in the Experimental section. The basic configuration of the electrochemical cell was the same as that used for the non-aqueous solution experiments except that the reference electrode was a SSCE. As in the non-aqueous solution electrochemistry experiments, a CV of the pH 4.0 buffer was taken before and after bubbling with argon (Figures 49a and 49b) in order to locate any background signals from oxygen.

The CV's of $[Ru^{II}(H_2dcbpy)_2pptd](PF_6)_2$ in pH 4.0 acetate buffer are given in Figures 49c and 49d. Figure 49c shows a chemically reversible reduction wave that looks like two reductions close to each other ($E_{½}$ vs. SSCE of –0.50 V (Table 2). This wave can be assigned to the pptd ligand. Figure 49d shows the chemically reversible oxidation wave with a $E_{½}$ vs. SSCE of +1.16 V (Table 2).

The CV's of $[Ru^{II}(H_2dcbpy)_2pptd](PF_6)_2$ in pH 7.0 acetate buffer are given in Figures 50c-e. Figure 50a and 50b show the CVs of pH 7.0 acetate buffer before and after bubbling with Ar. Figure 50c and 50d show one reduction wave with an $E_{½}$ vs. SSCE of –0.67 V (Table 2). The metal-centered oxidation wave was not observed in pH 7.0 acetate buffer (Figure 50e).

It is evident from the CV's that the pptd-centered reduction of $[Ru^{II}(H_2dcbpy)_2pptd](PF_6)_2$ is indeed pH dependent. The reduction in pH 7.0 acetate buffer required a more negative potential (-0.67 V) than in pH 4.0 acetate buffer (-0.50 V). The difference in potential between pH 4.0 and pH 7.0 is 0.17 V which is very close to the predicted theoretical value of 0.178 V (Appendix A).

3) Surface electrochemistry: Cyclic Voltammetry of $[Ru^{II}(H_2dcbpy)_2pptd](PF_6)_2$ attached to a TiO_2 coated conducting glass (ITO) electrode.

The first major goal of these experiments was to see if the $[Ru^{II}(H_2dcbpy)_2pptd](PF_6)_2$ complex actually absorbed on to a TiO_2-coated glass (ITO) electrode. The second major goal was to observe the electrochemical activity of the modified glass electrode in aqueous buffer solutions. It was expected that the bound pptd ligand would show pH-dependent behavior similar to that observed in solution experiments. The range of pH values that could be used to test this expectation was thought to be limited since, according to Grätzel et al.[11], the carboxy-ester linkage between the TiO_2 and the dcbpy ligand of the ruthenium complex would only be stable at $pH \leq 4.5$. A buffer solution of $pH > 4.5$ would apparently result in the breakage of the linkage between the dye and the TiO_2 surface.

The making and coating of the TiO_2 electrode is described in Experimental sections 2.9 and 2.10. The thickness of the TiO_2 coating on the glass electrode was controlled by using scotch tape as described in the Experimental section. According to the literature[12], this was supposed to give fairly reproducible and uniform coatings approximately 12 μm thick. The actual coatings, however, did not seem that uniform, with some electrodes having a very thick coating while other electrodes were transparent. After the TiO_2 electrodes had been heated they were stored in a dessicator in order to prevent water absorption.

Coating of the TiO_2-coated glass electrodes with the dye ($[Ru^{II}(H_2dcbpy)_2pptd](PF_6)_2$) was fairly challenging because the dye was only partially soluble in ethanol. Absolute ethanol was used as the solvent to dissolve the dye because it was usually the solvent of choice in the literature.[12] To ensure maximum solubility of the dye in ethanol, the dye was allowed to sit in the ethanol for a day. Once the ethanol solution was colored orange, the TiO_2-coated electrode was soaked until the dye was absorbed on to the TiO_2. The coating of the dye also depended on how thick the TiO_2 layer was on the glass electrode. If the coating was fairly thick, it took a longer time to coat it completely and the coloration was intense. On the other hand, if the coating was transparent, the dye coating process was much faster and the color was less intense. The figure below illustrates this idea.

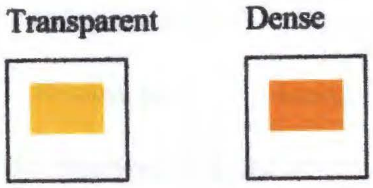

Figure 51: TiO_2-coated glass electrodes

a) CV experiments of bare TiO_2-coated electrodes in pH 3.5 and pH 4.0 acetate buffers

Cyclic voltammetry experiments on the bare TiO_2-coated glass electrode were done in order to identify any background signals from the TiO_2 that would overlap with signals from the bound ruthenium complex. As with solution electrochemistry, CVs of pH 3.5 and pH 4.0 acetate buffer solutions were taken before and after bubbling with Ar (Figures 52a-b and 53a-b). It is evident from Figures 52 and 53 that the bare TiO_2 coated electrode is electroactive. In fact the signals seen in Figures 52a-b and 53a-b are typical of bare TiO_2 coated electrodes. According to Durrant et. al.[13] the cathodic current that is observed when scanning negatively is due to the reduction of trap and/or conduction band states of the TiO_2 film. The reverse scan results in a more pronounced peak-shape signal that is due to oxidation (unfilling) of the trap/conduction band states of the TiO_2 film. Durrant et. al.[13] also note that the current doesn't start to increase until about -0.3 V, which is also true of the signals seen in Figures 52 and 53. Therefore, the electrodes used in these experiments with the ruthenium complex appear to be acting normally.

b) CV experiments of Ru-TiO_2 coated TiO_2 electrodes in pH 3.5 and pH 4.0 acetate buffers

The TiO_2 electrodes with adsorbed $[Ru^{II}(H_2dcbpy)_2(pptd)]^{2+}$ (Ru-TiO_2 electrodes) were used directly in the electrochemistry experiments. The buffer solution was bubbled with Ar for approximately 15-20 minutes prior to placing the Ru-TiO_2 electrode in solution. The Ru-TiO_2 electrode was removed from the ethanol/Ru-complex solution, air dried for a few minutes and then placed directly in the buffer solution. Figure 52c shows the CV in pH 3.5 acetate buffer. The background reverse wave from TiO_2 is still present at approximately –0.35 V along with the forward and reverse reduction waves from the attached $[Ru^{II}(H_2dcbpy)_2pptd](PF_6)_2$ complex, at approximately –0.6 V. One thing to notice from Figure 52c compared to the solution electrochemistry CVs is that the reverse wave is exactly on top of the forward wave. This was the expected behavior for the surface electrochemistry experiments. From a theoretical point of view, it is expected that the forward wave and the reverse wave would be exactly on top of each other since the diffusion layer is no longer present. The reason why this diffusion layer is not present is because the $[Ru^{II}(H_2dcbpy)_2pptd](PF_6)_2$ is actually attached to the electrode surface, hence when the potential is at the correct voltage, the $[Ru^{II}(H_2dcbpy)_2pptd](PF_6)_2$ molecules are reduced. When the potential is reversed, the reduced $[Ru^{II}(H_2dcbpy)_2pptd](PF_6)_2$ molecules which are still attached to the electrode are oxidized. This process does not involve any movement of $[Ru^{II}(H_2dcbpy)_2pptd](PF_6)_2$ molecules through a diffusion layer, which is why there is no separation on the x-axis between reduction and oxidation potentials.

It is instructive to compare the $E_{1/2}$ value for the reduction of $[Ru^{II}(H_2dcbpy)_2pptd](PF_6)_2$ in solution with pH 4.0 acetate buffer (Figure 49c) with that of the "$E_{1/2}$" value of the sample complex adsorbed on to the TiO_2-coated electrode in pH 3.5 acetate buffer (Figure 52c). In solution at pH 4.0, $E_{1/2}$ = -0.50 V (ΔE_p = 132 mV) while the adsorbed complex at pH 3.5 showed $E_{1/2}$ = -0.61 V (Table 3, $\Delta E_p \cong 0$). The apparent problem with this is that the reduction became harder at the lower pH. This could be explained by assuming that the immediate environment of the bound complex is not identical to that of the complex in solution. Alternately, one could conjecture that reduction of the complex adsorbed on TiO_2 is not centered on the pptd ligand. There are no compelling reasons to conclude this, but it can not be ruled out with the data available.

Ignoring the conventional wisdom of never repeating an apparently successful experiment, a second set of CV experiments of the Ru-TiO_2 electrodes were done in pH 4.0 acetate buffer. The pH 4.0 acetate buffer solution was bubbled with Ar in order to remove as much oxygen as possible before placing the coated electrode in it. The CV of $[Ru^{II}(H_2dcbpy)_2pptd](PF_6)_2$ dye attached to TiO_2 coated glass electrode in pH 4.0 acetate buffer is shown in Figure 53c. It was expected that Figure 53c would be virtually identical to 52c considering the small difference in pH. When the two figures are compared, it is evident that the forward reduction wave is around –0.60 V in both scans. Also, both figures show two reverse waves. The similarities end there. The differences can be summarized:

Figure 52c (pH 3.5)	Figure 53c (pH 4.0)
One of the reverse waves is at the same potential of the reverse wave of the bare electrode (Figure 52b)	Neither reverse wave is at the same potential of the reverse wave of the bare electrode (Figure 53b)
Both reverse waves show current levels significantly reduced compared to the reverse wave of the bare electrode (Figure 52b)	Both reverse waves show current levels somewhat reduced compared to the reverse wave of the bare electrode (Figure 53b)

A possible explanation for the position of one of the reverse waves in Figure 53c (~ -0.4 V) could be that the Ru-complex desorbed after reduction at –0.6 V. Reoxidation of solution Ru-complex at pH 4.0 was previously measured to be ≈ -0.44 V (Figure 49c). However, this would not explain the cathodic shift of the other reverse wave from ≈ -0.6 V in Figure 52c to ~ -0.75 V in Figure 53c

The initial goal of performing electrochemistry experiments using the synthesized target ruthenium complex $[Ru^{II}(H_2dcbpy)_2pptd](PF_6)_2$ was to observe pH-dependent electrochemical activity. Based on the experiments performed, this goal was achieved. In addition, the pH-dependent behavior conformed to expectations based on earlier work with RuII-pptd complexes.

The second goal of attaching the $[Ru^{II}(H_2dcbpy)_2pptd](PF_6)_2$ complex onto a TiO_2 coated glass electrode was also accomplished. Also, the adsorbed complex-electrode assembly appears to show some electrochemical activity when exposed to aqueous buffers.

4) FUTURE DIRECTIONS

Due to the lack of time, a more comprehensive characterization of the Ru-TiO_2 electrode was not possible. Hence, any future work on this project should begin with reattaching the $[Ru^{II}(H_2dcbpy)_2pptd](PF_6)_2$ on to a TiO_2 coated glass electrode and conducting electrochemical experiments. The electrochemical experiments should be conducted at more tightly controlled pH values between 2.5 and 3.5 since the carboxy-ester linkage may be susceptible to breakage beyond this pH range.

Also, since the initial difficulty with this project was the actual synthesis of the target complex, it might be wise to move away from the synthesis of the dicarboxy ruthenium complex and maybe use another ligand for attachment to the TiO_2 coated electrodes.

References

[1] Nelissen, H.F.M.; Feiters, M.C.; Nolte, R.J.M. *J. Org. Chem.* **2002**, *67*, 5901-5906.

[2] Yanagida, M.; Singh, L. P.; Sayama, K.; Hara, K.; Katoh, R.; Islam, A.; Sugihara, H.; Arakawa, H.; Nazeeruddin, M. K.; Grätzel, M. *J. Chem. Soc., Dalton, Trans.* **2000**, 2817-2822.

[3] http://www.sigmaaldrich.com/cgi (08/2003)

[4] Nazeeruddin, M.K.; Kalyanasundaram, K. *Inorg. Chem.* **1989**, *28*, 4251-4259.

[5] Liska, P.; Vlachopoulos, N.; Nazeeruddin, M. K.; Comte, P; Grätzel, M. *J. Am. Chem. Soc.* **1988**, *110*, 3686-3687.

[6] Pavinato, R. M.S. Thesis, Eastern Illinois University, 1994.

[7] Wolfbauer, G.; Bond, A. M.; MacFarlane, D. R. *Inorg. Chem* **1999,** *38*, 3836-3846.

[8] Patterson, B. T.; Keene, R. F. *Aust. J. Chem.* **1998**, *51,* 999-1002.

[9] Black, K. J.; Huang, H.; High, S.; Starks, L.; Olson, M.; McGuire, M.E. *Inorg. Chem.* **1993**, *32*, 5591-5596.

[10] Evans, D. H.; O'Connell, K. M.; Petersen, R. A.; Kelly, M. J *J. Chem. Ed.*, **1993,** *60*, 290-292.

[11] Kalyanasundaram, K.; Grätzel, M. *Coord. Chem. Rev.*, **1998**, *77*, 347-414.

[12] Nazeeruddin, M.K.; Kay, A.; Rodicio, I.; Humphrey-Baker, R.; Mueller E.; Liska, P.; Vaichopoulos, N.; Gratzel, M. *J. Am. Chem. Soc.* **1993**, *115*, 6382-6390.

[13] Topoglidis, E.; Campbell, C. J.; Cass, A. E. G.; Durrant, J. R. *Langmuir*, **2001**, *17*, 7899-7906.

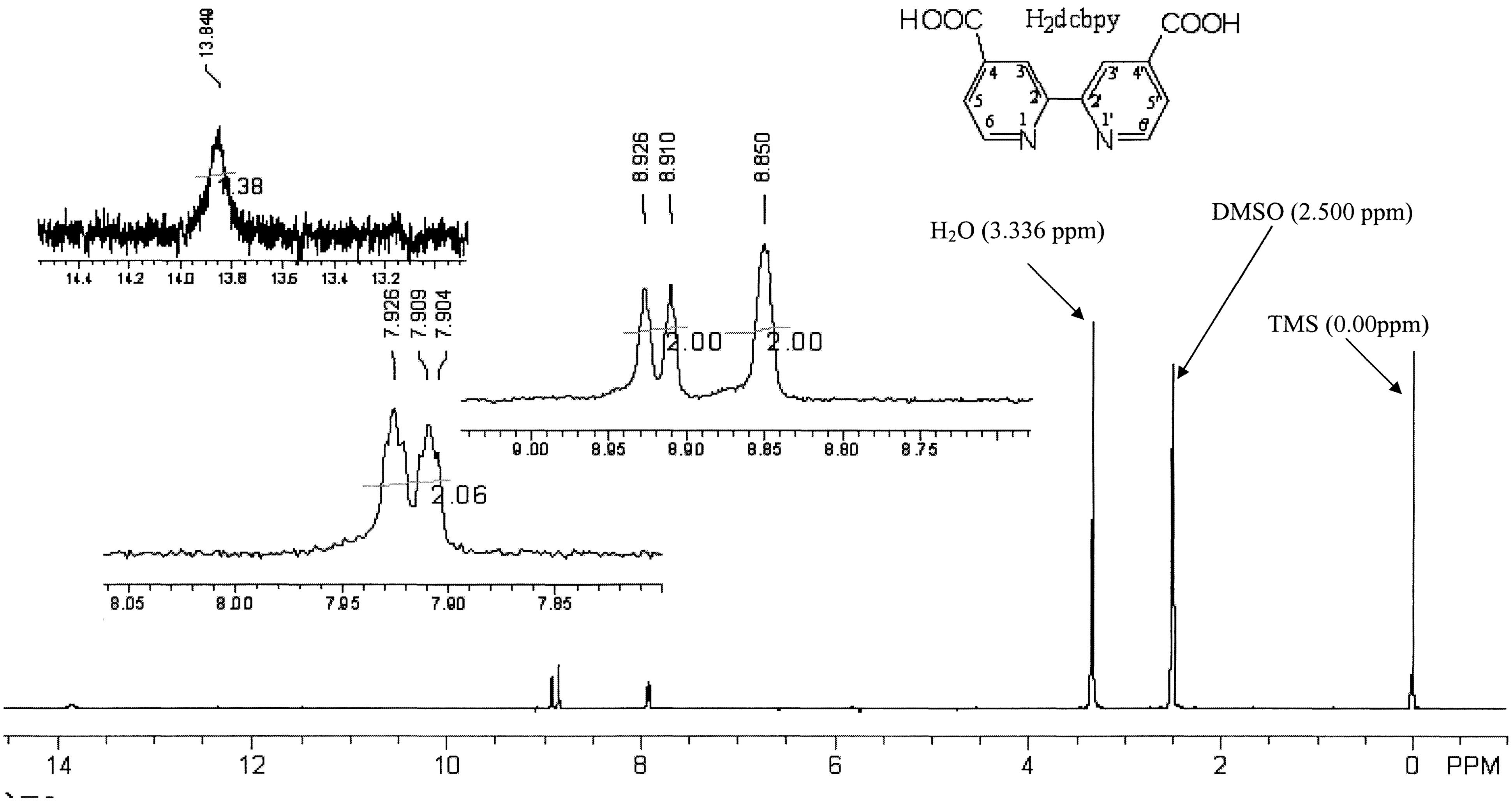

Figure 14a: ^{1}H-NMR of 2,2'-bipyridine-4,4'-dicarboxylic acid in d_6-DMSO

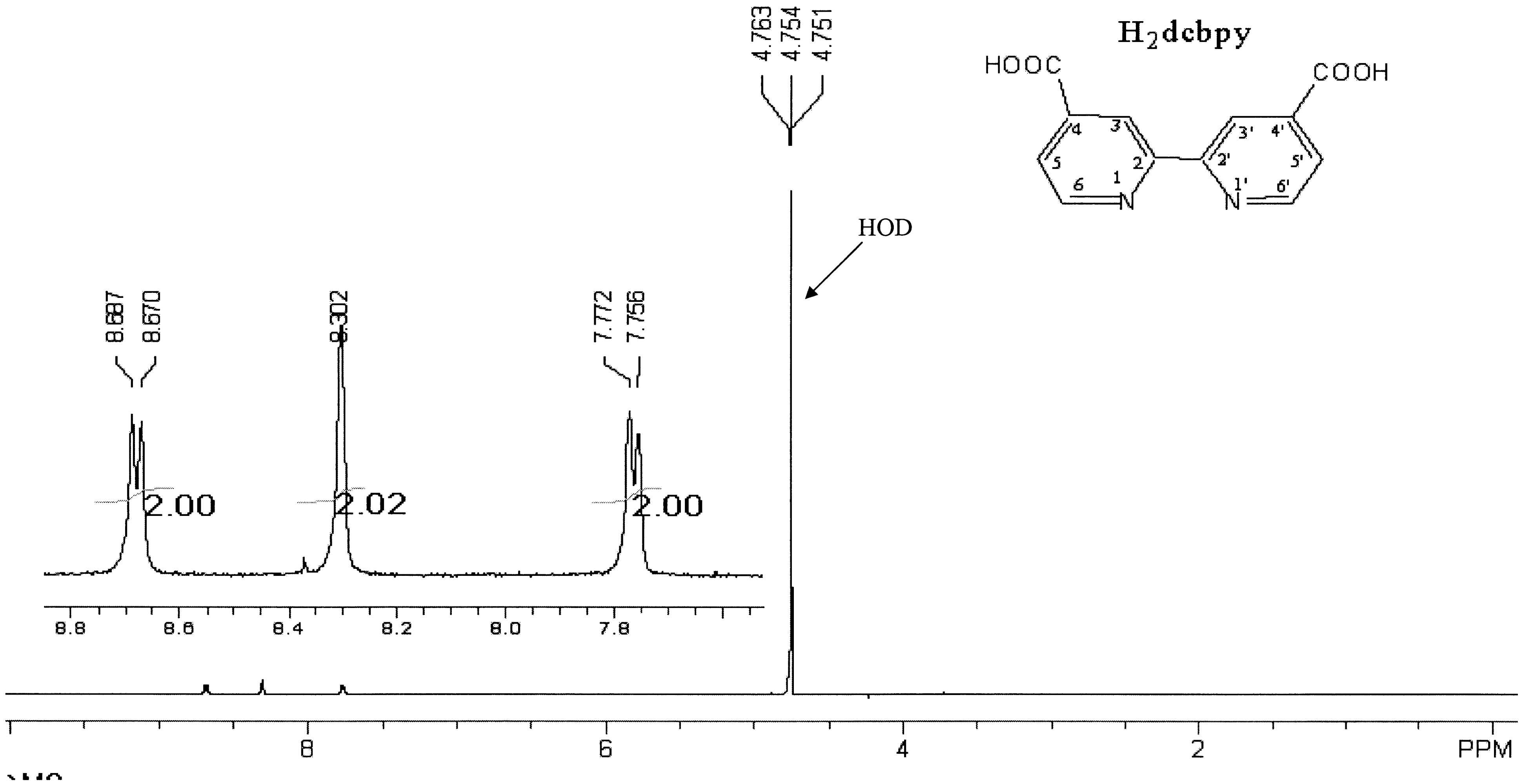

Figure 14b: ^{1}H-NMR of 2,2’-bipyridine-4,4’-dicarboxylic acid in 0.01 M NaOD/D$_2$O

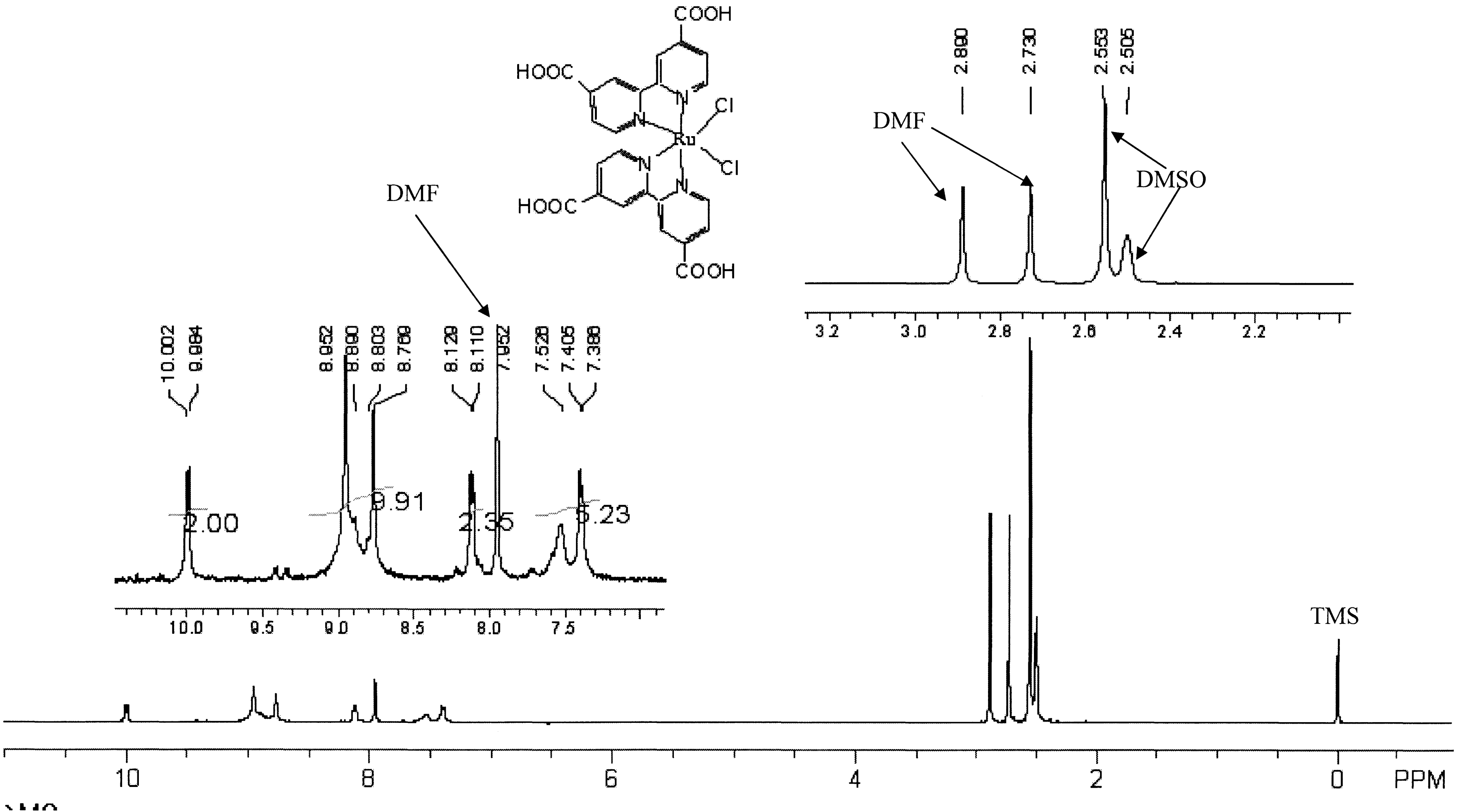

Figure 15: ^{1}H-NMR of Ru^{II}(H$_2$dcbpy)$_2$Cl$_2$ (020102-A) in d$_6$-DMSO

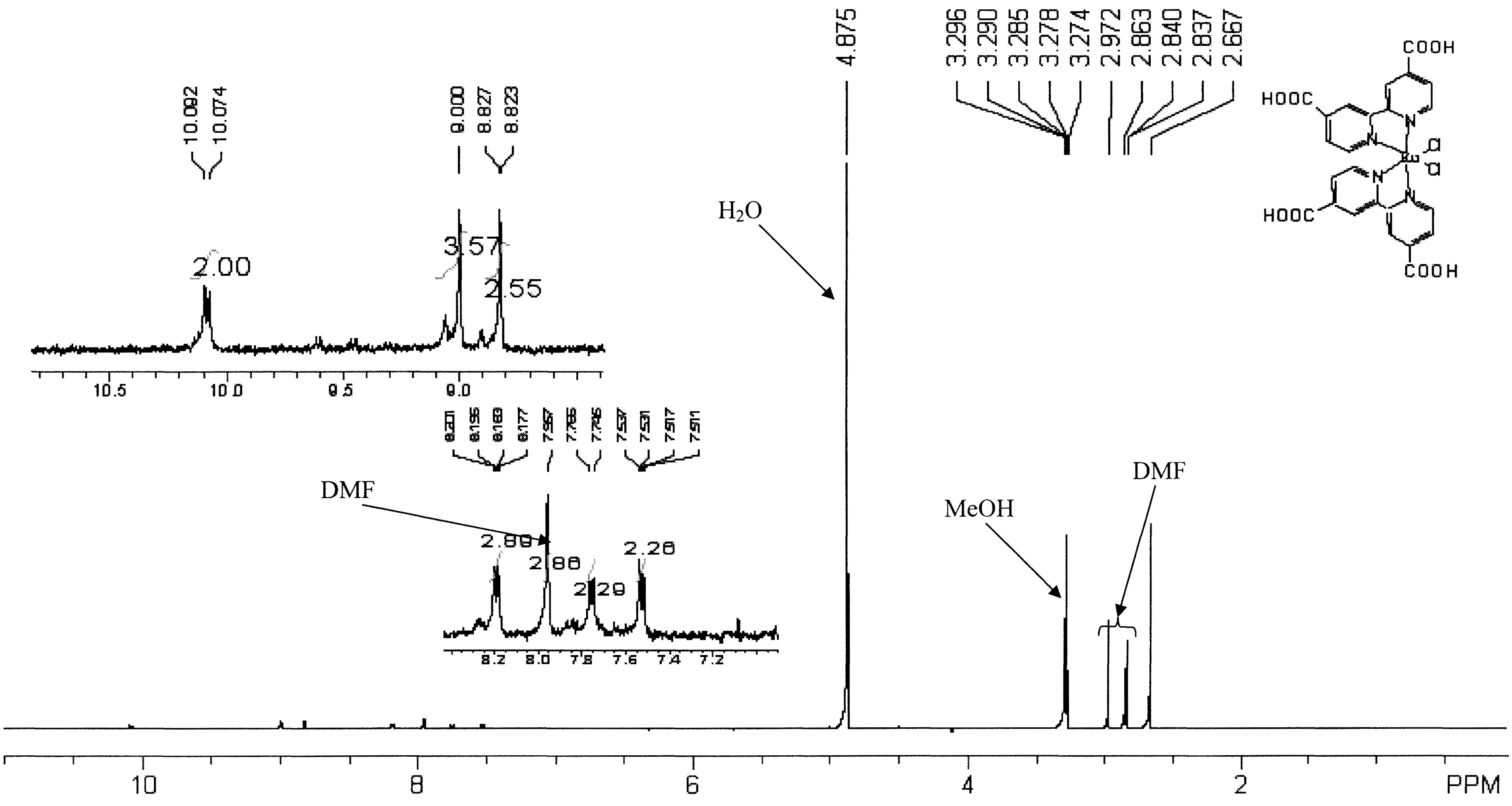

Figure 16: ^{1}H-NMR of Ru(H_2dcbpy)$_2$$Cl_2$ (020102-A) in d_4-MeOH

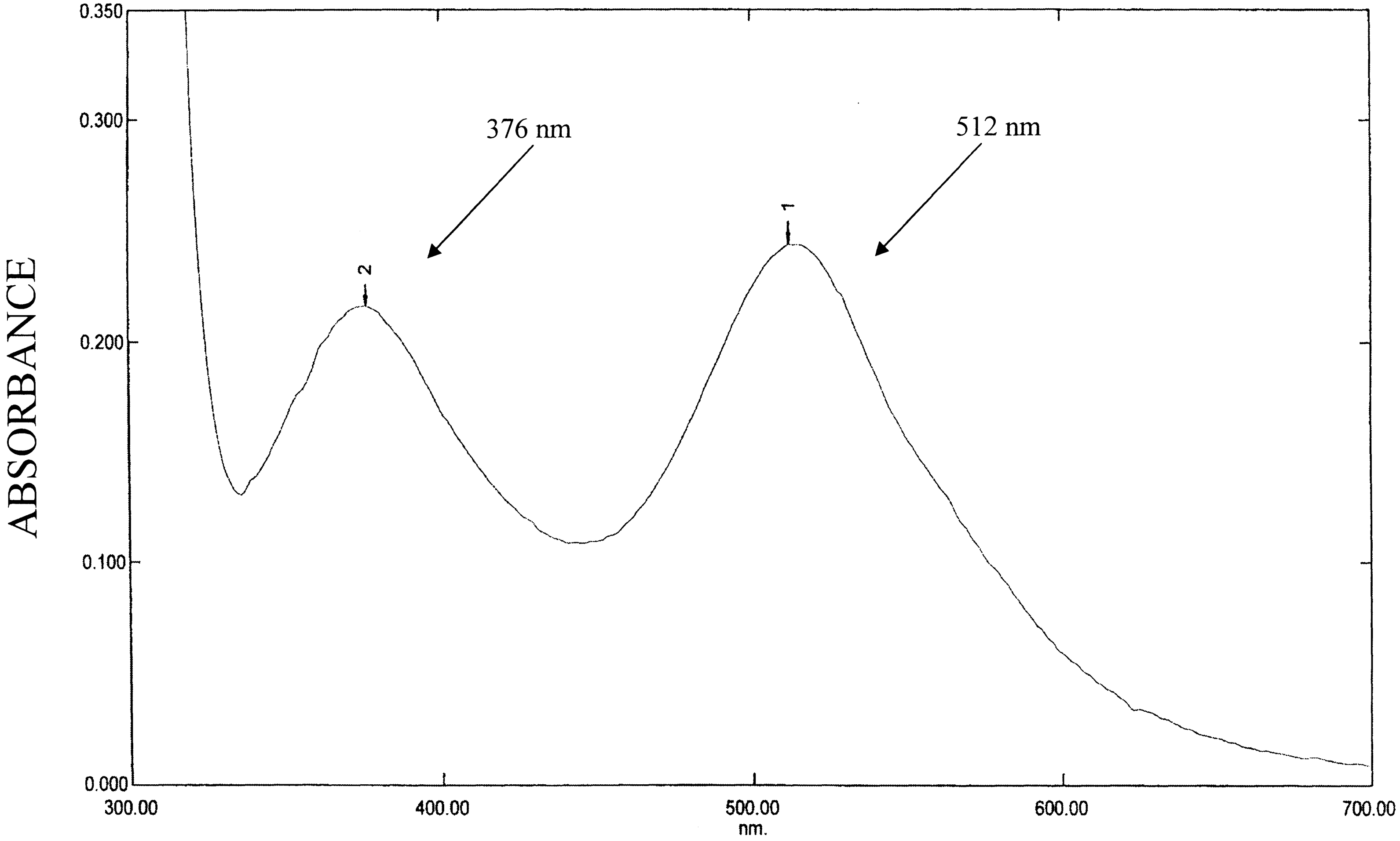

Figure 17: UV-Vis of $Ru(H_2dcbpy)_2Cl_2$ (021802-F) in pH 4.9 phthalate buffer

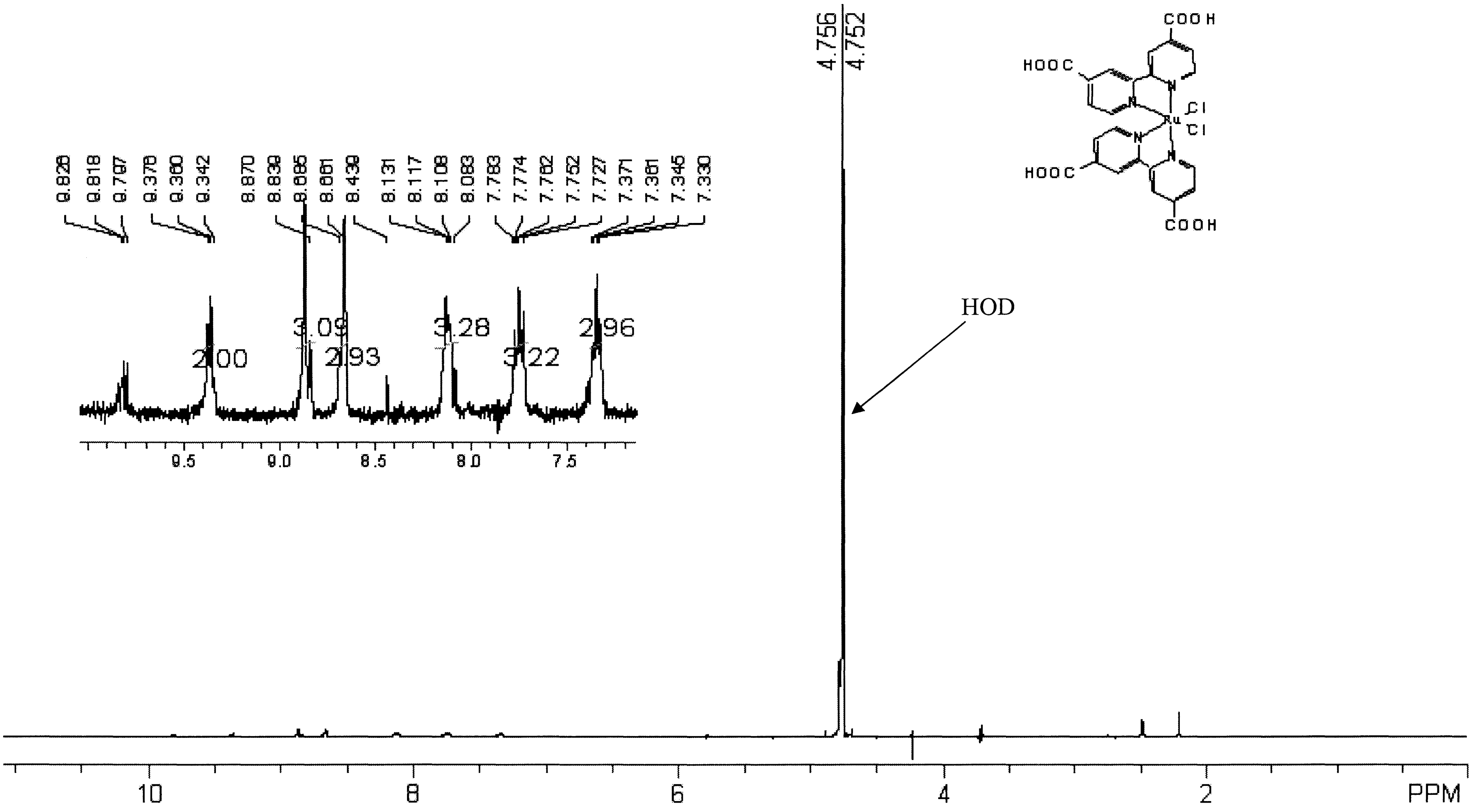

Figure 18: ^{1}H-NMR of Ru^{II}(H_2dcbpy)$_2$$Cl_2$ in 0.01 M NaOD/D_2O

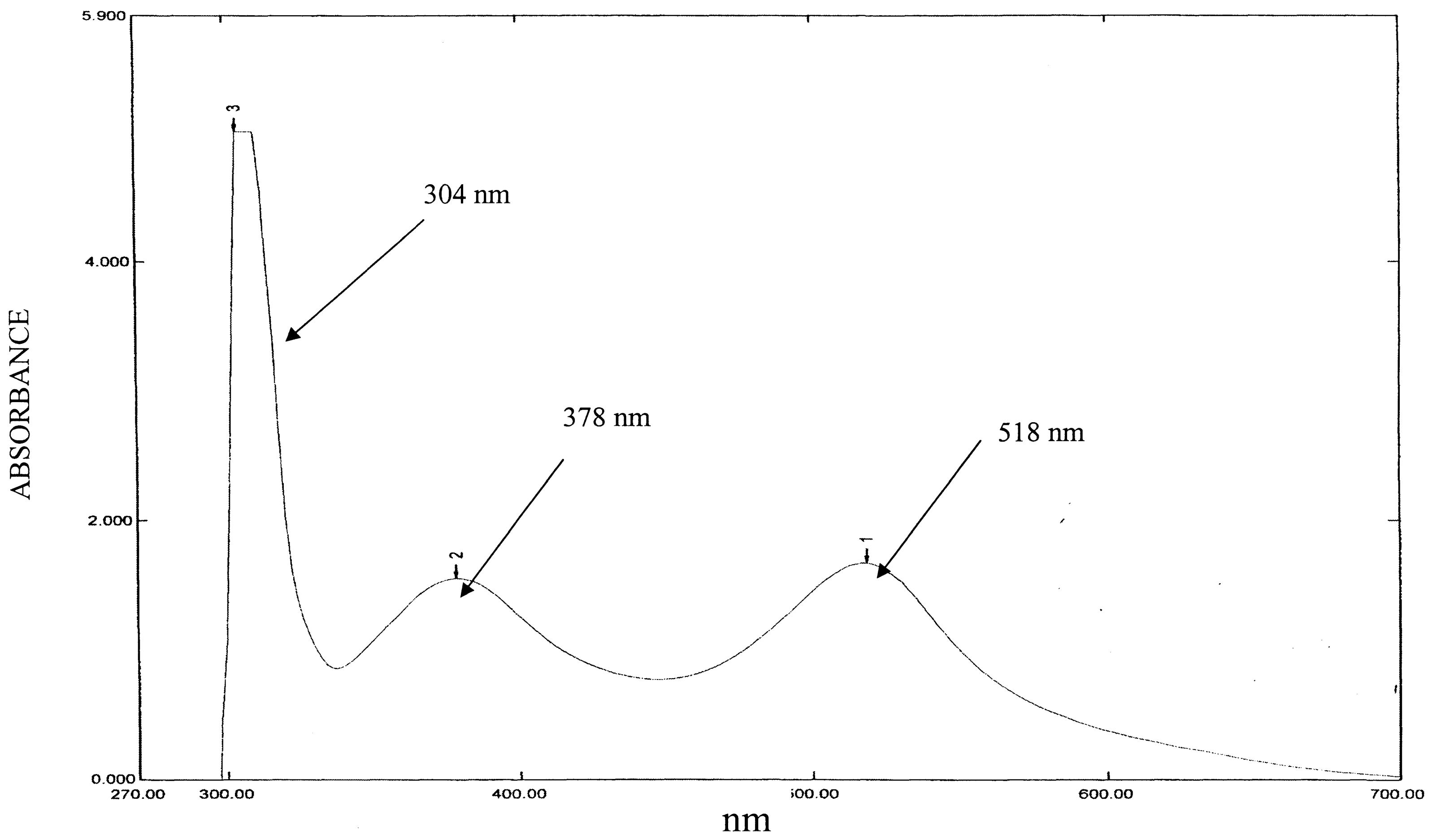

Figure 19: UV-Vis of $Ru^{II}(H_2dcbpy)_2Cl_2$ (062702-B) in 4.8 phthalate buffer

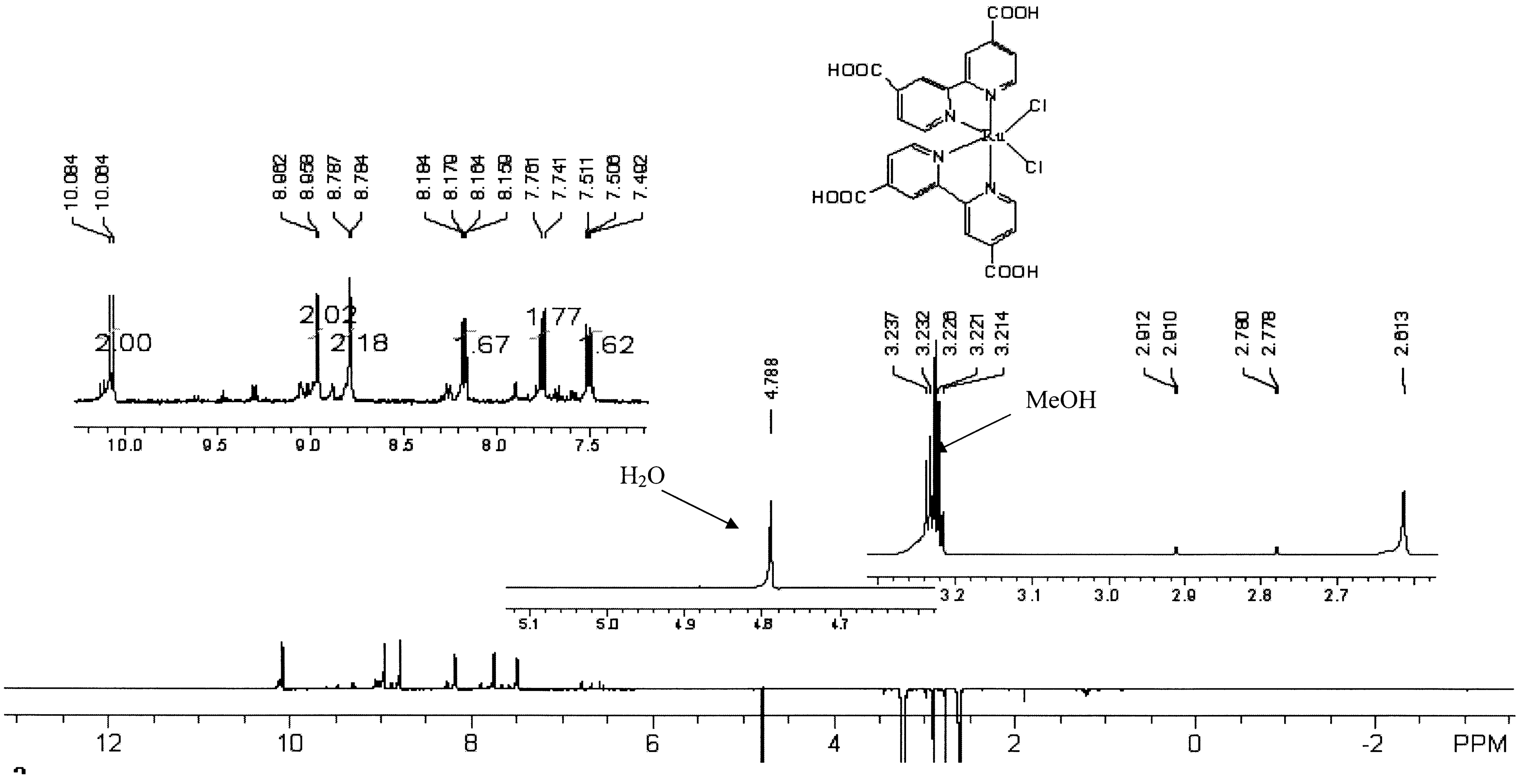

Figure 20: ^{1}H-NMR of Ru^{II}(H$_2$dcbpy)$_2$Cl$_2$ in d$_4$-MeOH with H$_2$O solvent suppression

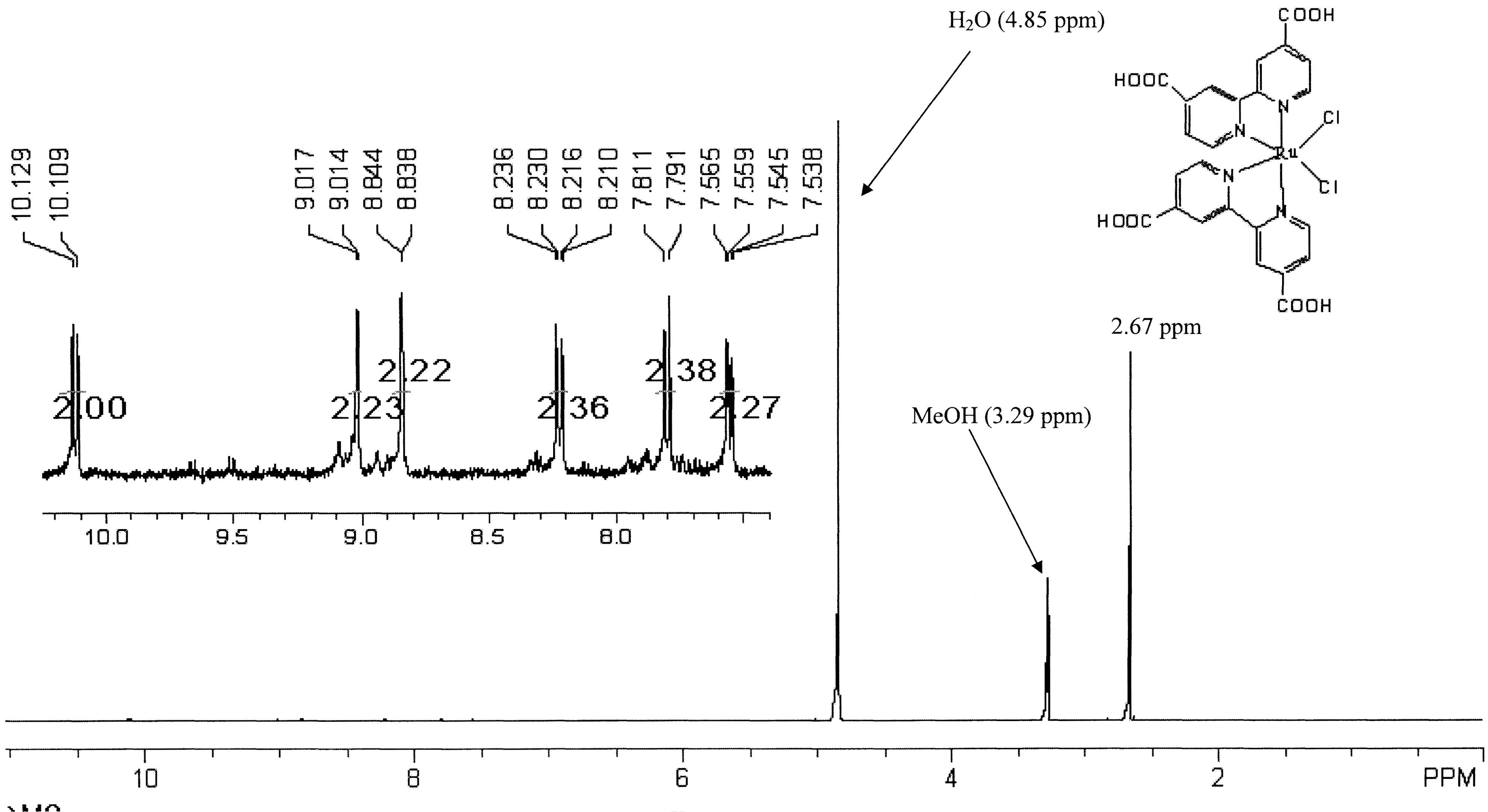

Figure 21: ^{1}H-NMR of Ru^{II}(H$_2$dcbpy)$_2$Cl$_2$ (071602-B) d$_4$-MeOH

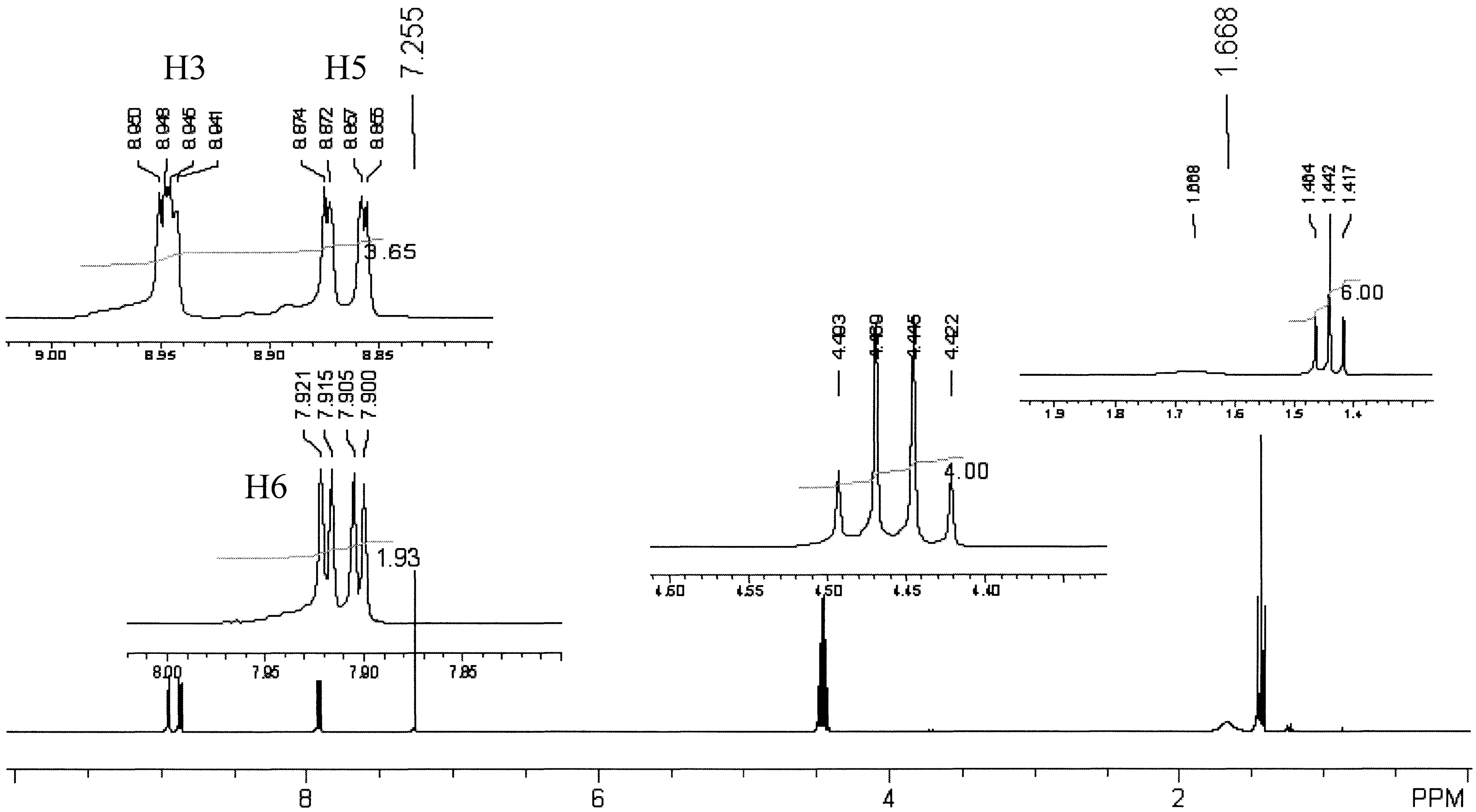

Figure 22: ^{1}H-NMR of Et_2dcbpy in $CDCl_3$

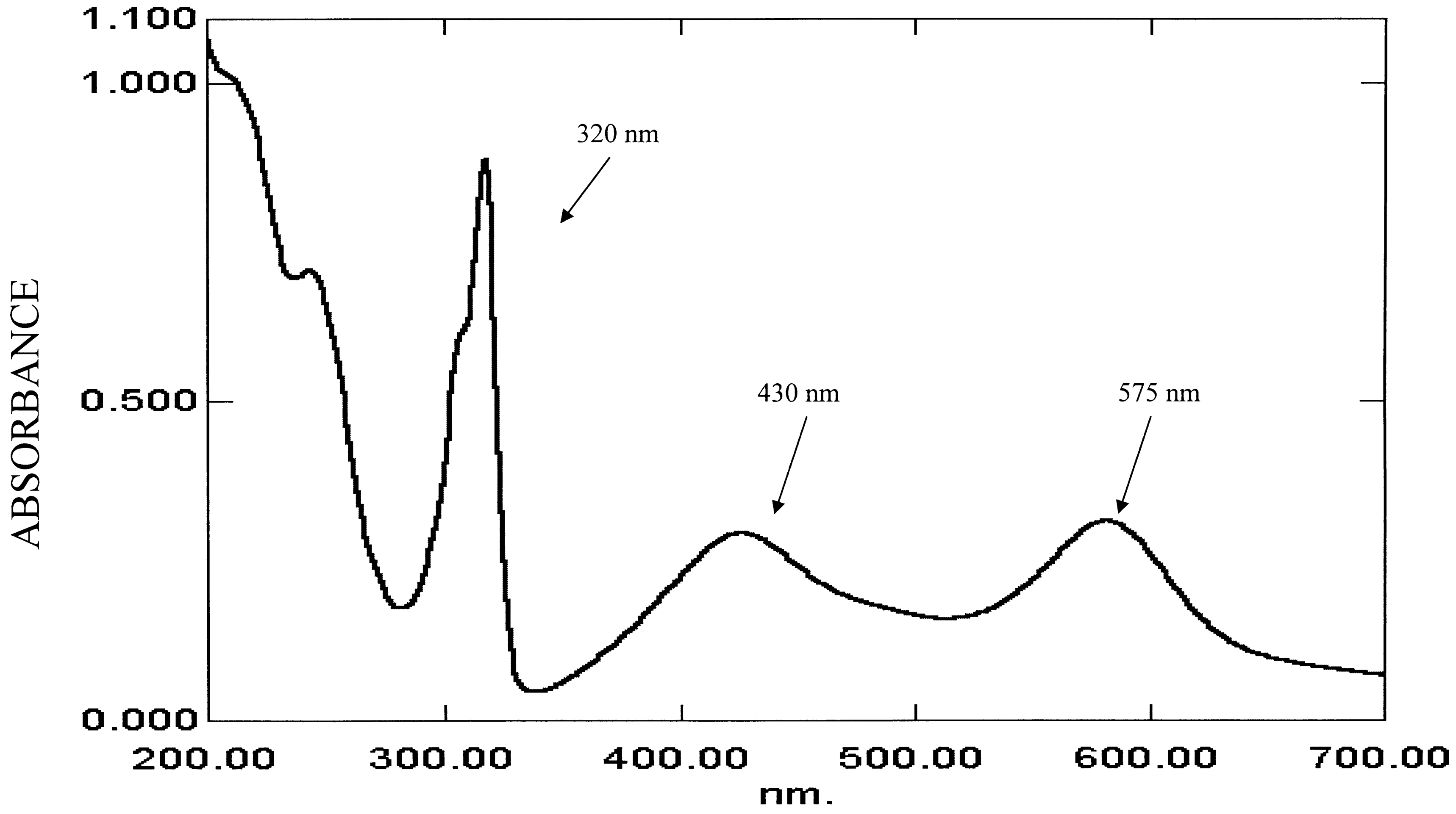

Figure 23: UV-Vis of $Ru^{II}(Et_2dcbpy)_2Cl_2$ in CH_3CN

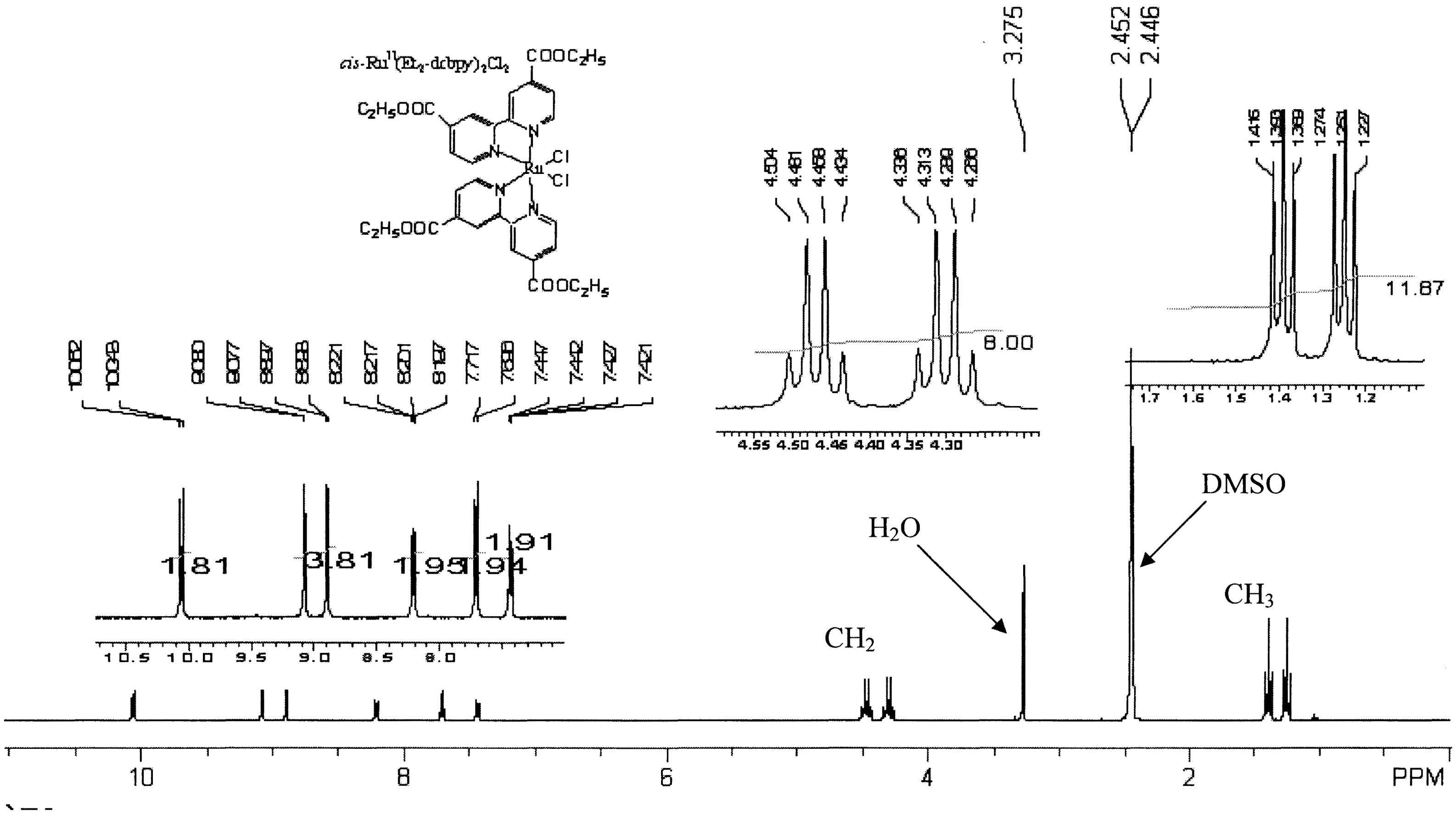

Figure 24: ^{1}H-NMR of $Ru^{II}(Et_2dcbpy)_2Cl_2$ in d_6-DMSO

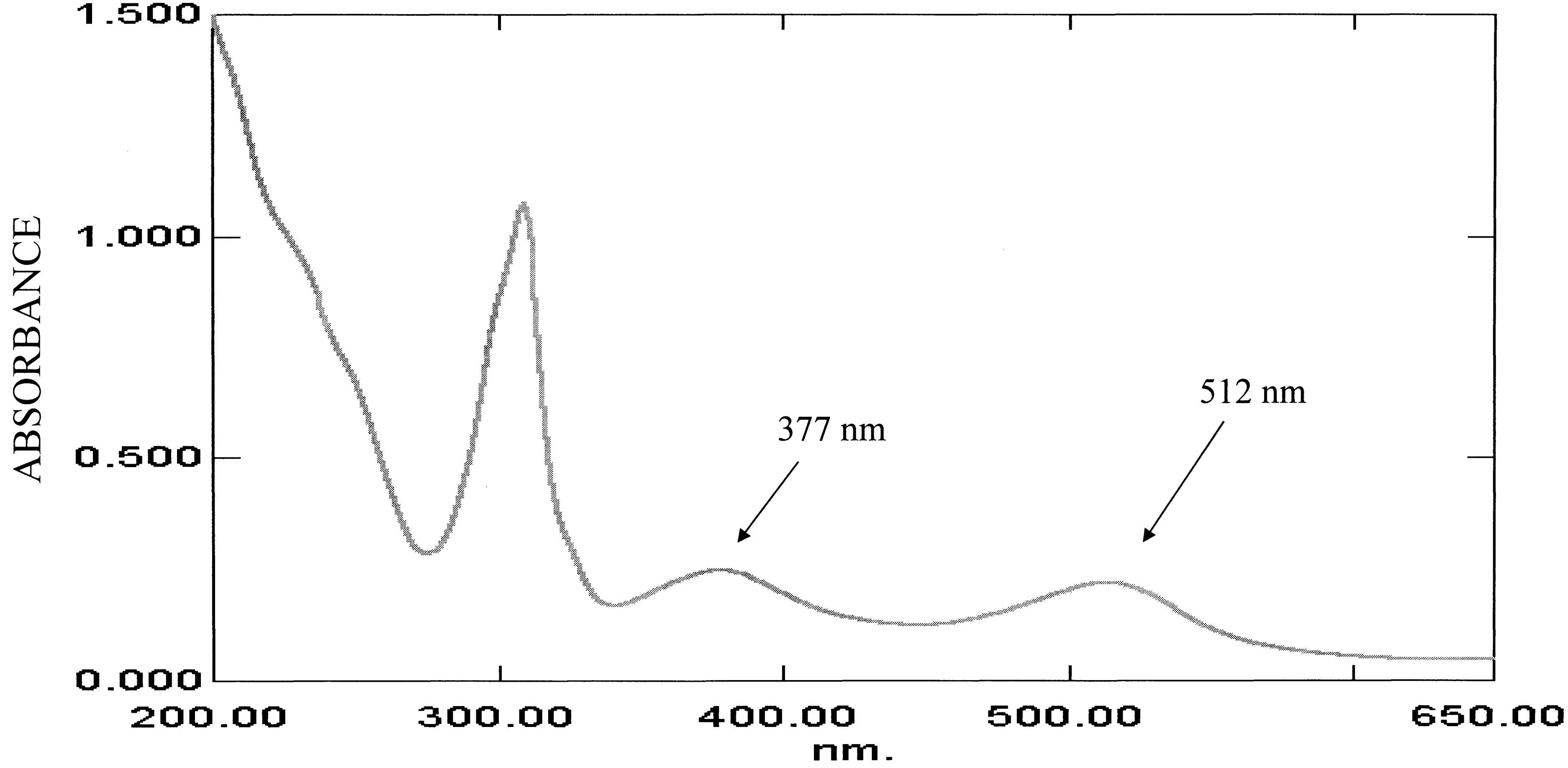

Figure 25: UV-Vis of $Ru^{II}(H_2dcbpy)_2Cl_2$ in pH 5.0 phosphate buffer

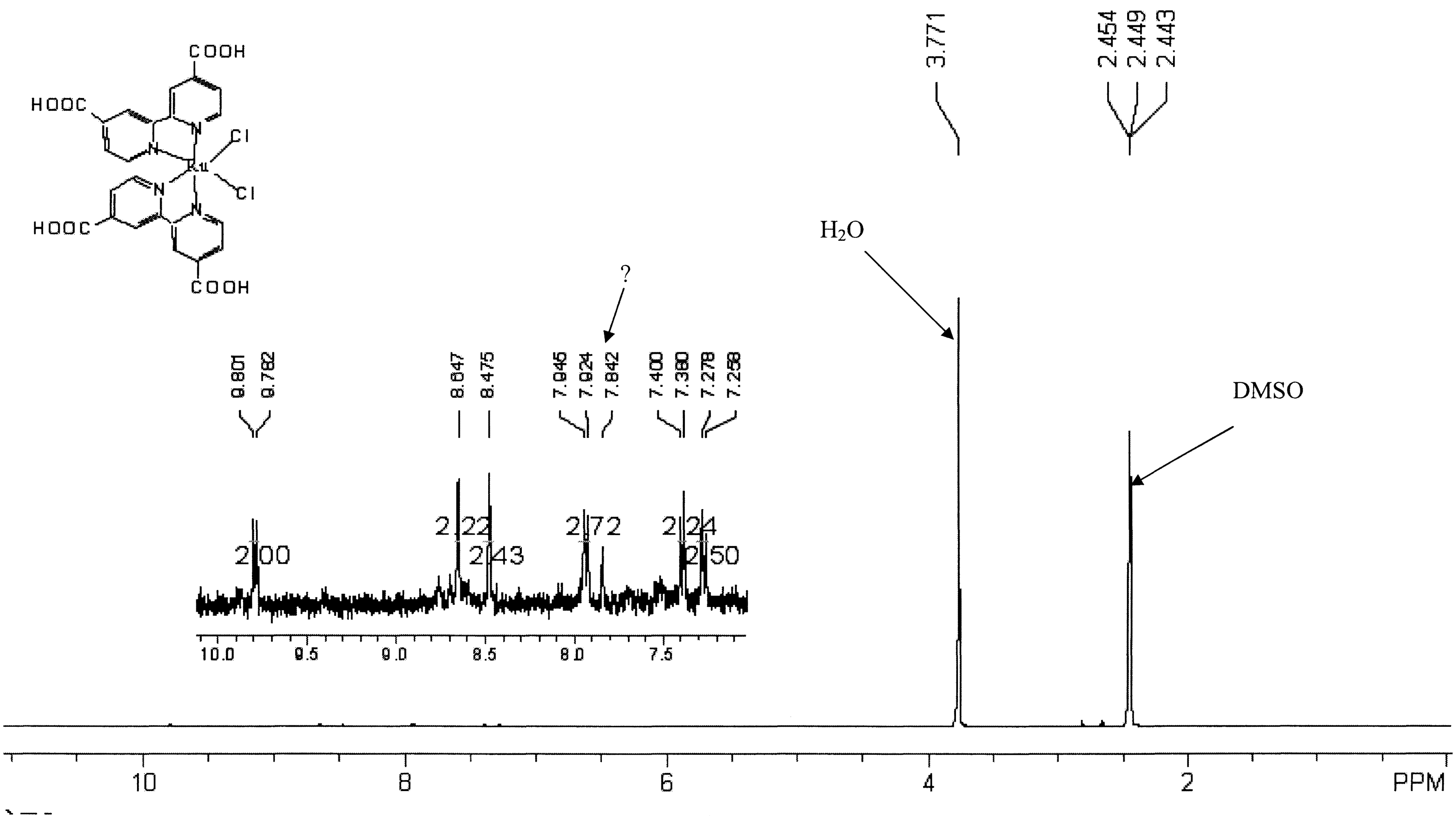

Figure 26: ^{1}H-NMR of $Ru^{II}(H_2dcbpy)_2Cl_2$ in d_6-DMSO

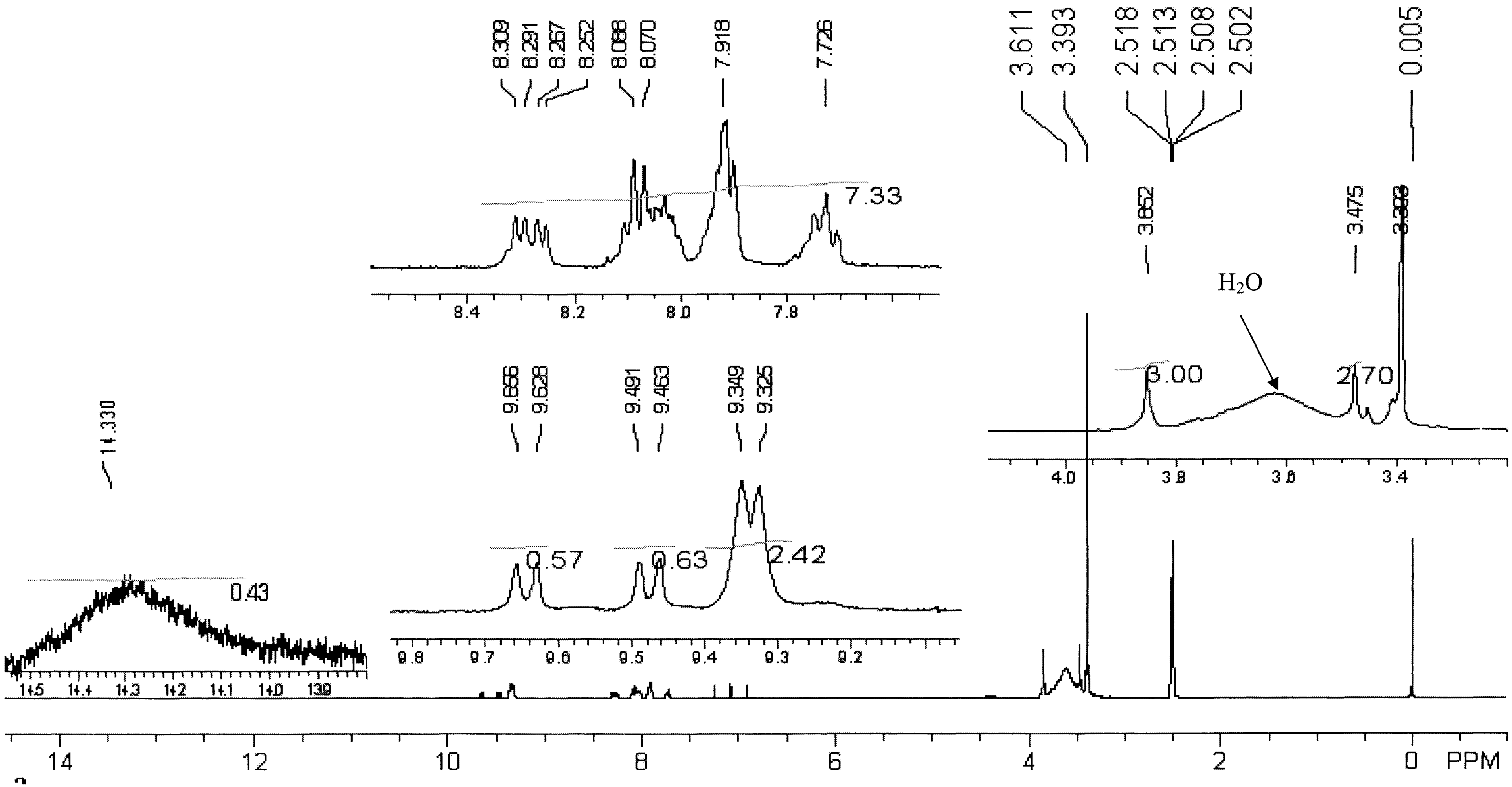

Figure 27: ^{1}H-NMR of $[Ru^{II}(H_2dcbpy)_2pptd](PF_6)_2$ in d_6-DMSO

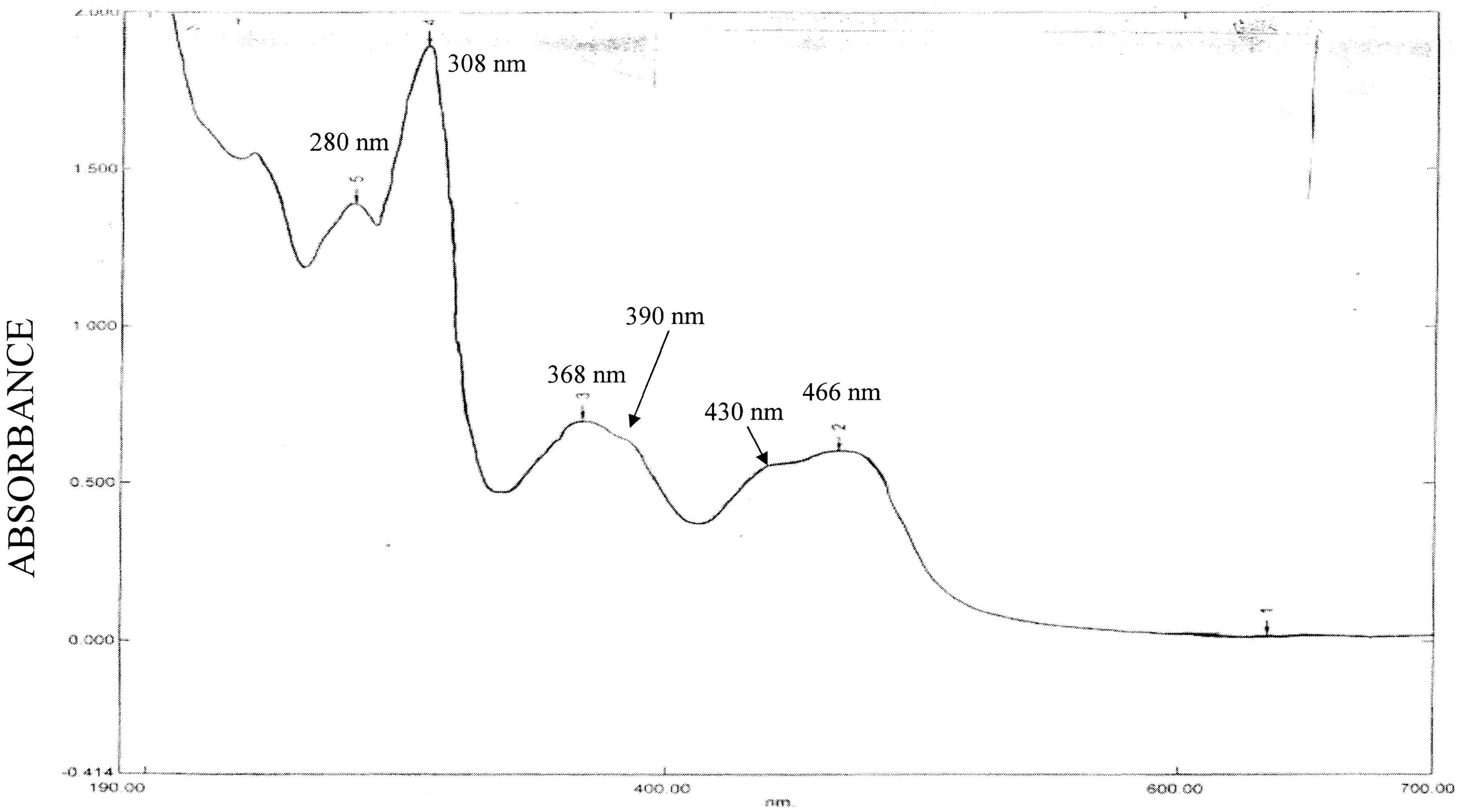

Figure 28: UV-Vis of $[Ru^{II}(H_2dcbpy)_2pptd](PF_6)_2$ in CH_3CN

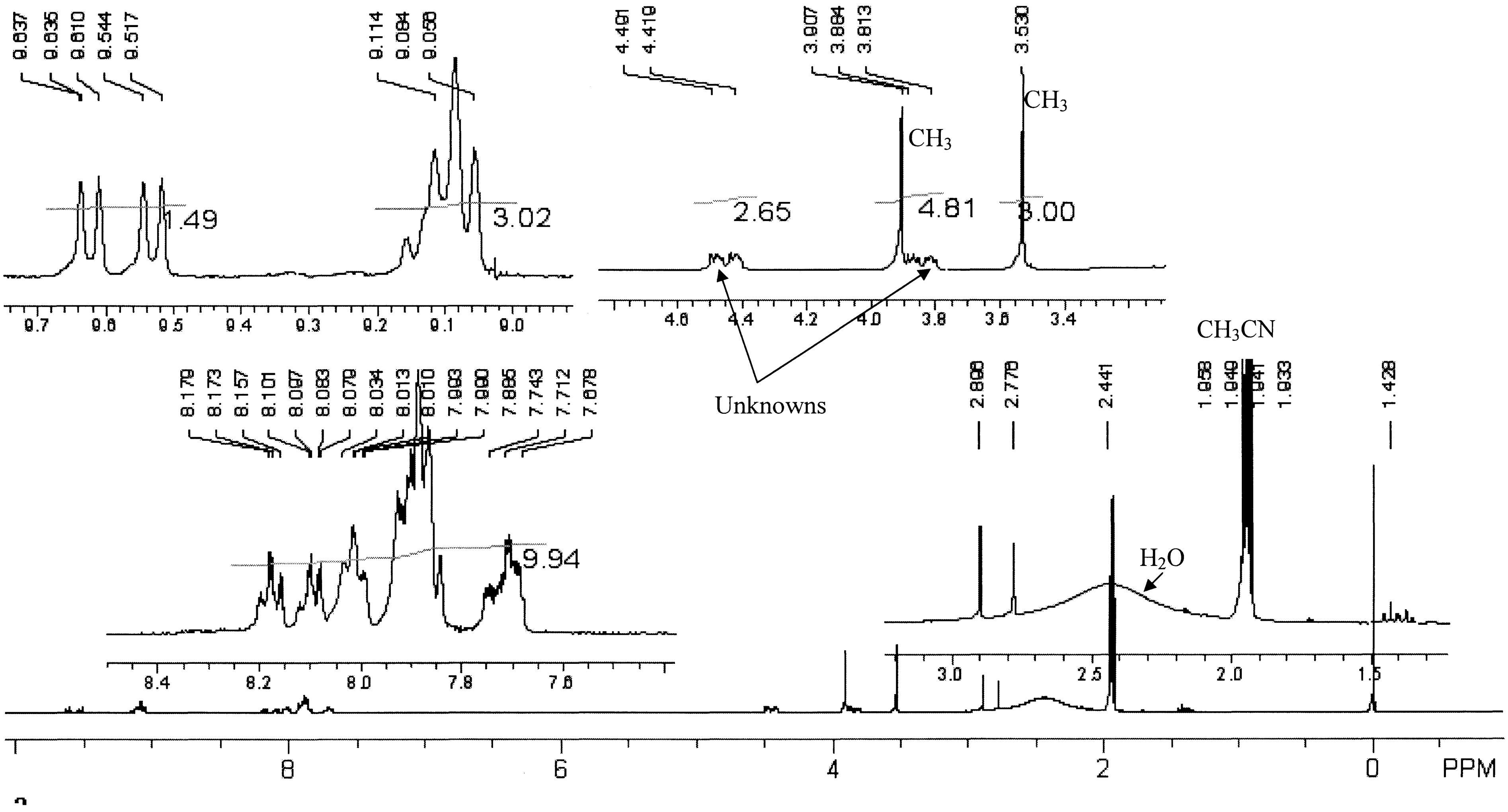

Figure 29: ^{1}H-NMR of $[Ru^{II}(H_2dcbpy)_2pptd](PF_6)_2$ in CD_3CN

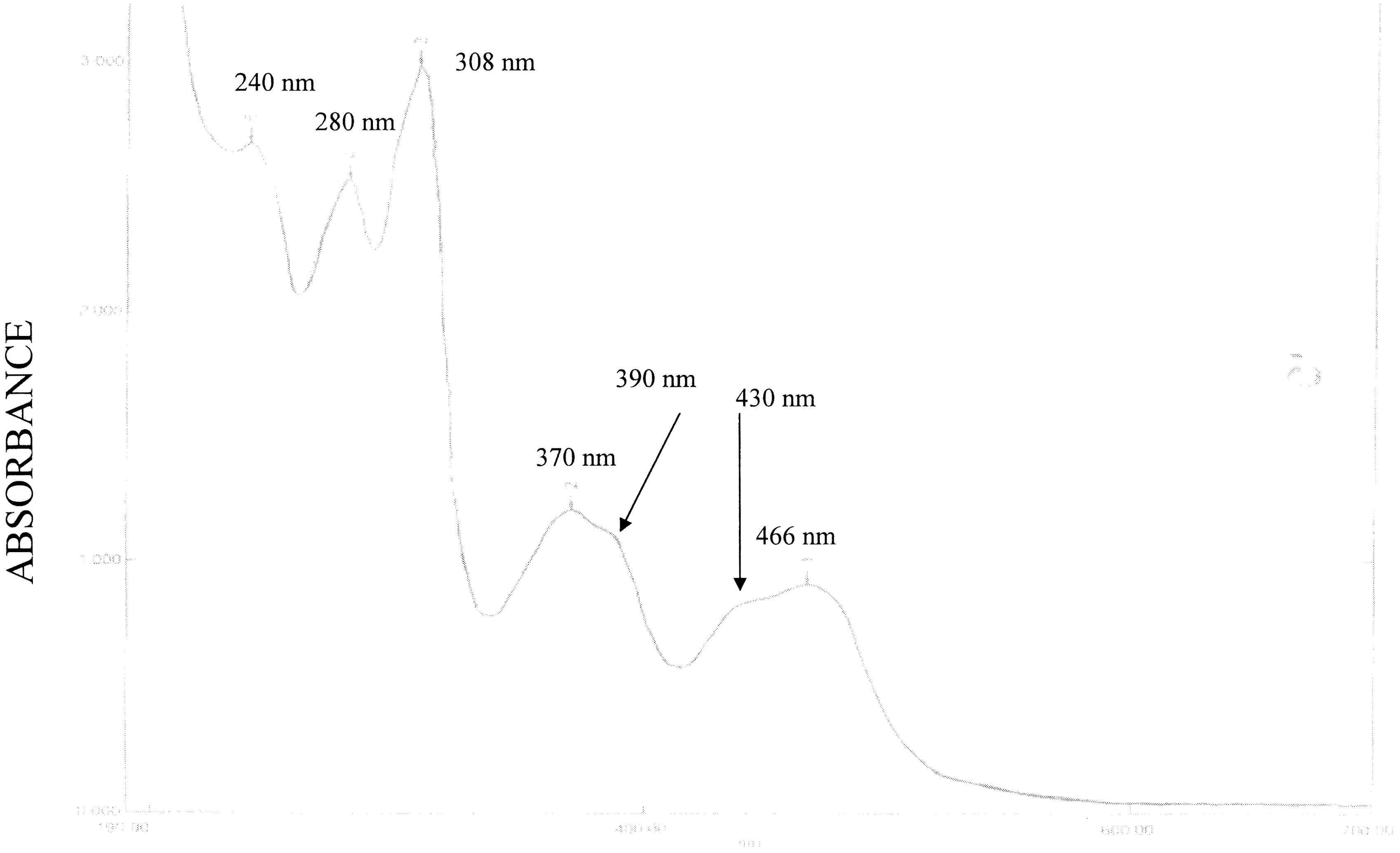

Figure 30: UV-Vis of $[Ru^{II}(H_2dcbpy)_2pptd](PF_6)_2$ in CH_3CN

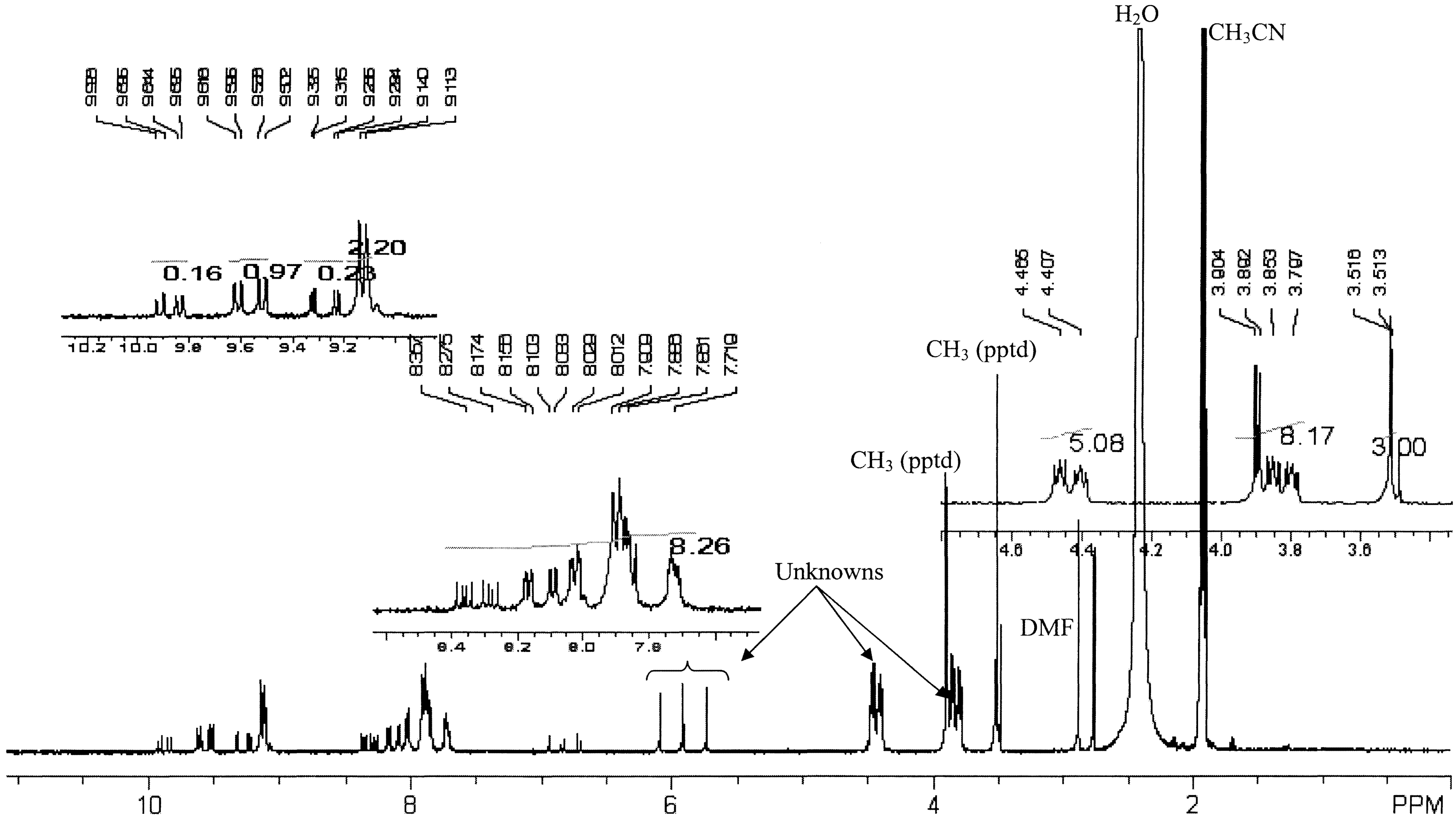

Figure 31: ^{1}H-NMR of [Ru^{II}(H$_2$dcbpy)$_2$pptd](PF$_6$)$_2$ in CD$_3$CN

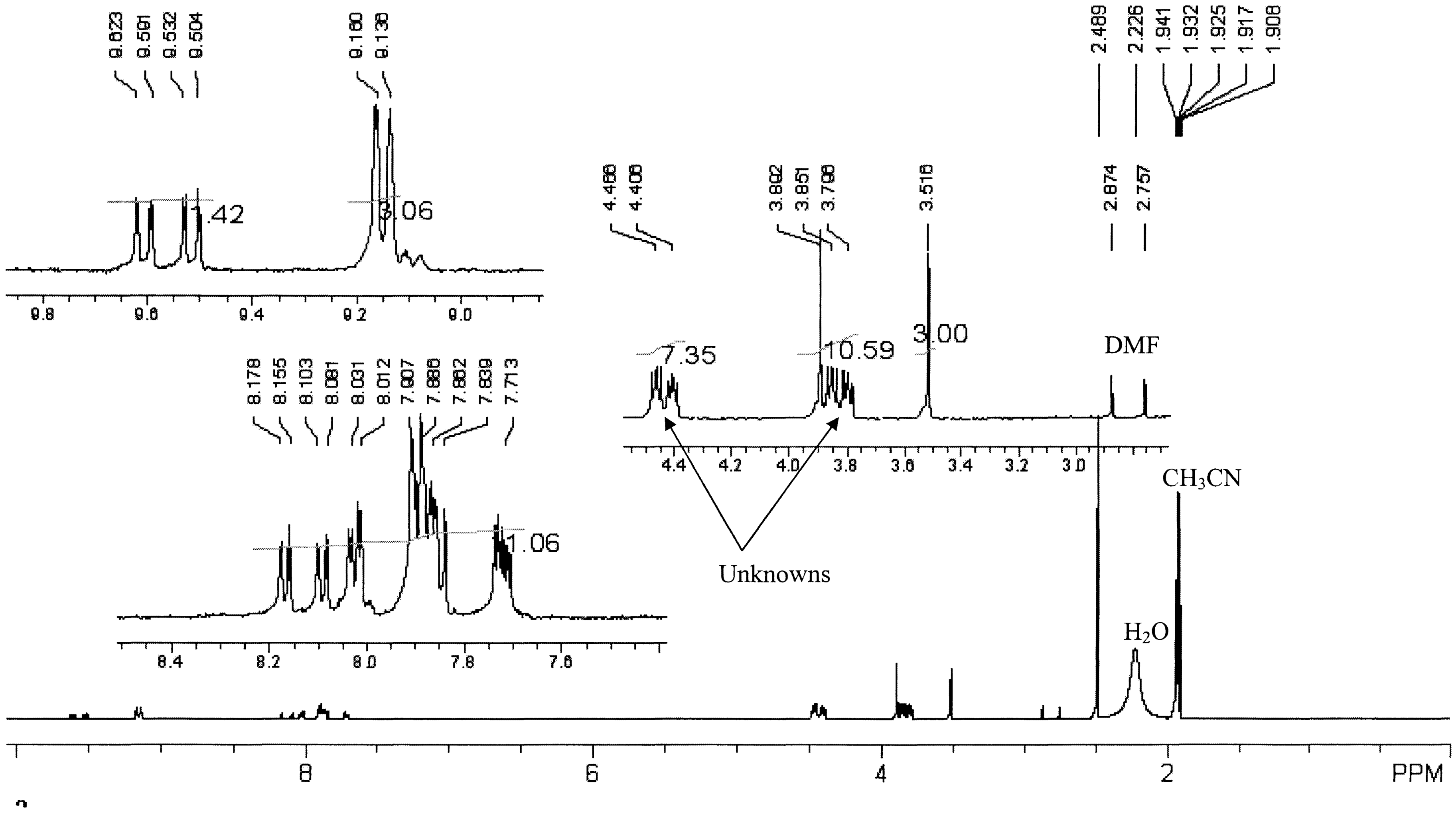

Figure 32: ^{1}H-NMR of $[Ru^{II}(H_2dcbpy)_2pptd](PF_6)_2$ in CD_3CN

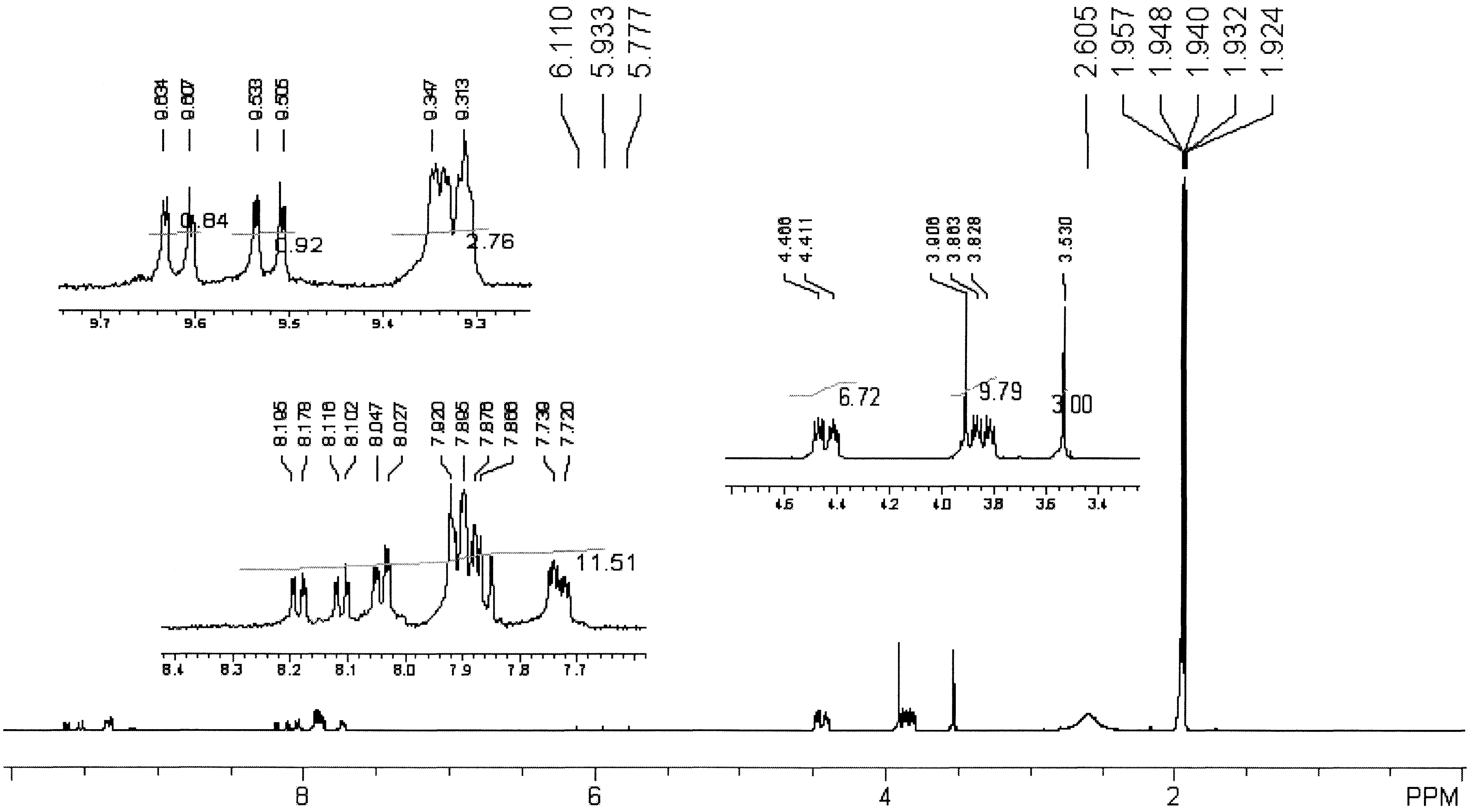

Figure 33: ^{1}H-NMR of [Ru^{II}(H$_2$dcbpy)$_2$pptd](PF$_6$)$_2$ in CD$_3$CN

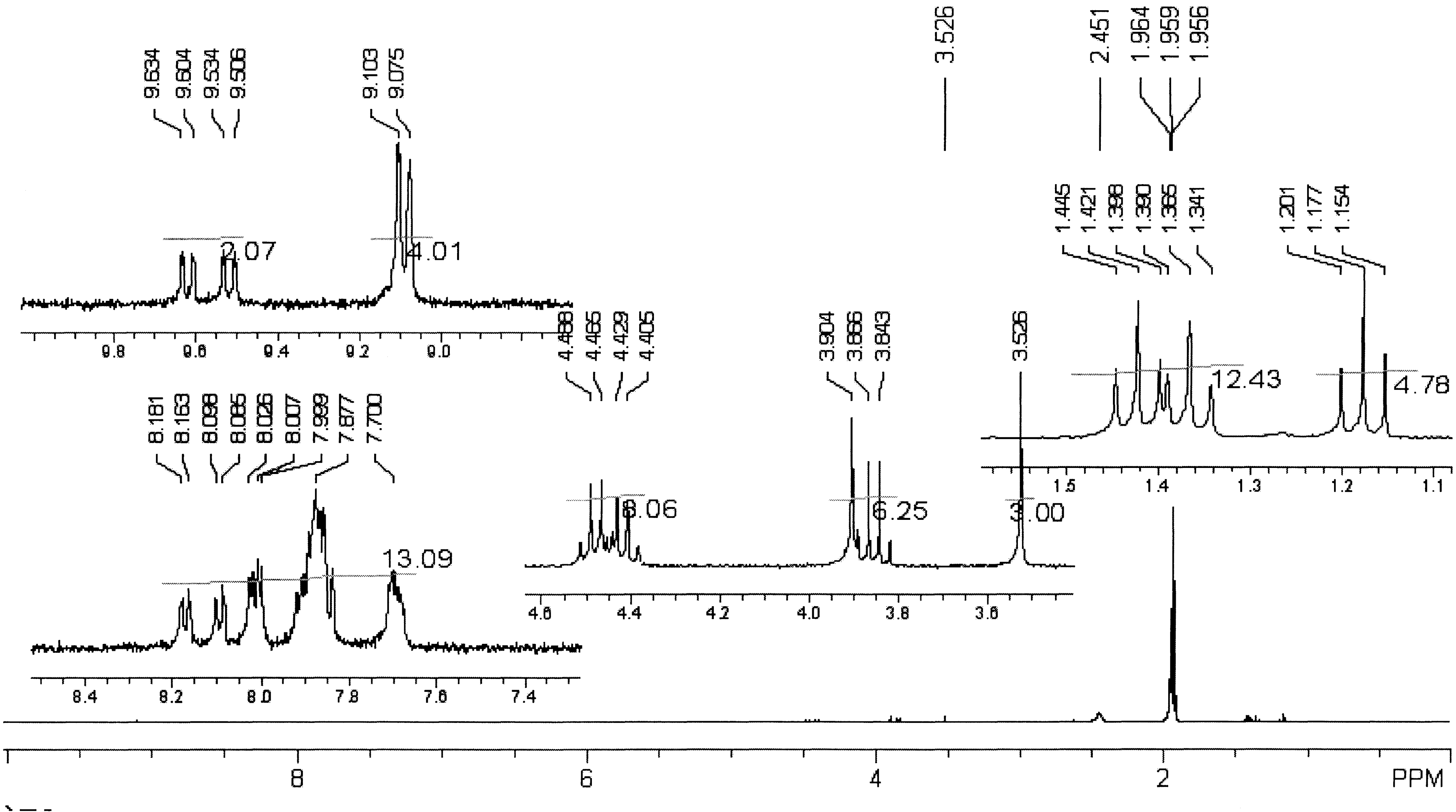

Figure 34: ^{1}H-NMR of [Ru^{II}(Et$_2$dcbpy)$_2$pptd](PF$_6$)$_2$ in CD$_3$CN

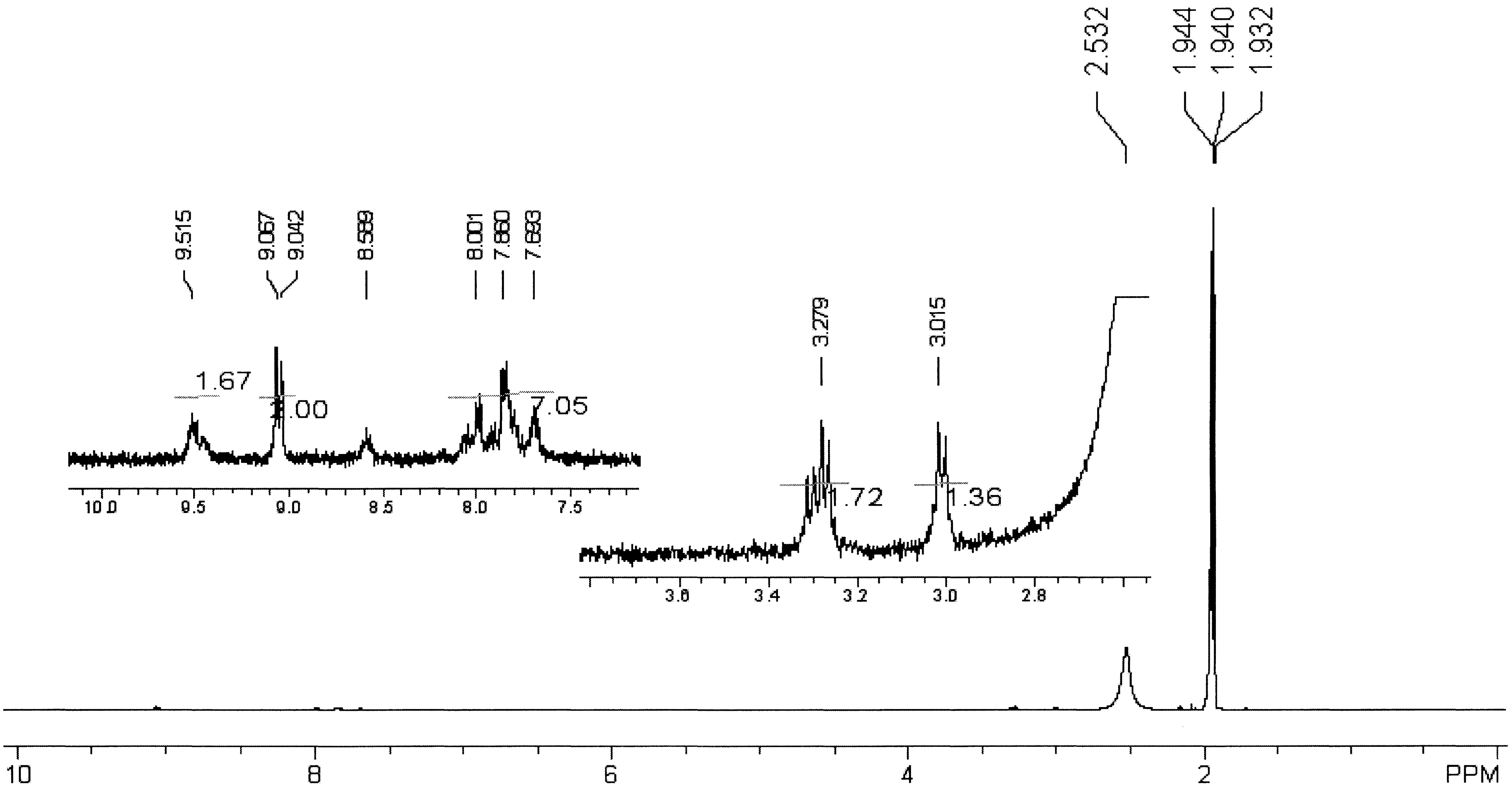

Figure 35: ^{1}H-NMR of [Ru^{II}(H$_2$dcbpy)$_2$pptd](PF$_6$)$_2$ (012403-A) in CD$_3$CN

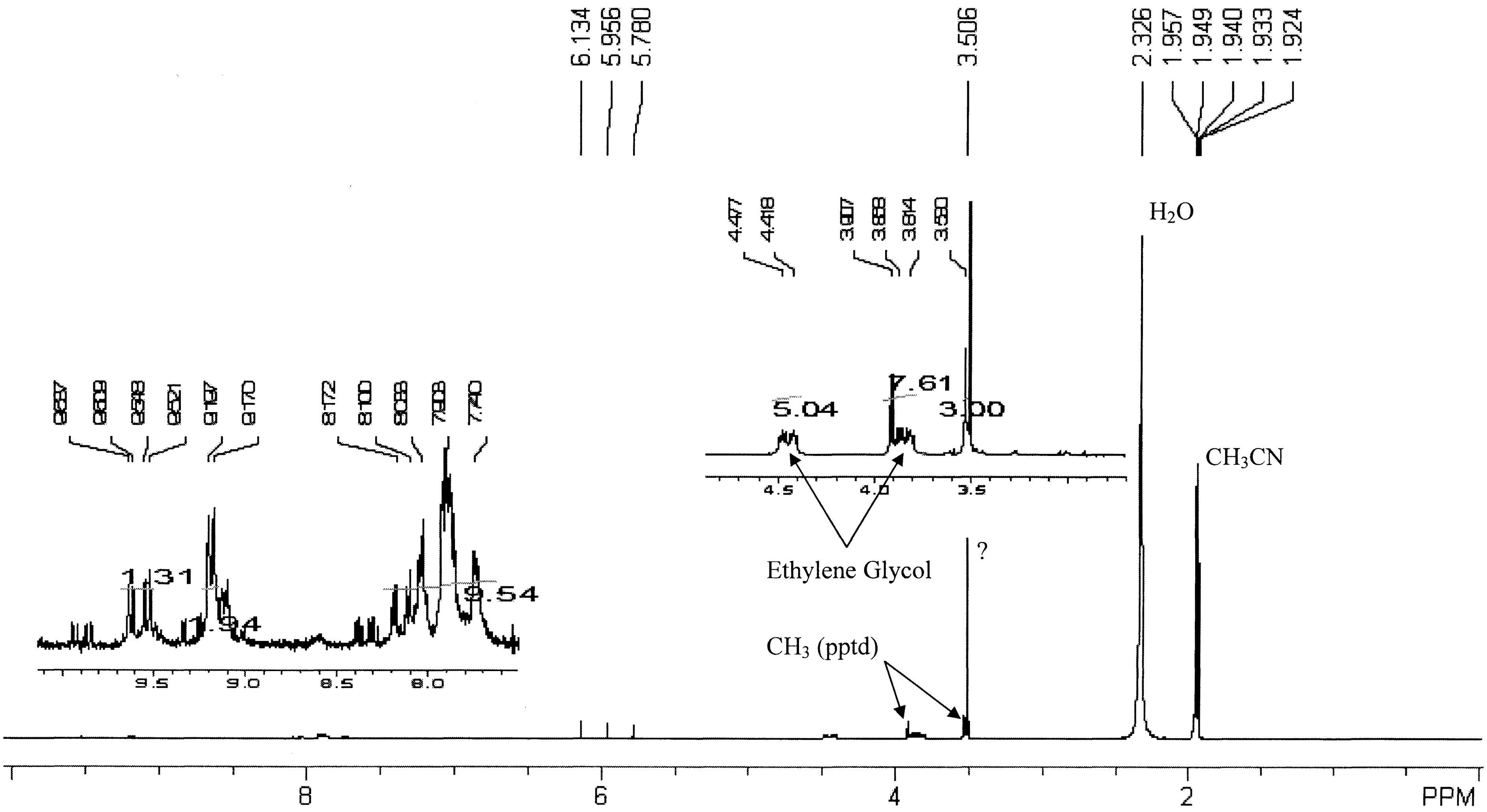

Figure 36: ^{1}H-NMR of [Ru^{II}(Et$_2$dcbpy)$_2$pptd](PF$_6$)$_2$ in CD$_3$CN

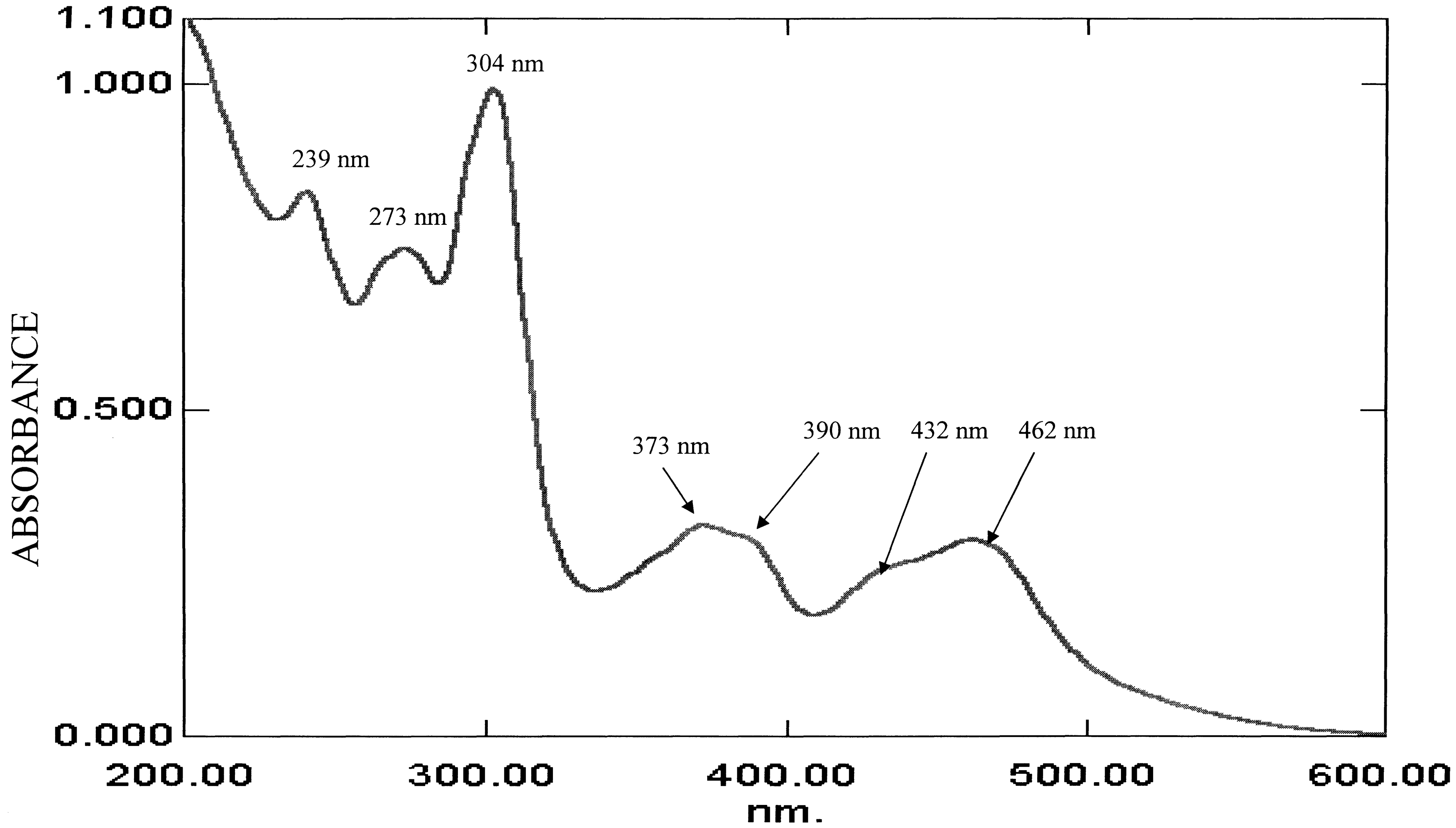

Figure 37: UV-Vis of $[Ru^{II}(dcbpy)_2pptd]^{2+}$ in pH 5.0 phosphate buffer

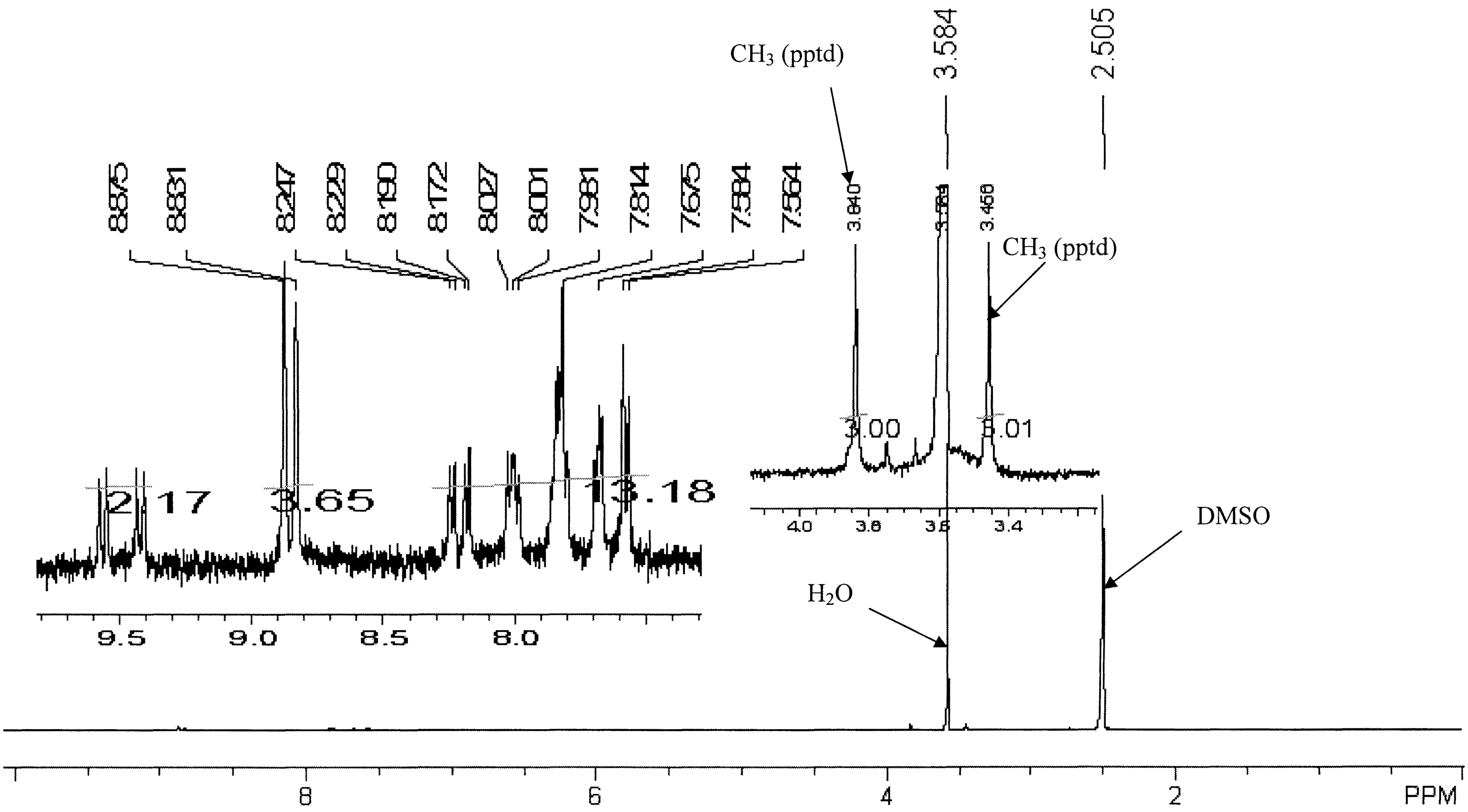

Figure 38: ^{1}H-NMR of [Ru^{II}(H$_2$dcbpy)$_2$pptd](PF$_6$)$_2$ in d$_6$-DMSO

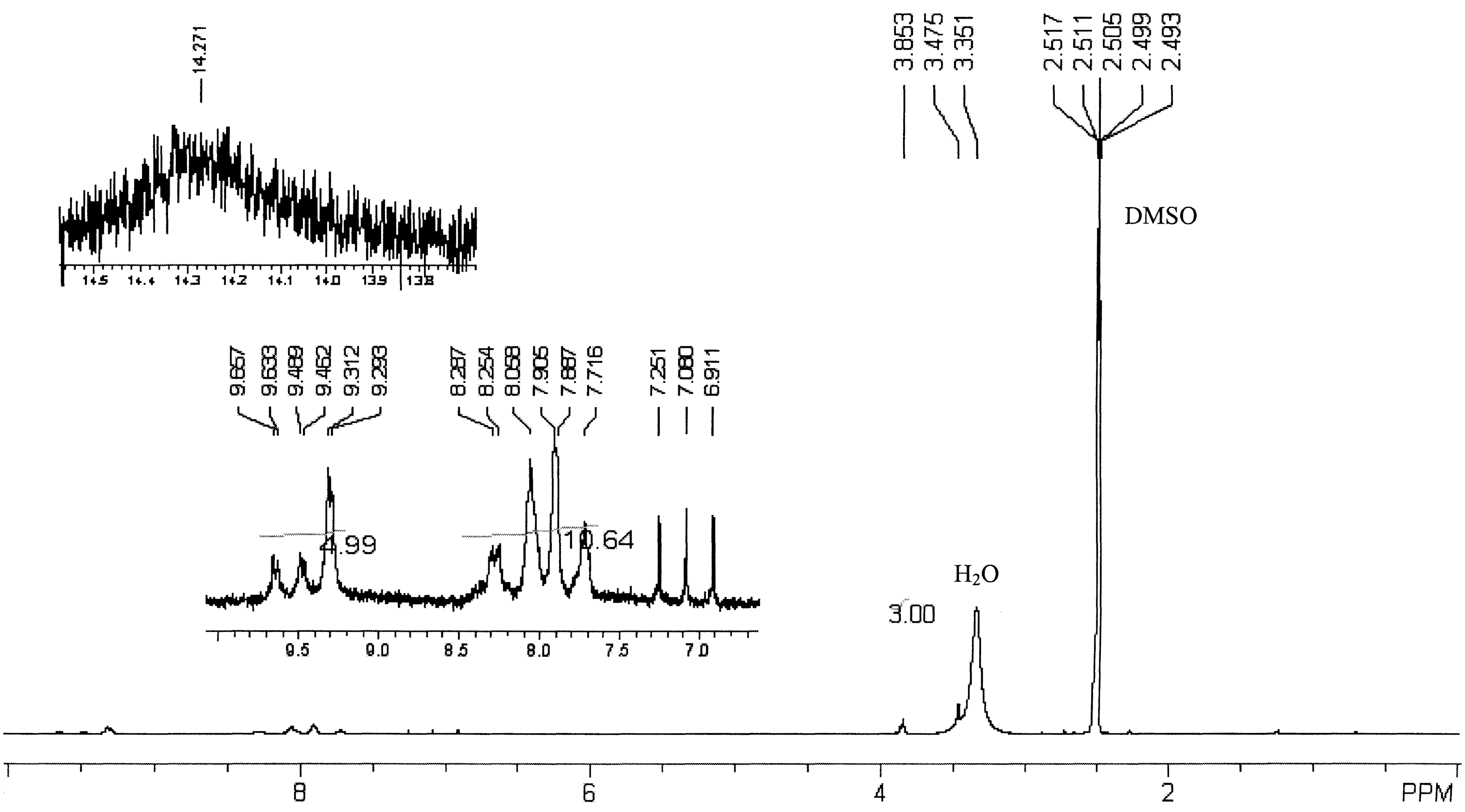

Figure 39: ^{1}H-NMR of $[Ru^{II}(H_2dcbpy)_2pptd](PF_6)_2$ in d_6-DMSO

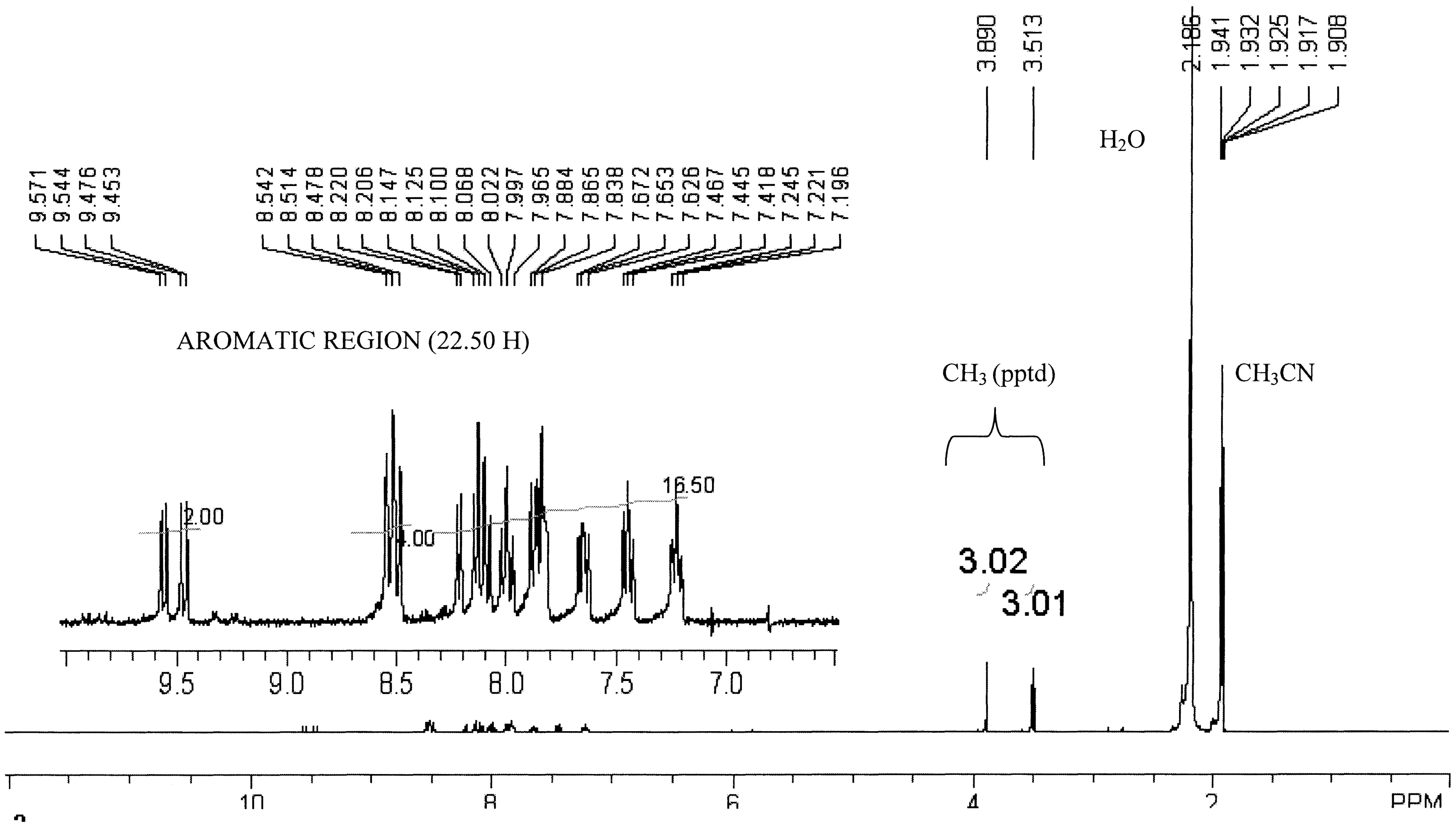

Figure 40: ^{1}H-NMR of $[Ru^{II}(bpy)_2pptd](PF_6)_2$ in CD_3CN

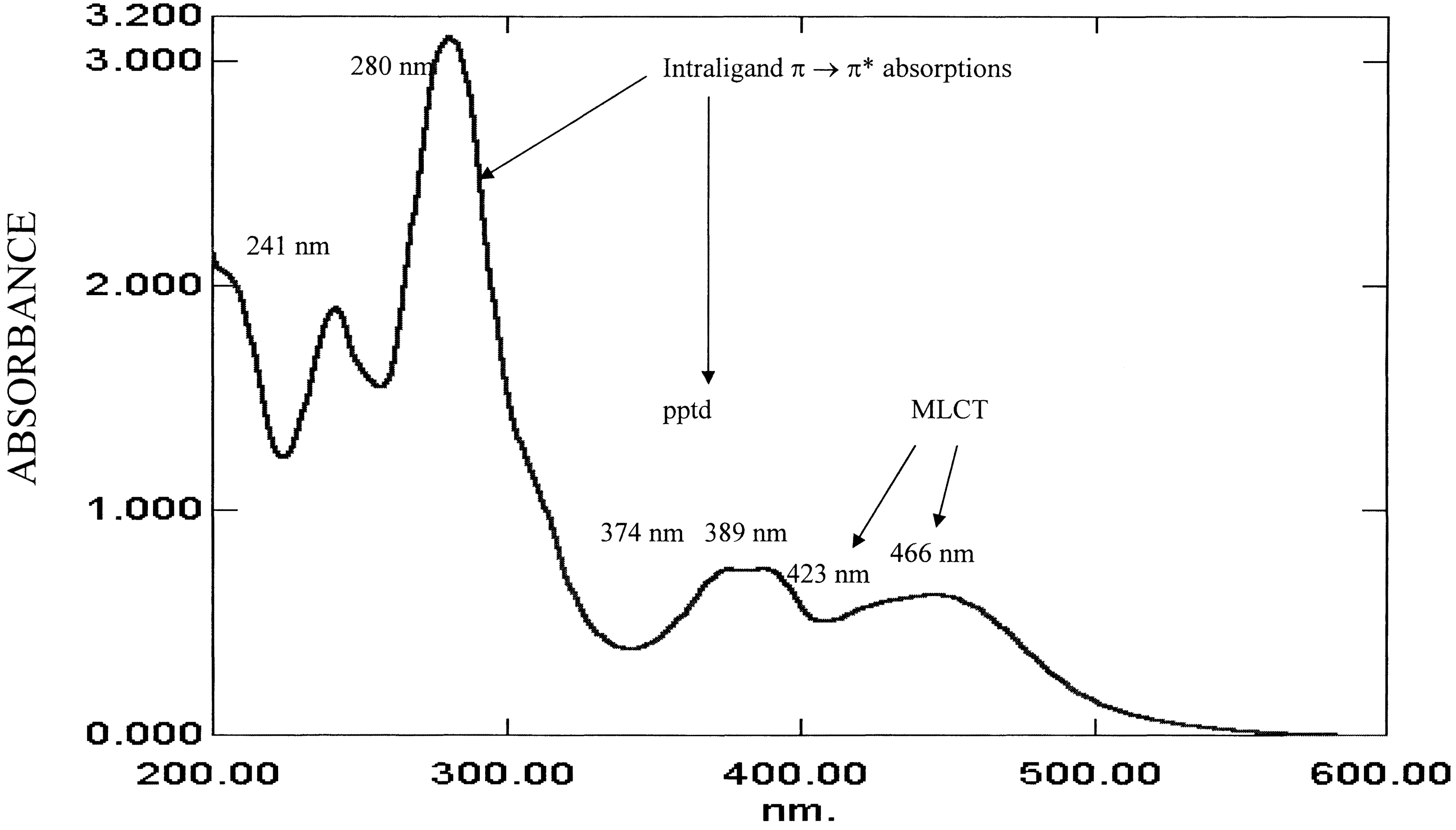

Figure 41: UV-Vis of $[Ru^{II}(bpy)_2pptd](PF_6)_2$ in pH 5.0 phosphate buffer

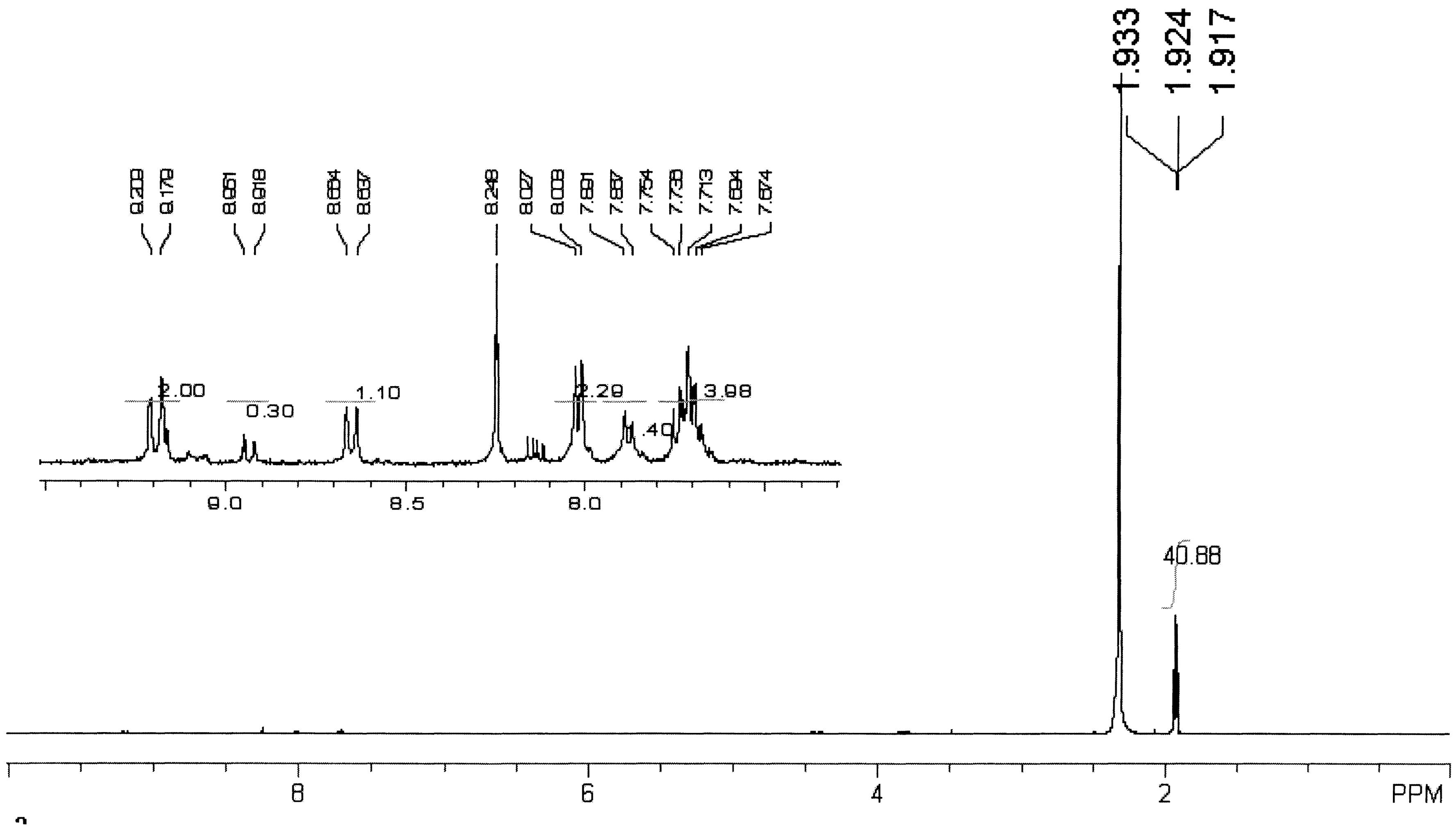

Figure 42: ^{1}H-NMR of of [Ru^{II}(H$_2$dcbpy)$_2$phen](PF$_6$)$_2$ in CD$_3$CN

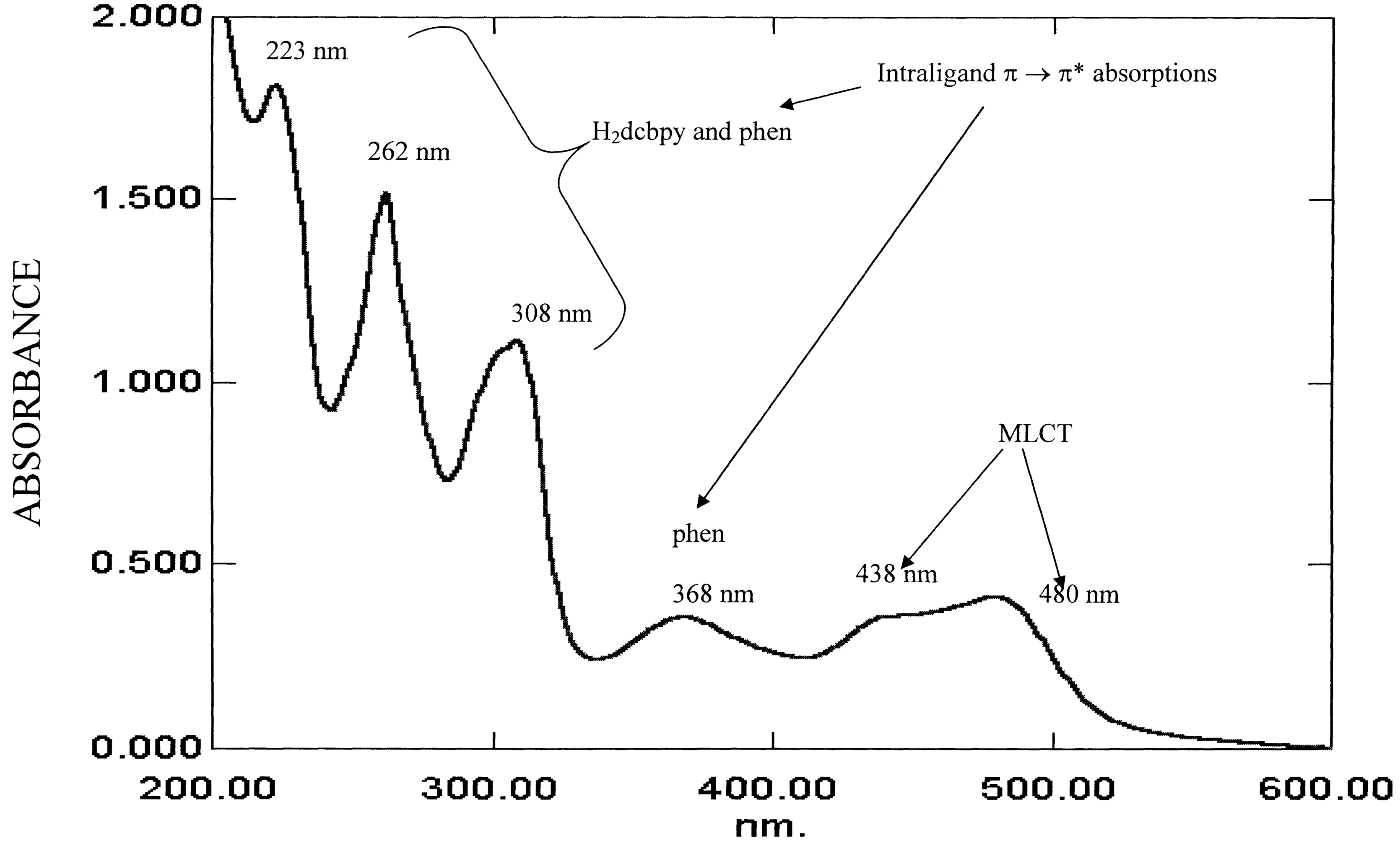

Figure 43: UV-Vis of $[Ru^{II}(H_2dcbpy)_2phen](PF_6)_2$ in pH 5.0 phosphate buffer

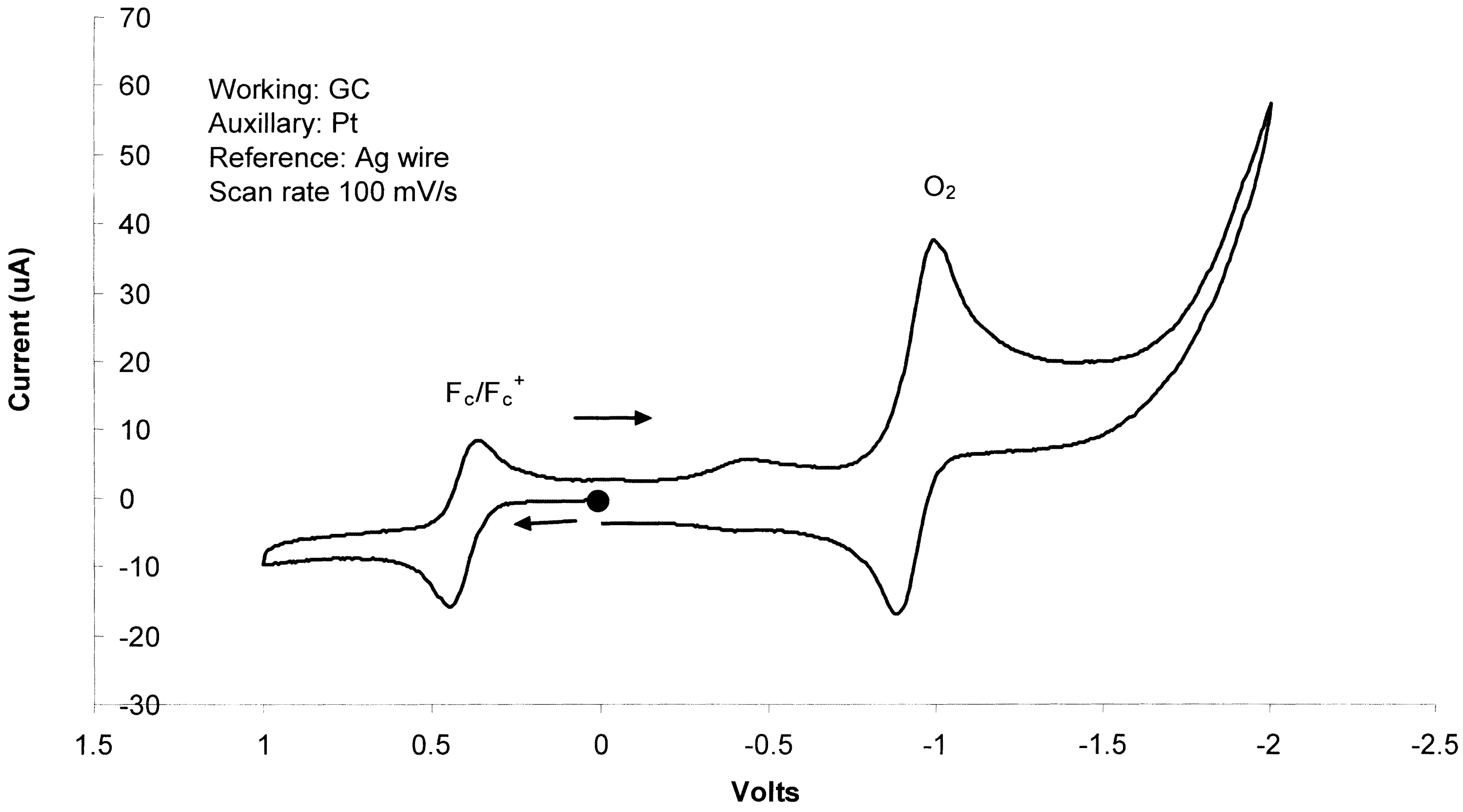

Figure 45a: CV of 0.1M TBAH/DMF with Oxygen present

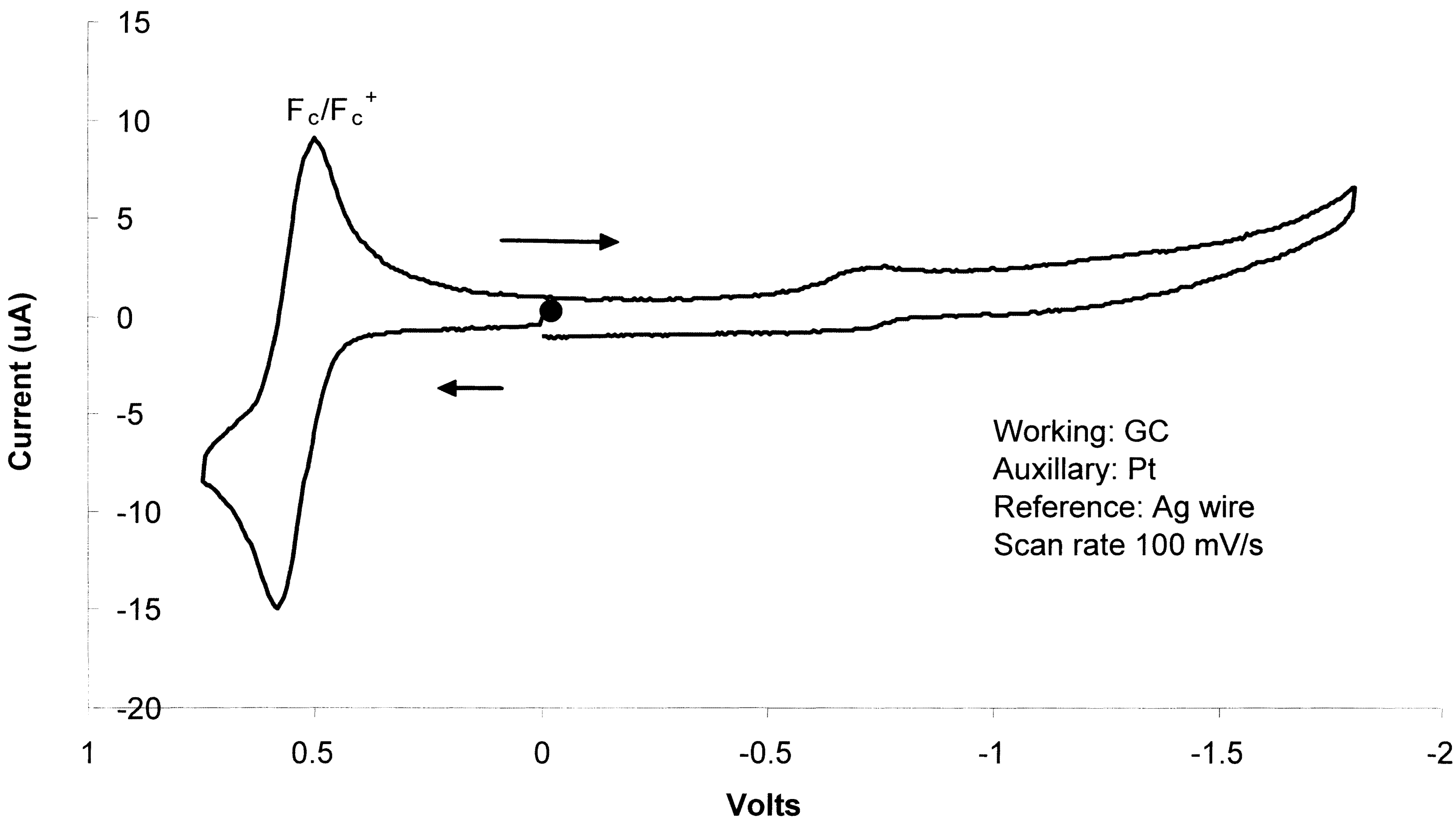

Figure 45b: CV of 0.1 M TBAH/DMF after bubbling with Ar

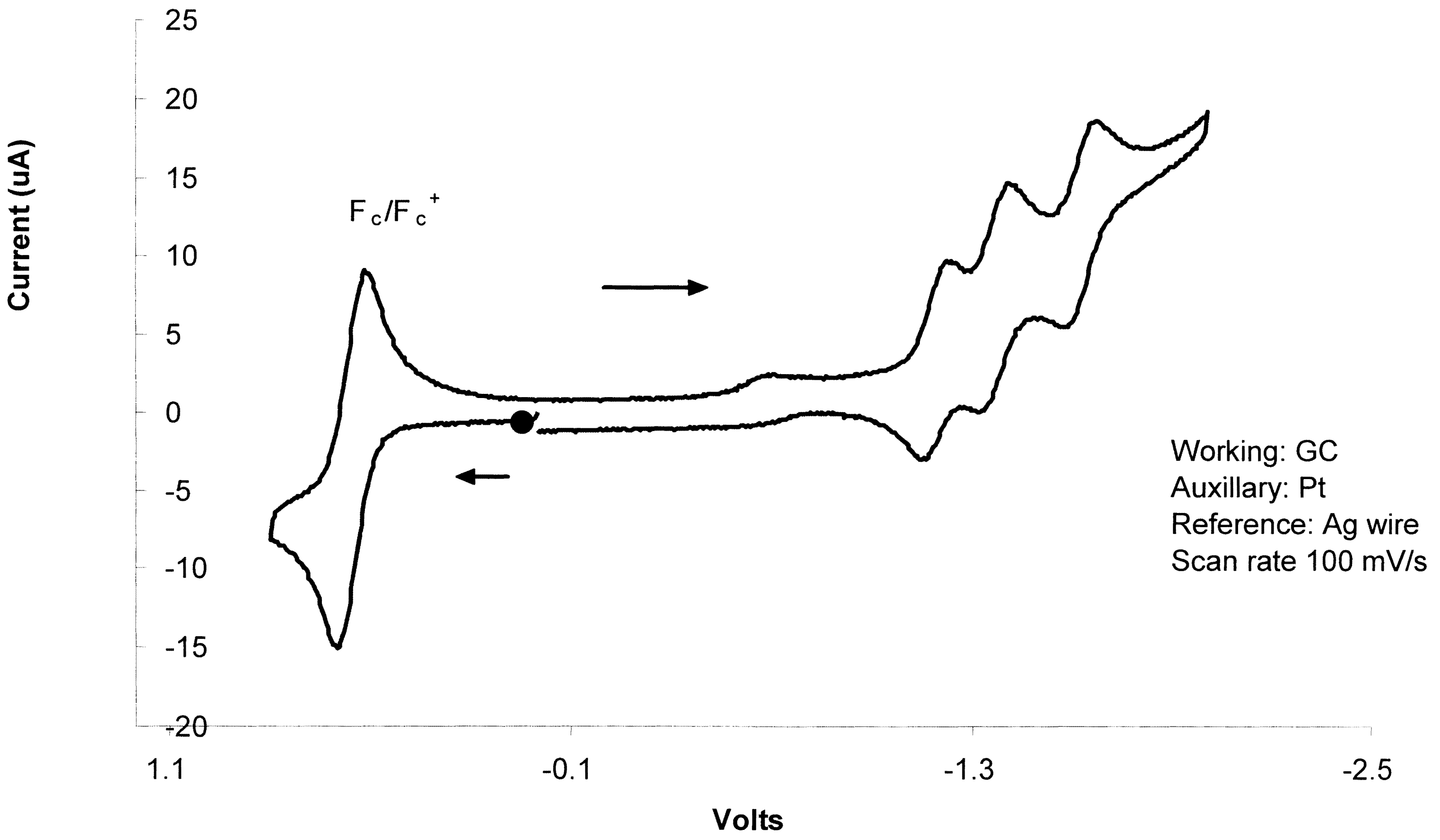

Figure 45c: CV of $[Ru^{II}(bpy)_2phen](PF_6)_2$ in 0.1 M TBAH/DMF

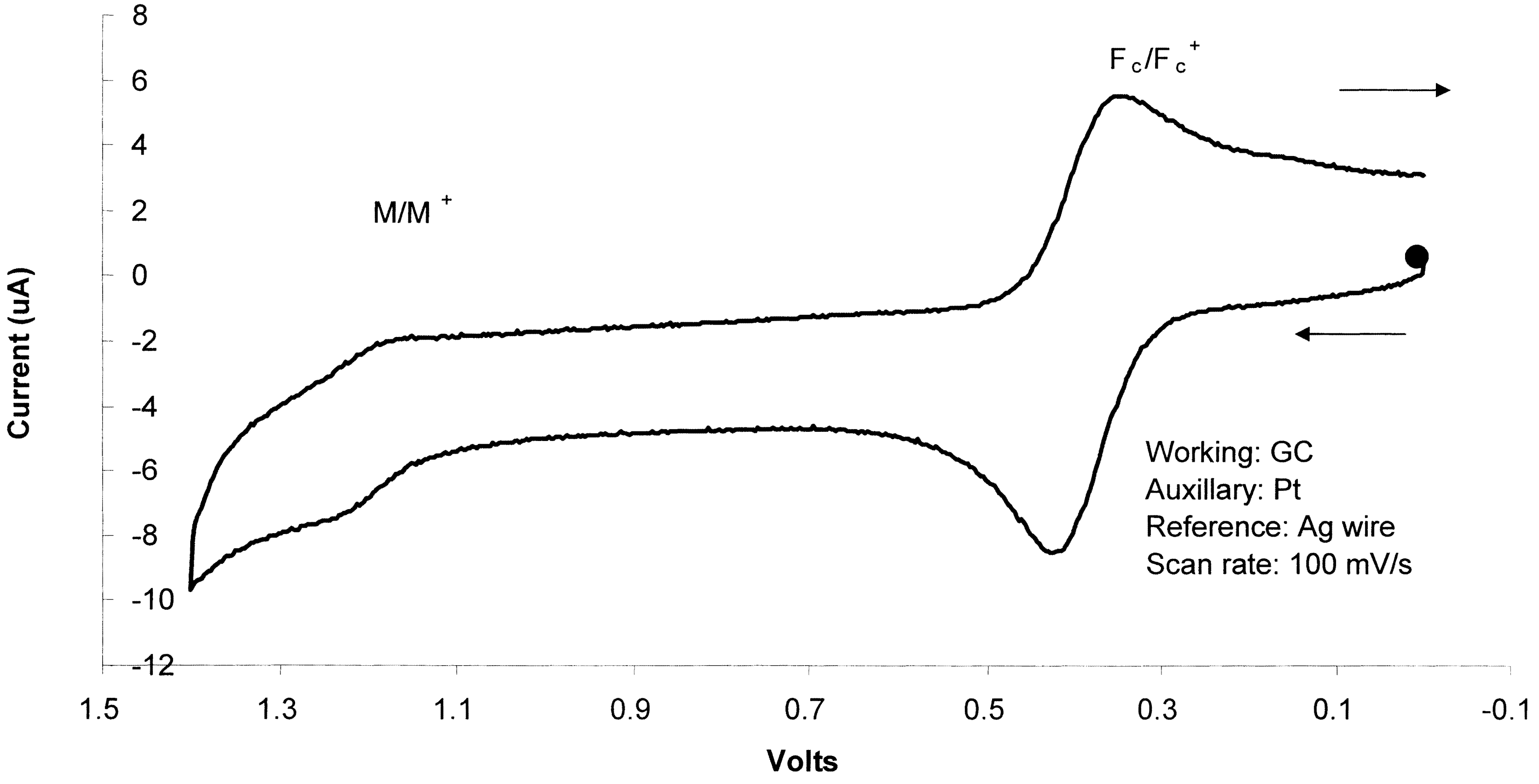

Figure 45d: CV of $[Ru^{II}(bpy)_2phen](PF_6)_2$ in 0.1 M TBAH/DMF

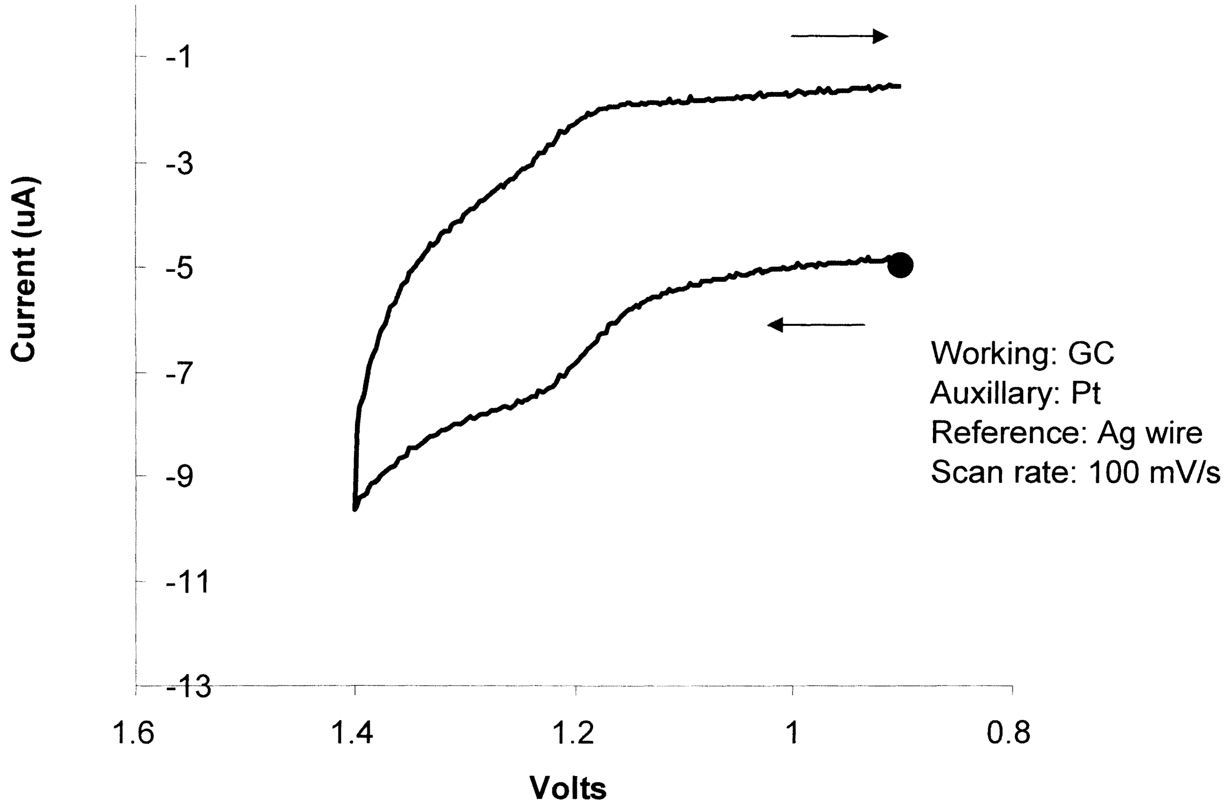

Working: GC
Auxillary: Pt
Reference: Ag wire
Scan rate: 100 mV/s

Figure 45e: CV of $[Ru^{II}(bpy)_2phen](PF_6)_2$ expanded

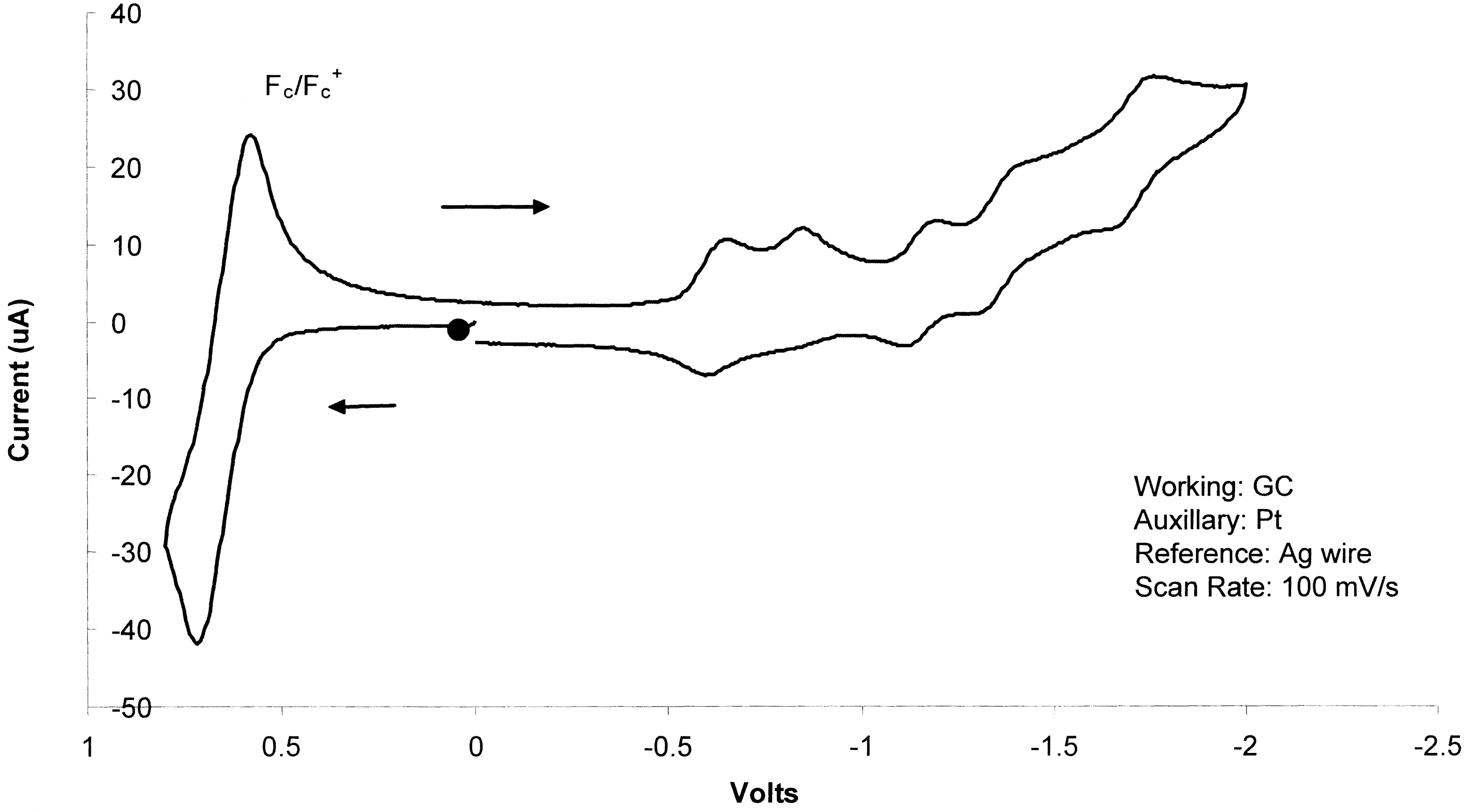

Figure 46a: CV of [Ru^{II}(bpy)$_2$pptd](PF$_6$)$_2$ in 0.1 M TBAH/DMF

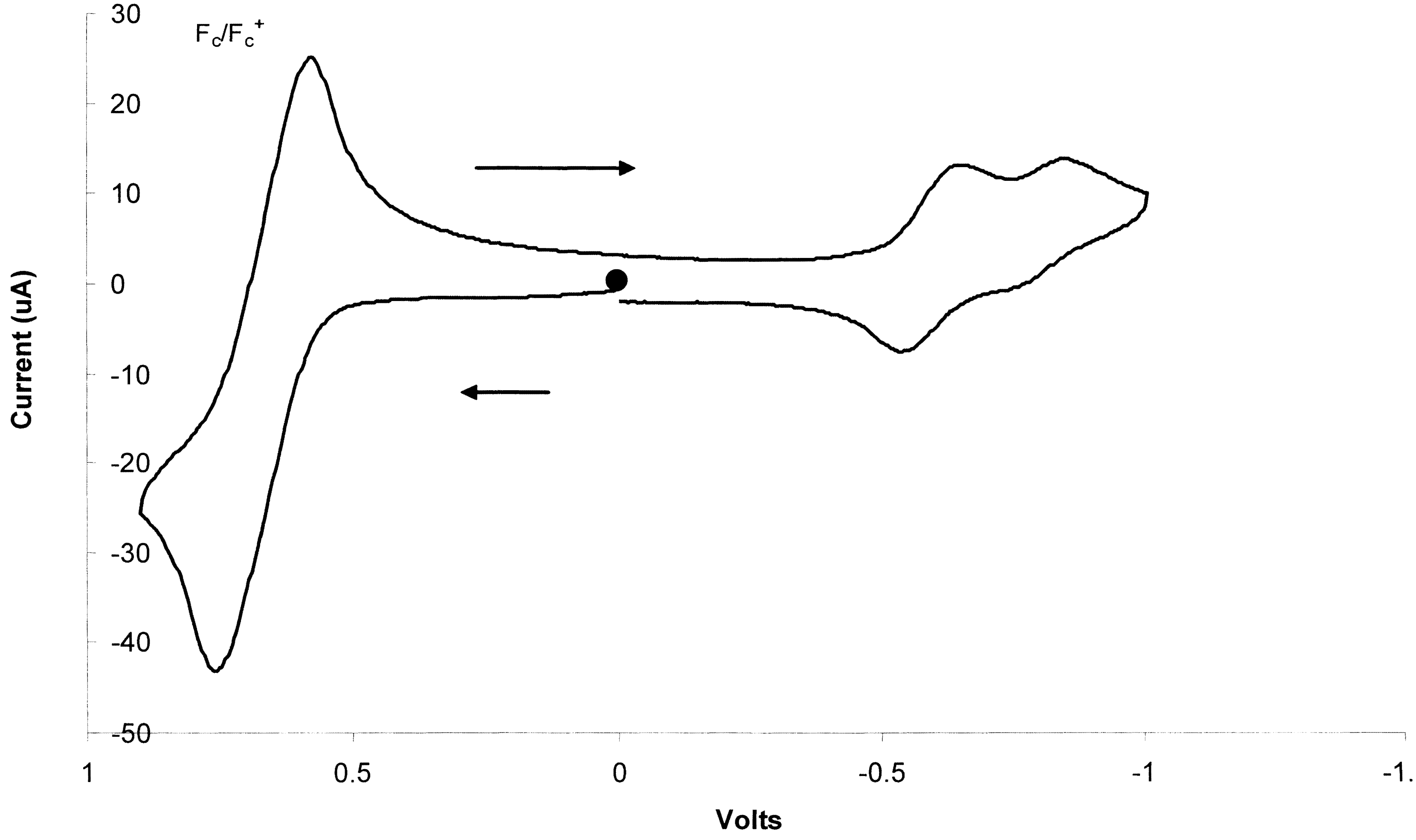

Figure 46b: CV of $[Ru^{II}(bpy)_2pptd](PF_6)_2$ in 0.1 M TBAH/DMF

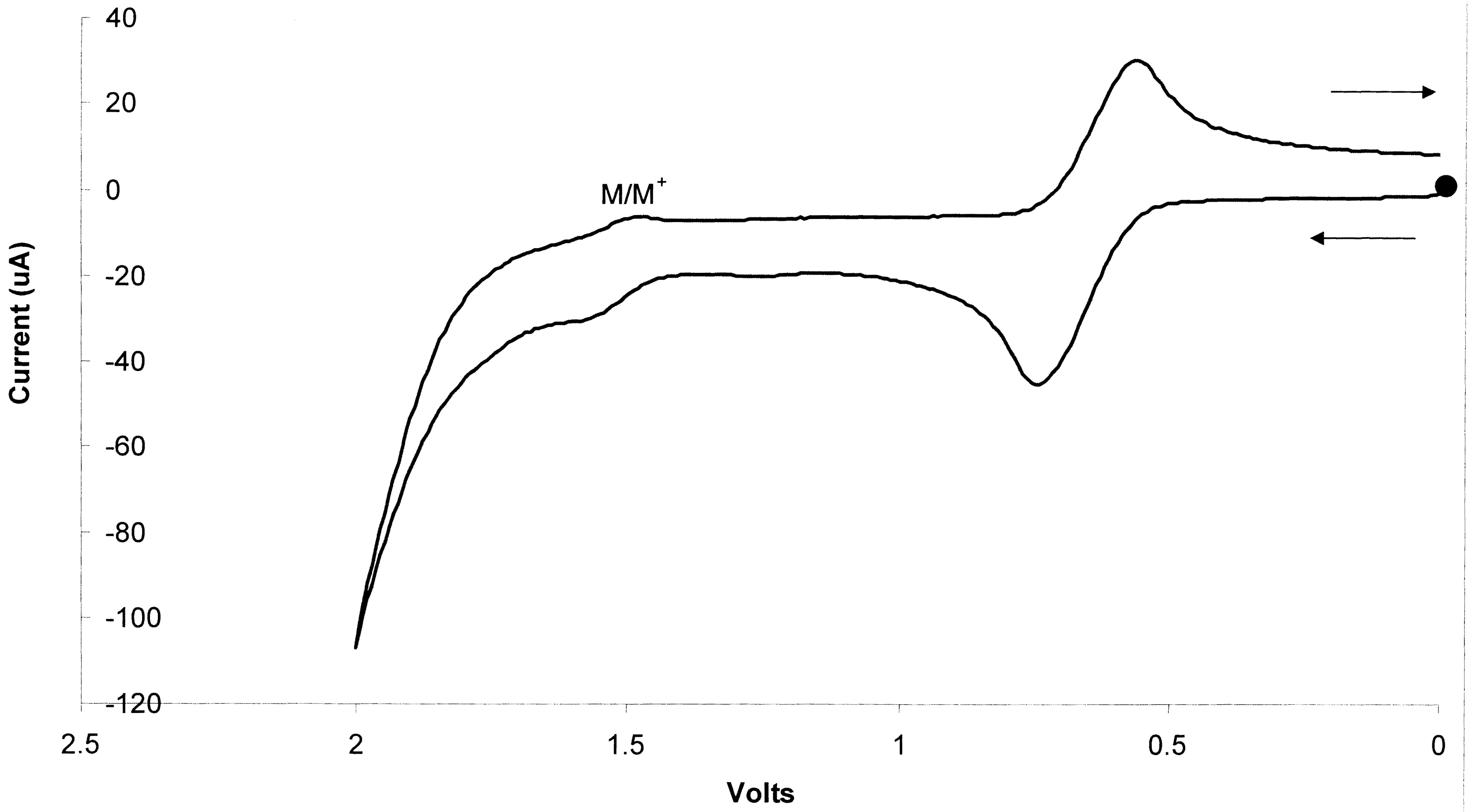

Figure 46c: CV of $[Ru^{II}(bpy)_2pptd](PF_6)_2$ in 0.1 M TBAH/DMF

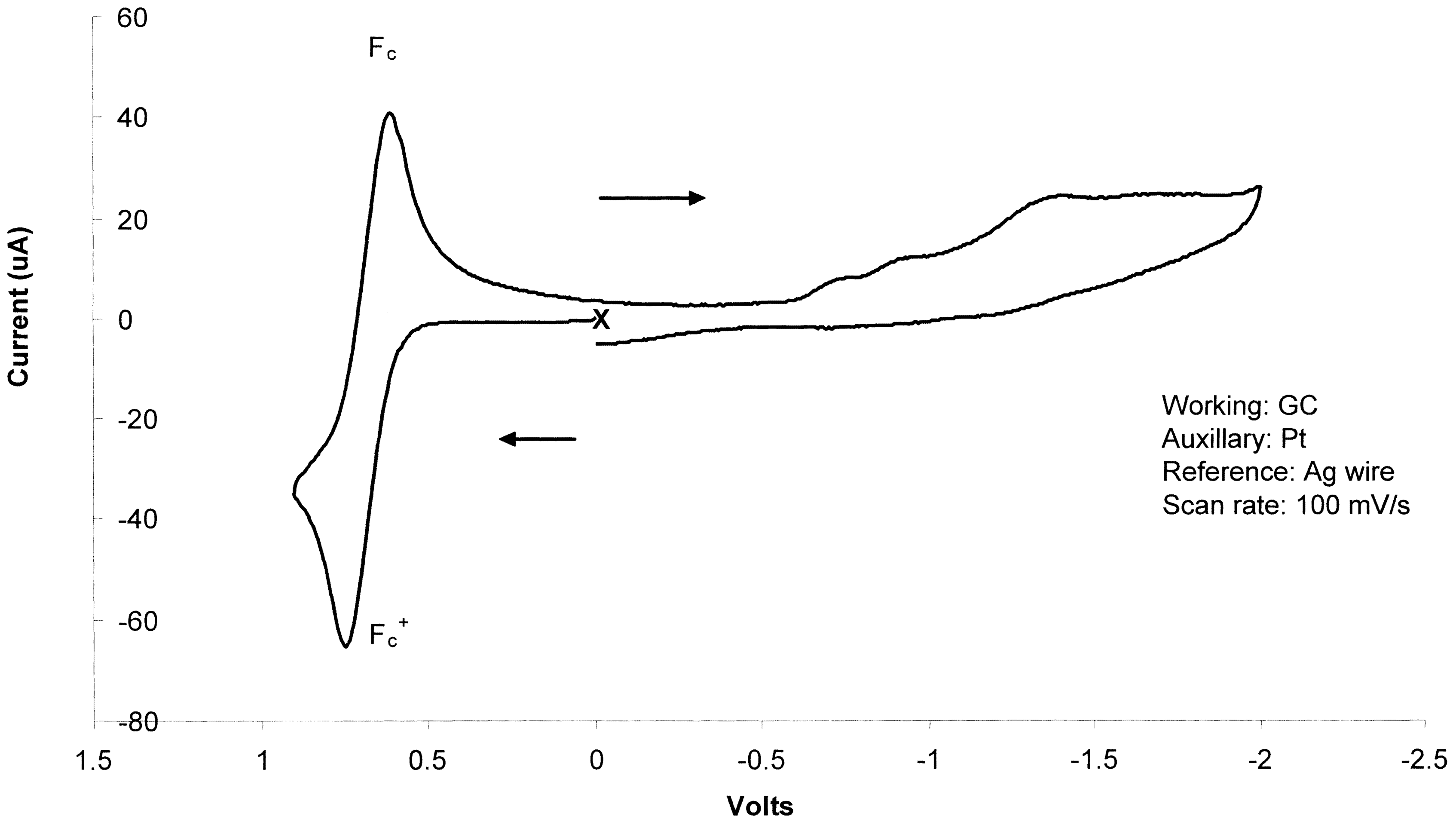

Figure 47a: CV of $[Ru^{II}(H_2dcbpy)_2phen](PF_6)_2$ in 0.1 M TBAH/DMF

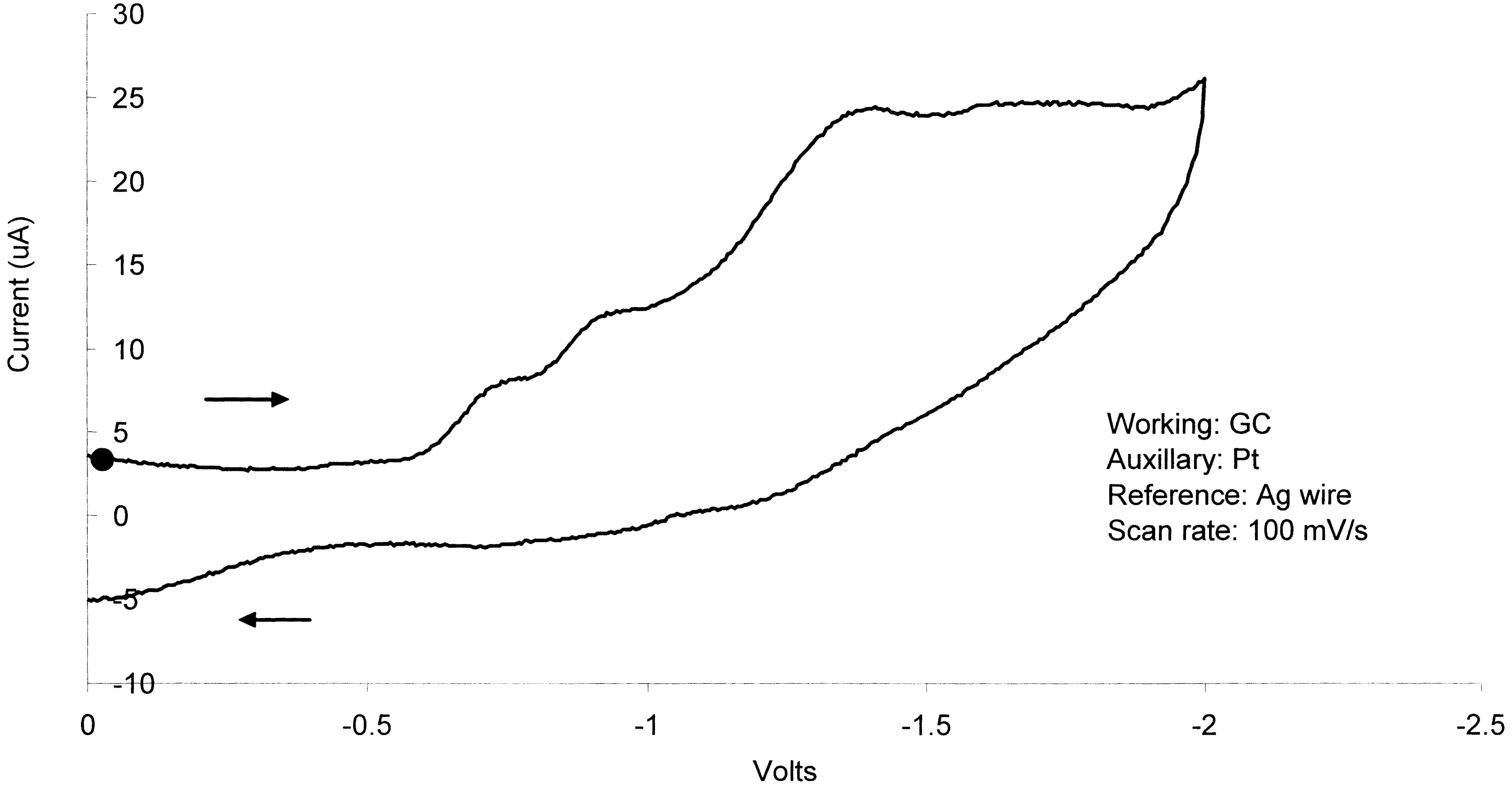

Figure 47b: CV of [Ru^{II}(H$_2$dcbpy)$_2$phen](PF$_6$)$_2$ in 0.1 M TBAH/DMF

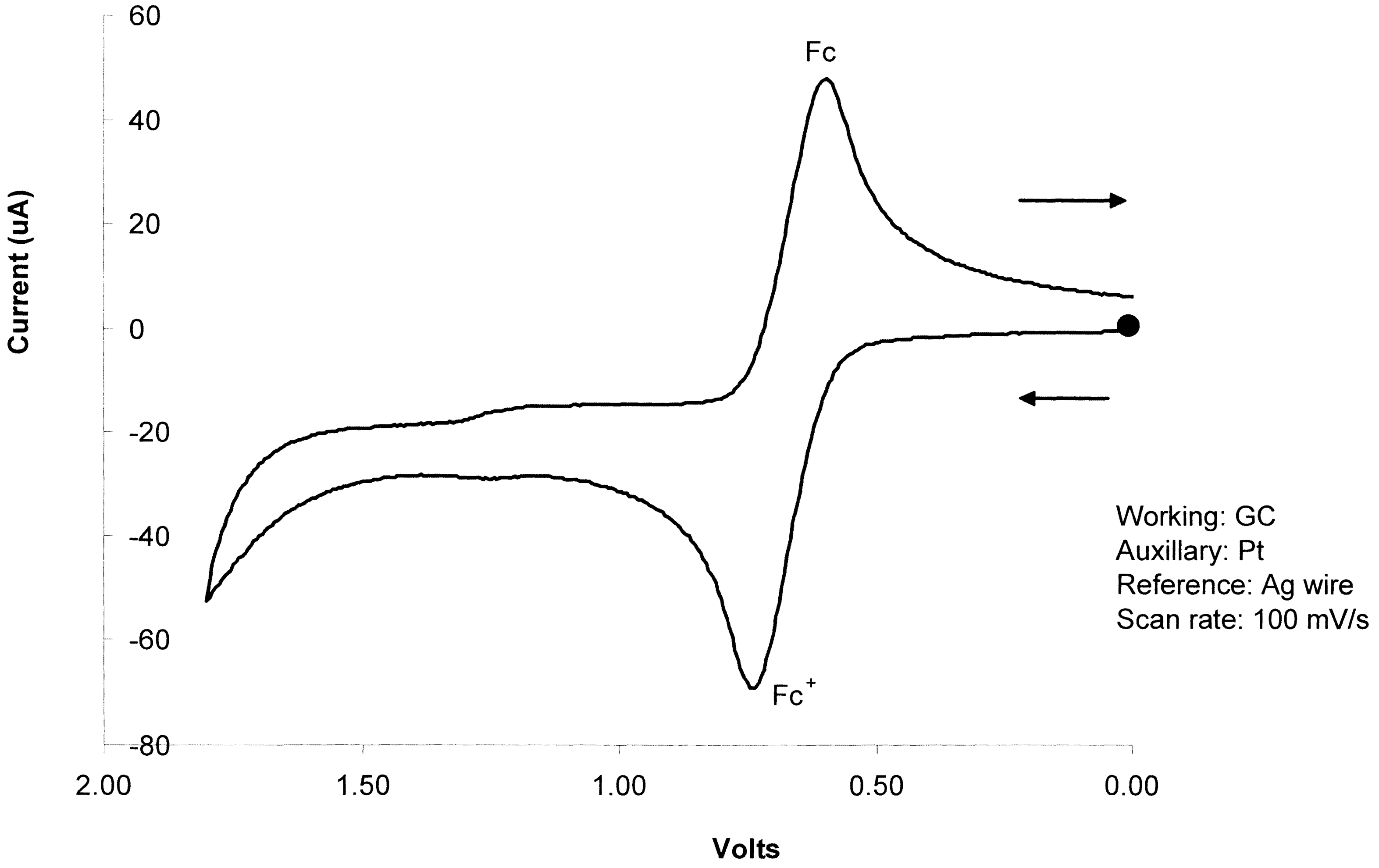

Figure 47c: CV of $[Ru^{II}(H_2dcbpy)_2phen](PF_6)_2$ in 0.1 M TBAH/DMF

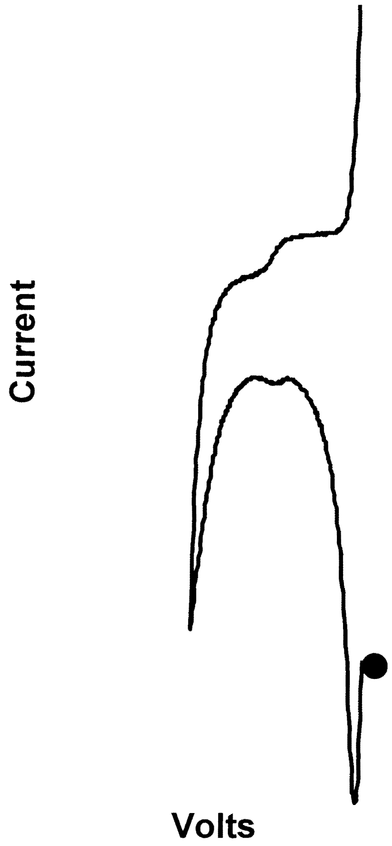

Working: GC
Auxillary: Pt
Reference: Ag wire
Scan rate: 100 mV/s

Figure 47d: CV of $[Ru^{II}(H_2dcbpy)_2phen](PF_6)_2$ in 0.1 M TBAH/DMF

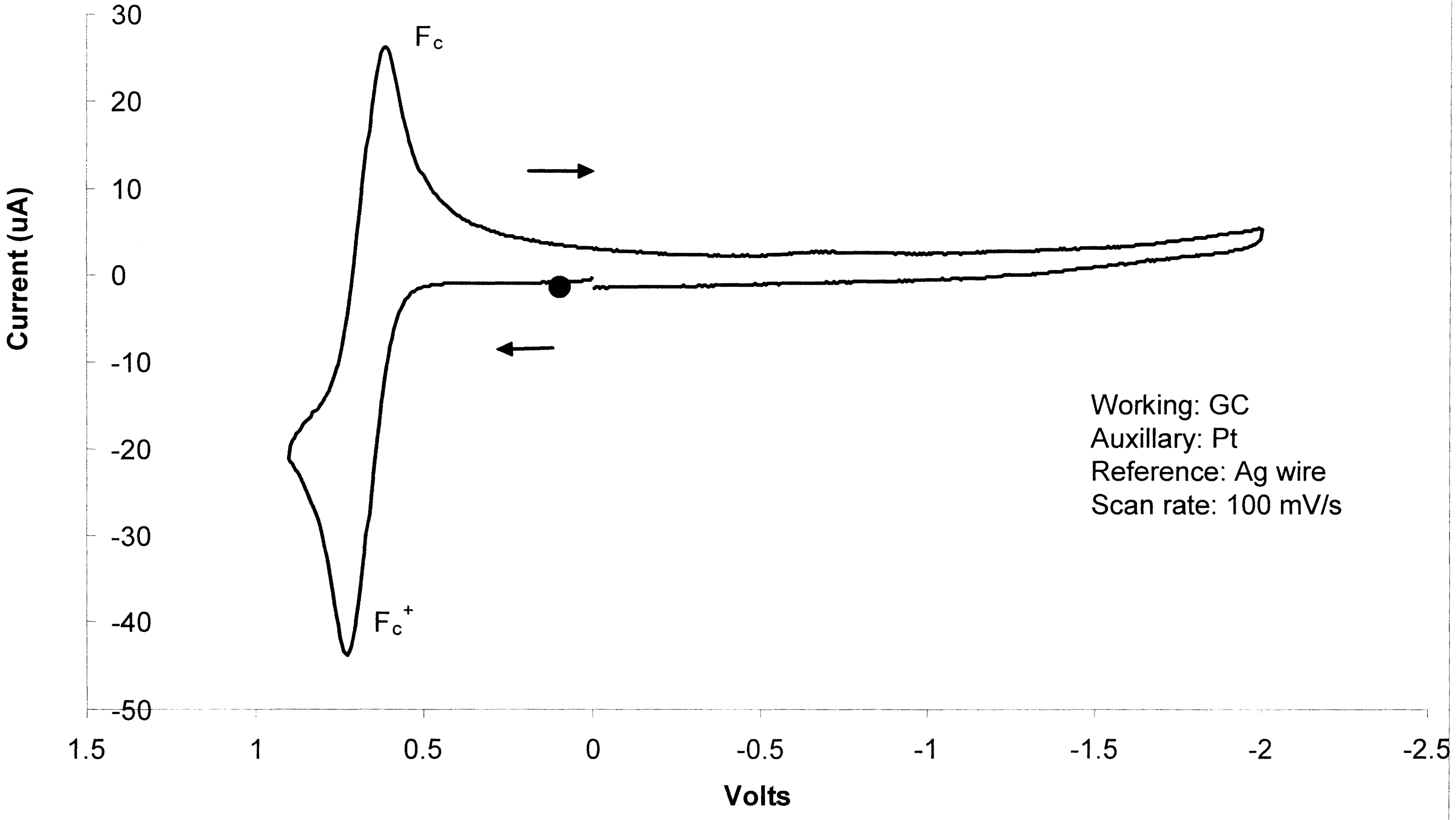

Figure 48a: Background CV of 0.1 M TBAH/DMF after bubbling with Ar

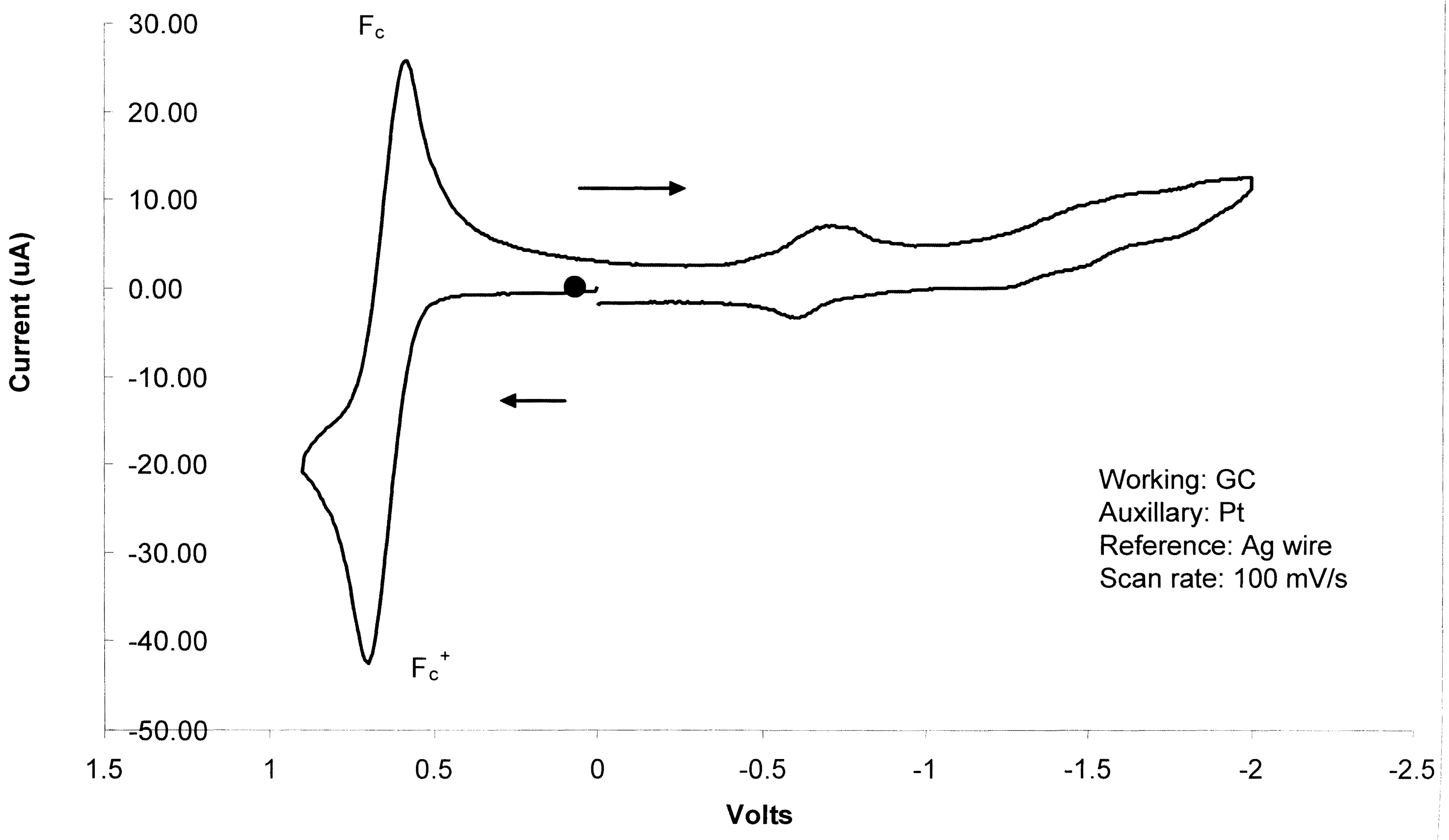

Figure 48b: CV of $[Ru^{II}(H_2dcbpy)_2pptd](PF_6)_2$ in 0.1 M TBAH/DMF

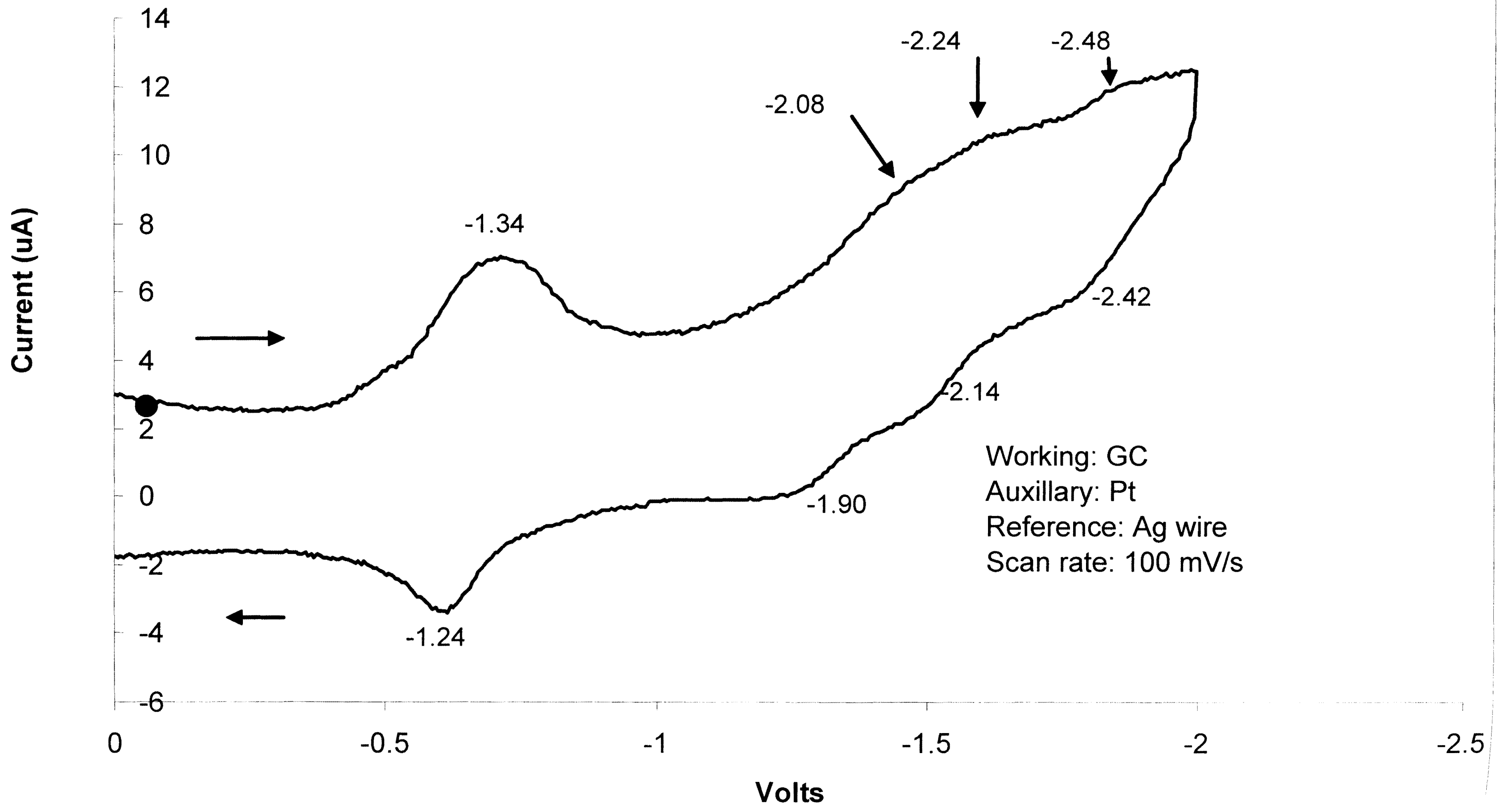

Figure 48c: CV of $[Ru^{II}(H_2dcbpy)_2pptd](PF_6)_2$ in 0.1 M *TBAH/DMF*

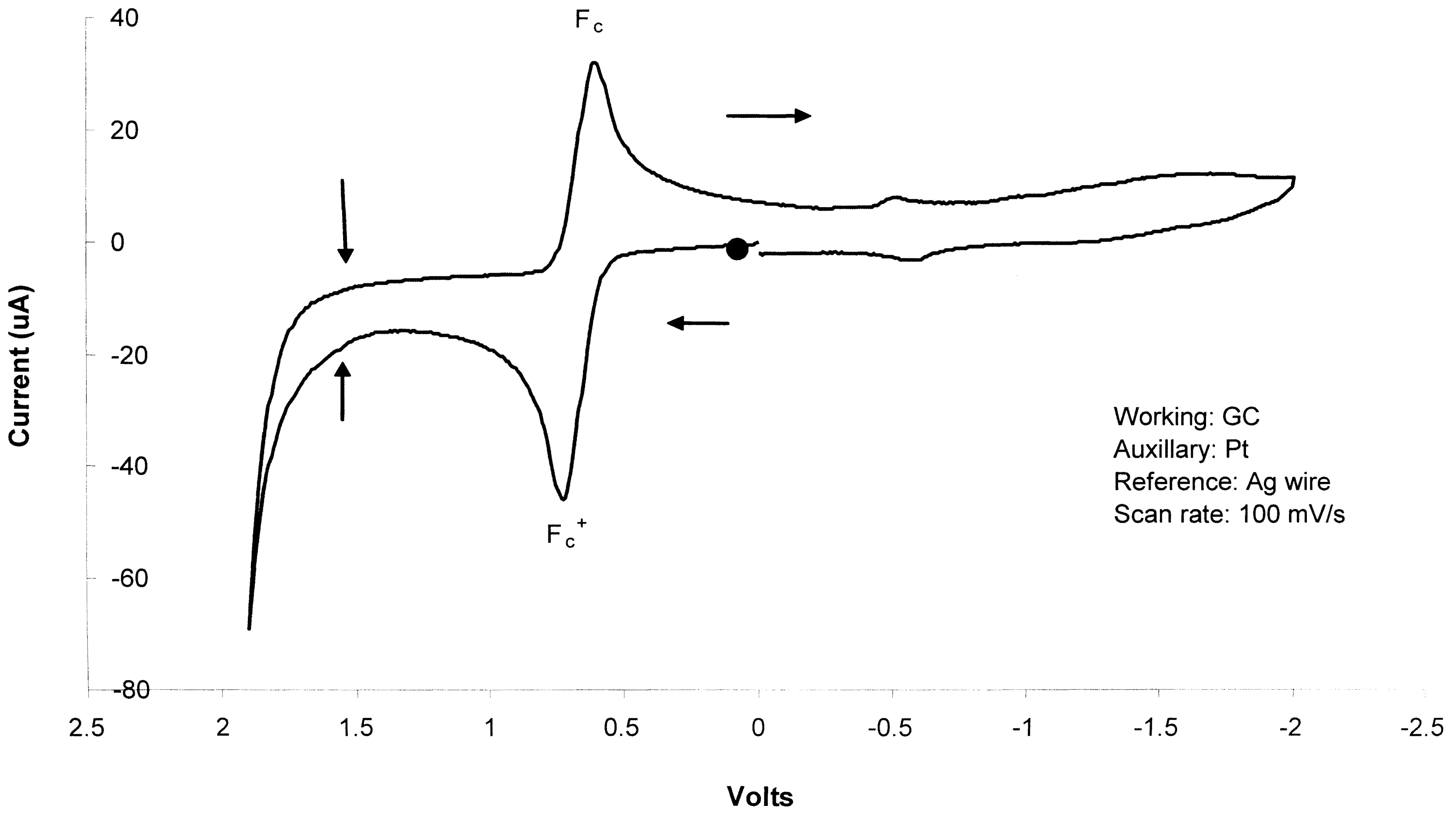

Figure 48d: CV of $[Ru^{II}(H_2dcbpy)_2pptd](PF_6)_2$ in 0.1 M TBAH/DMF

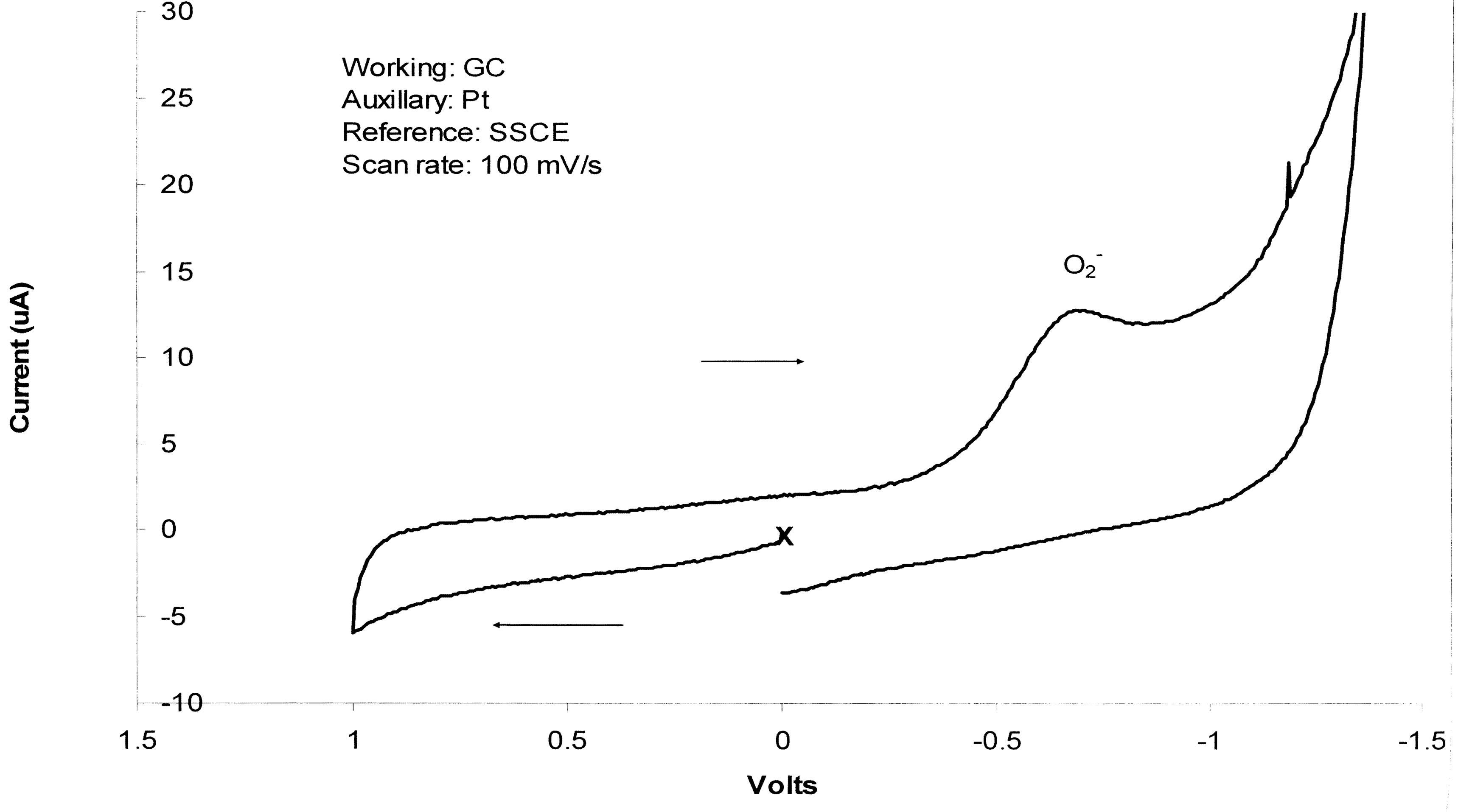

Figure 49a: CV of pH 4.0 acetate buffer with oxygen present

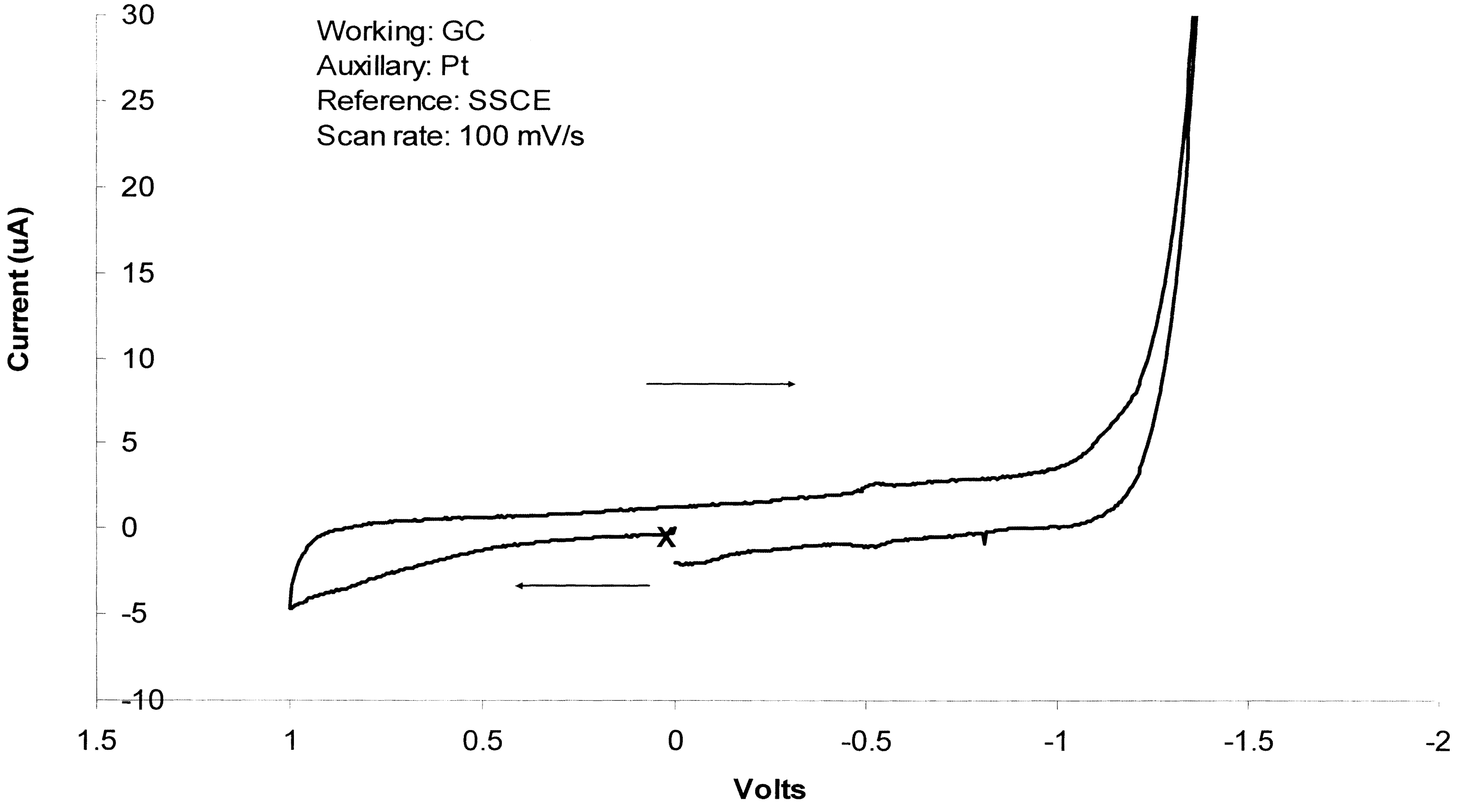

Figure 49b: CV of pH 4.0 acetate buffer after bubbling with Ar

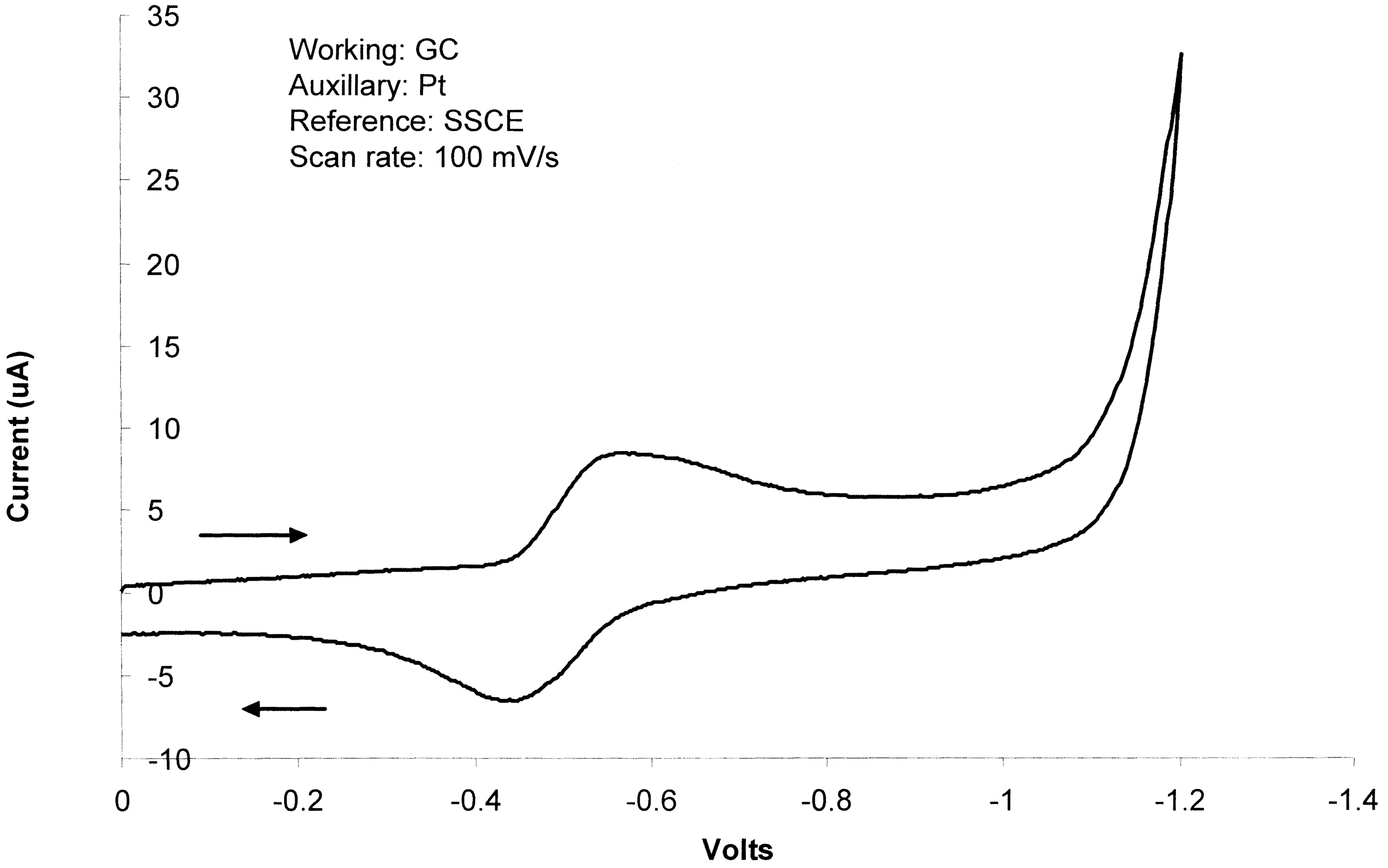

Figure 49c: CV of $[Ru^{II}(H_2dcbpy)_2pptd](PF_6)_2$ in pH 4.0 acetate buffer

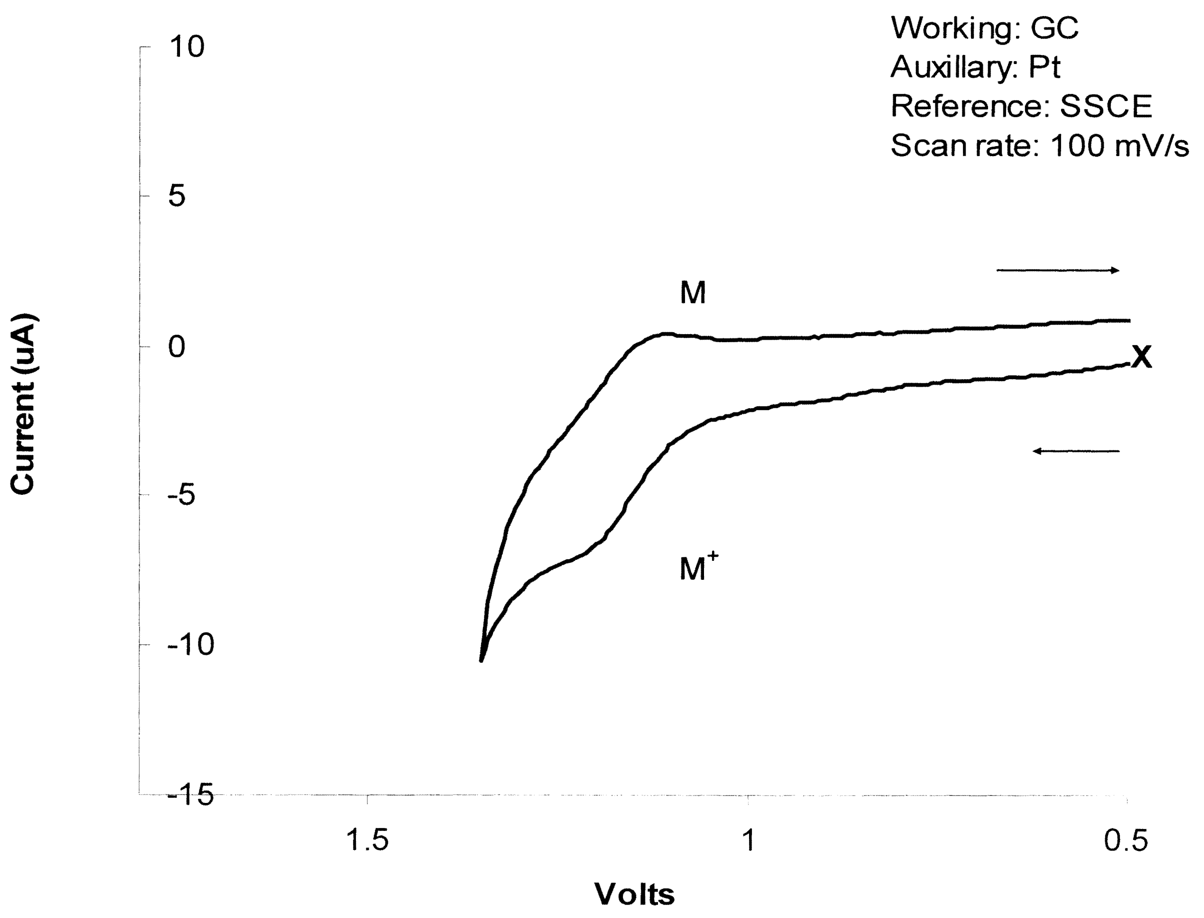

Figure 49d: CV of $[Ru^{II}(H_2dcbpy)_2pptd](PF_6)_2$ in pH *4.0 acetate* buffer

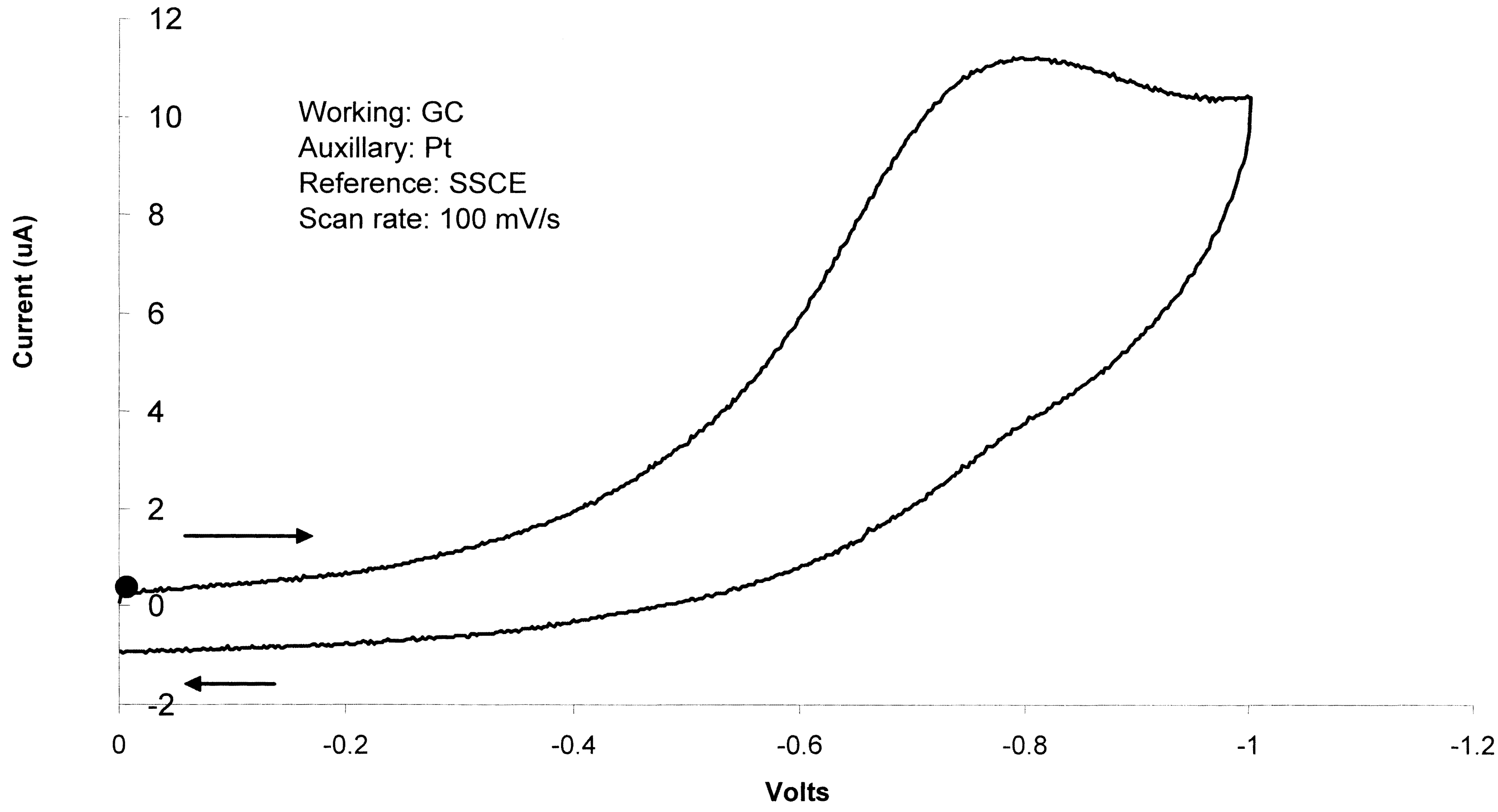

Figure 50a: CV of pH 7.0 acetate buffer with oxygen present

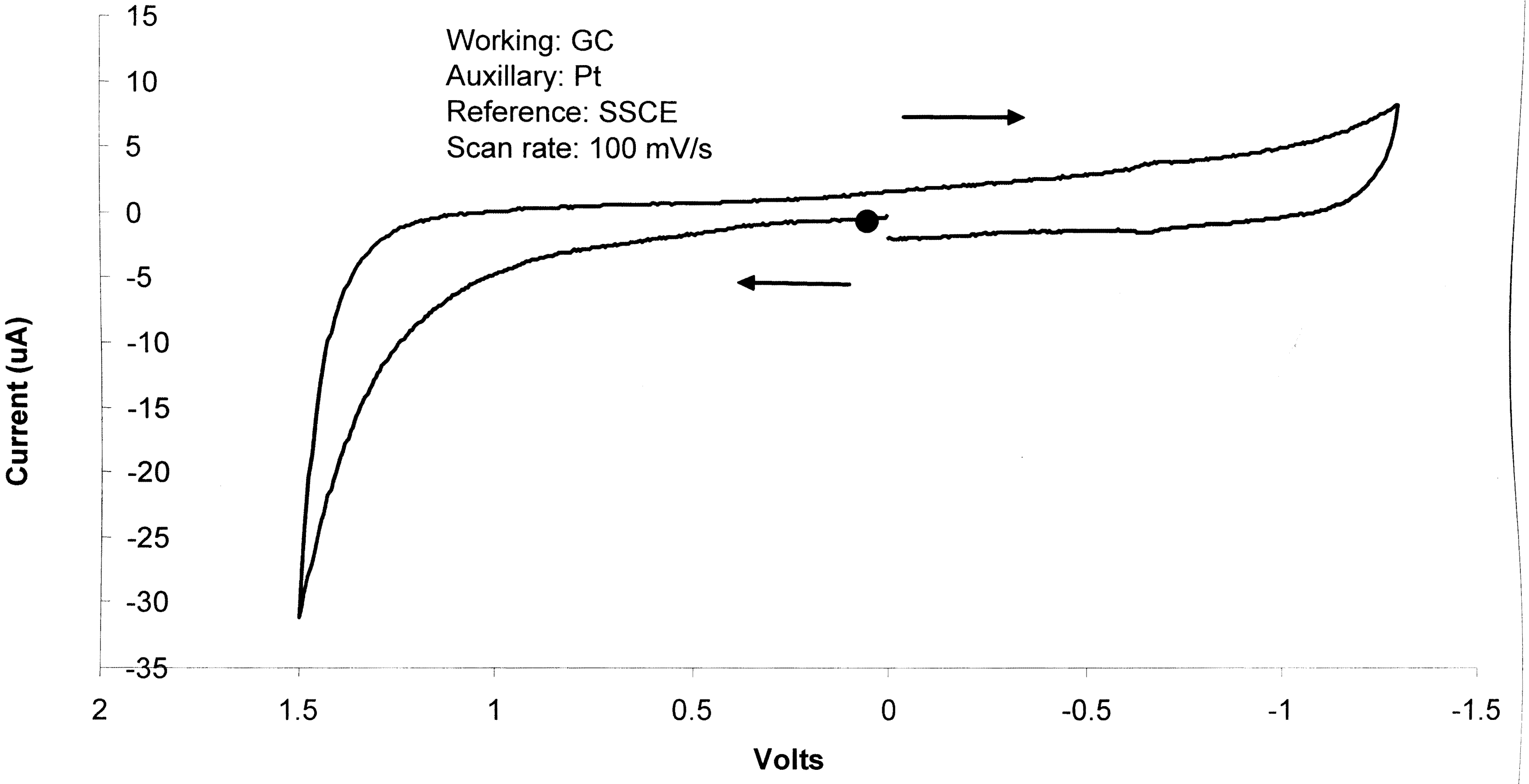

Figure 50b: CV of pH 7.0 sodium acetate buffer after bubbling with Ar

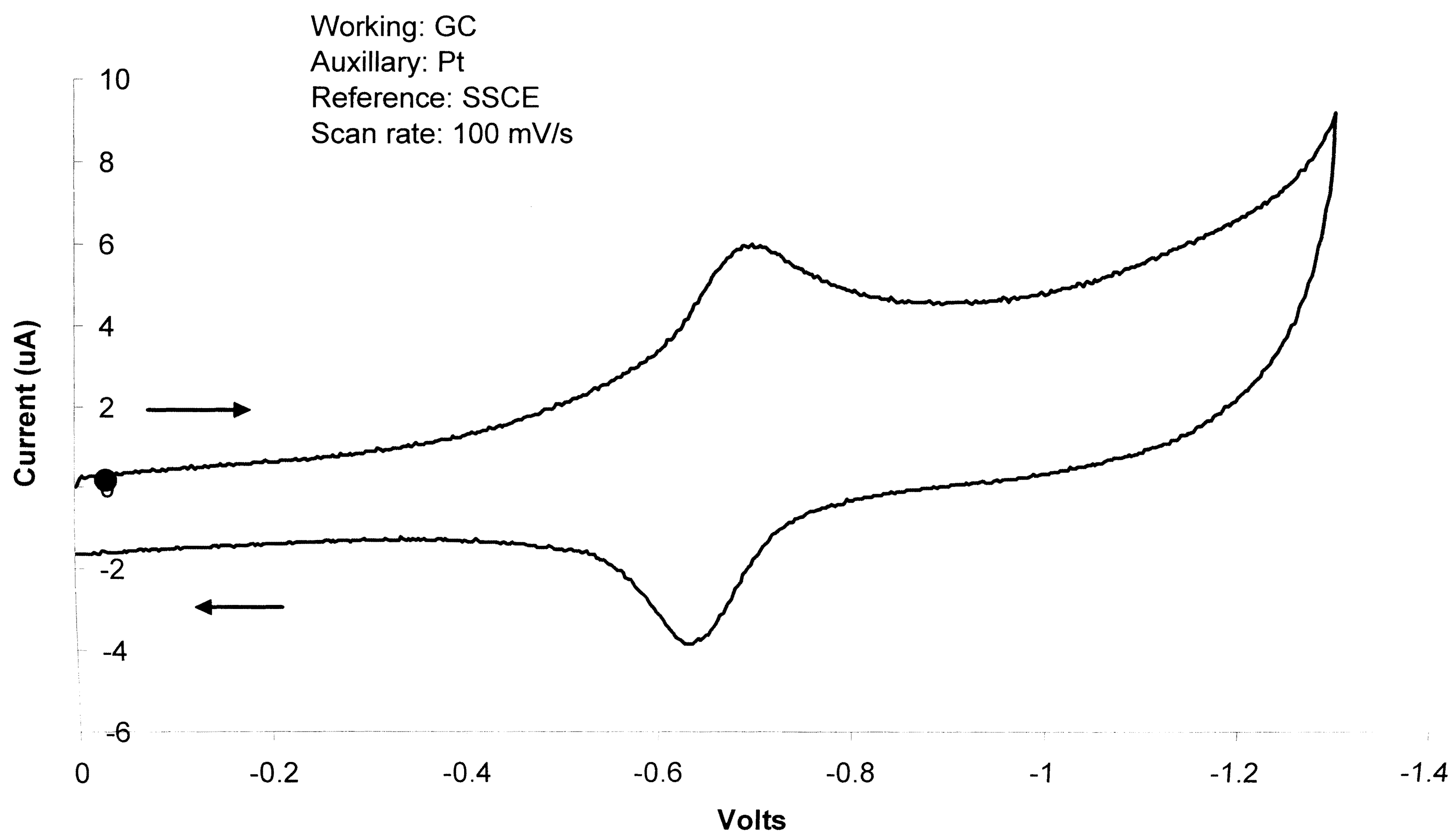

Figure 50c: CV of $[Ru^{II}(H_2dcbpy)_2pptd](PF_6)_2$ in pH 7.0 acetate buffer

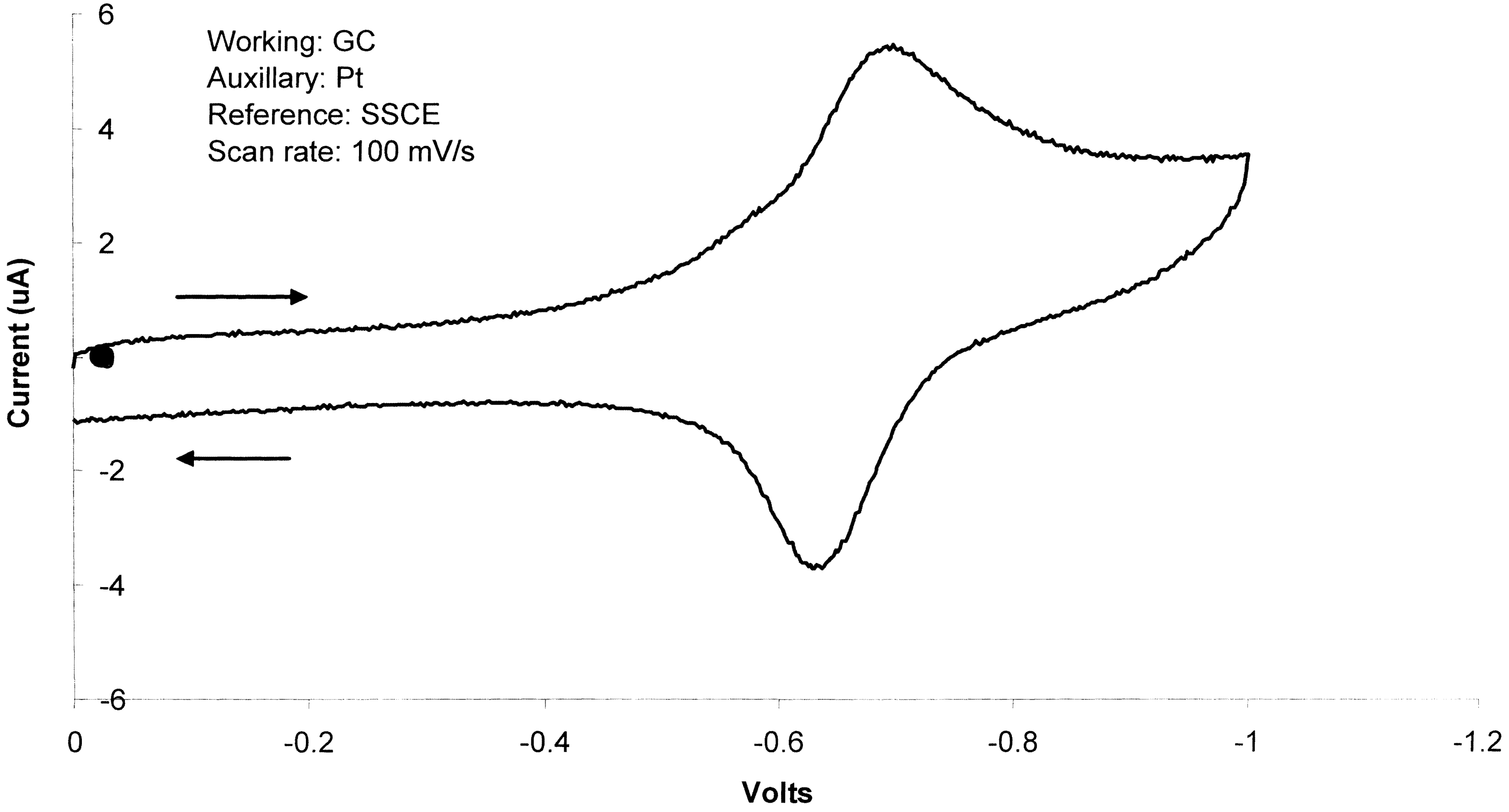

Figure 50d: CV of $[Ru^{II}(H_2dcbpy)_2pptd](PF_6)_2$ in pH 7.0 acetate buffer

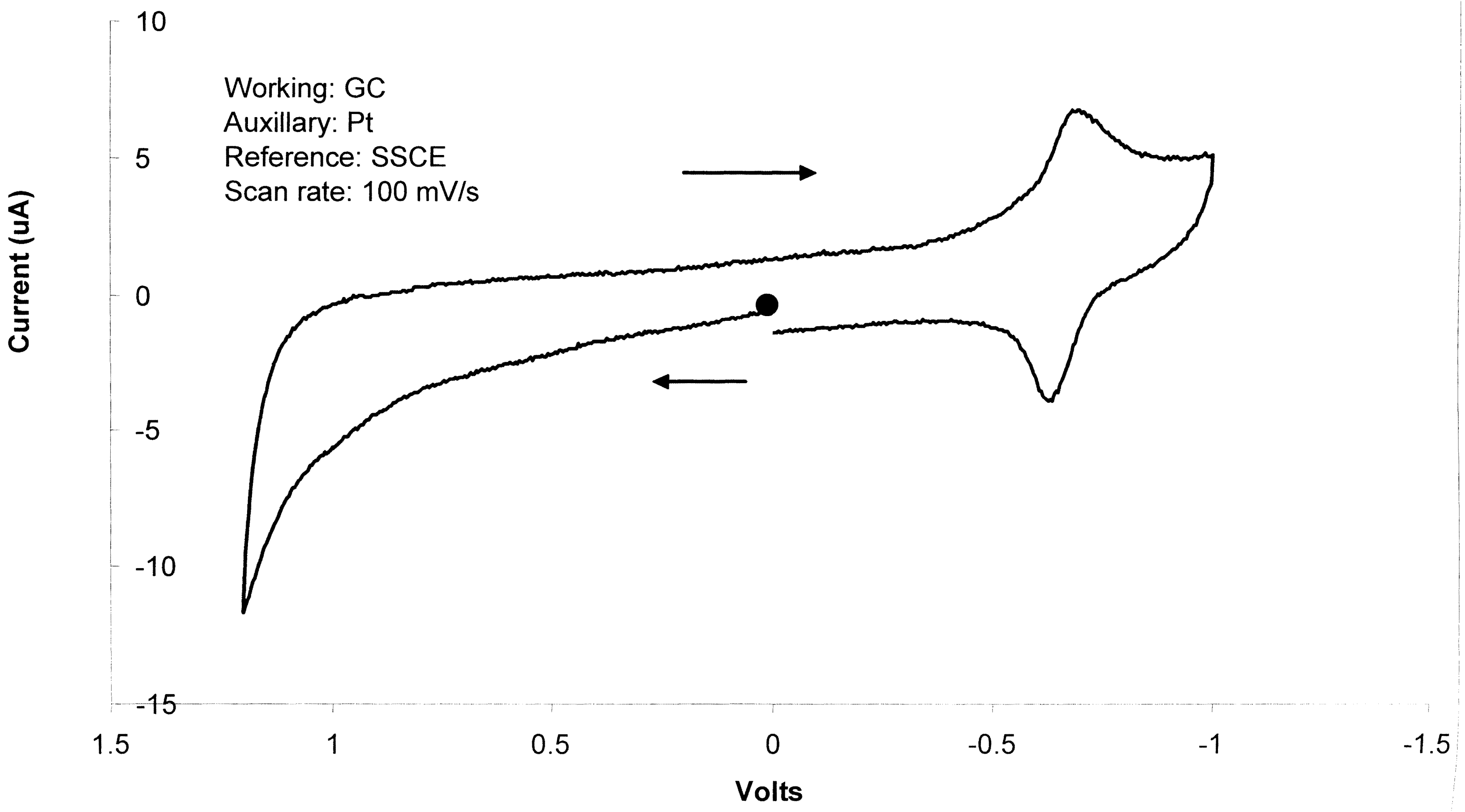

Figure 50e: CV of $[Ru^{II}(H_2dcbpy)_2pptd](PF_6)_2$ in pH 7.0 *acetate buffer*

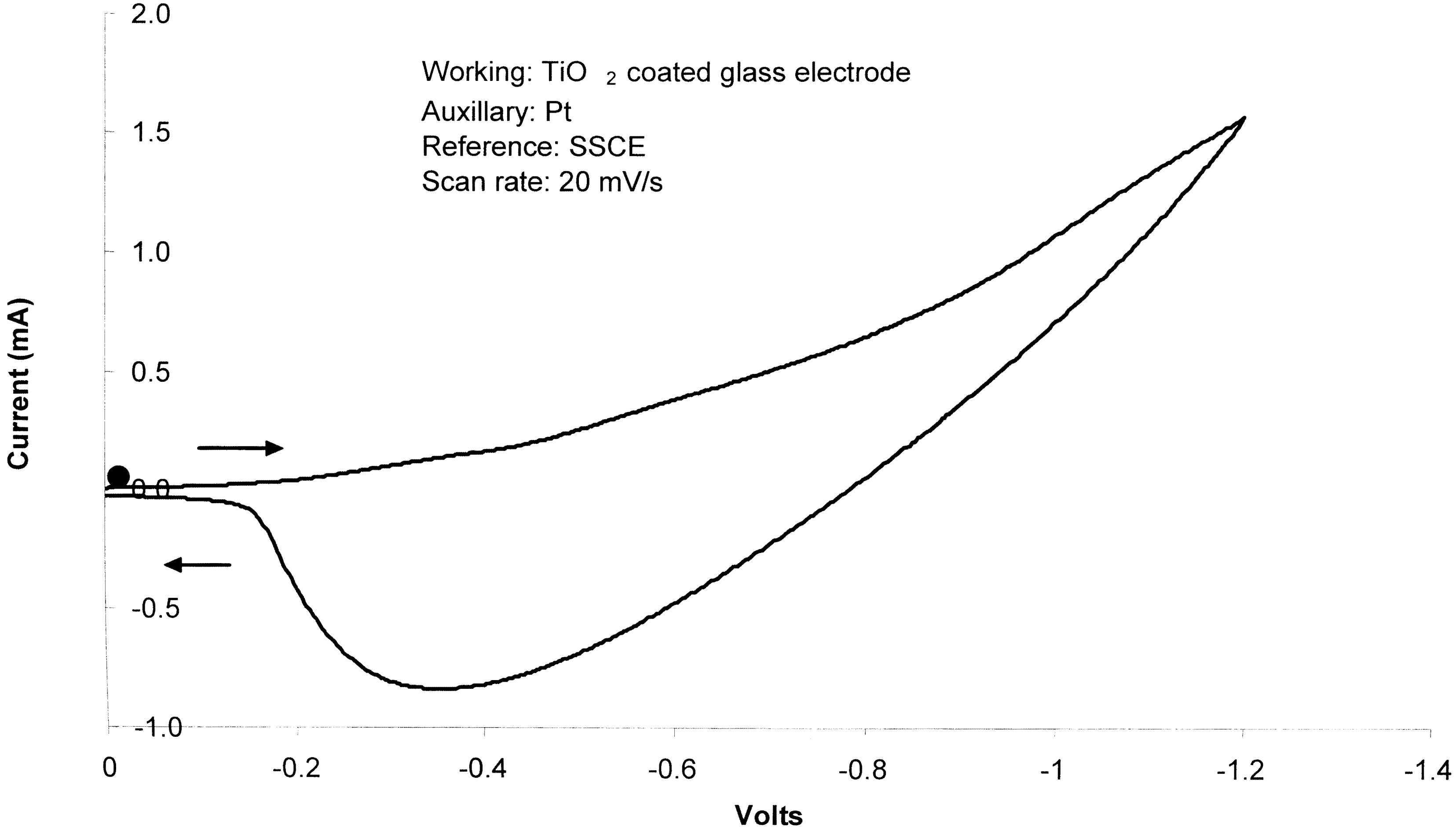

Figure 52a: CV of bare TiO_2 with O_2 present in pH 3.5 *acetate buffer*

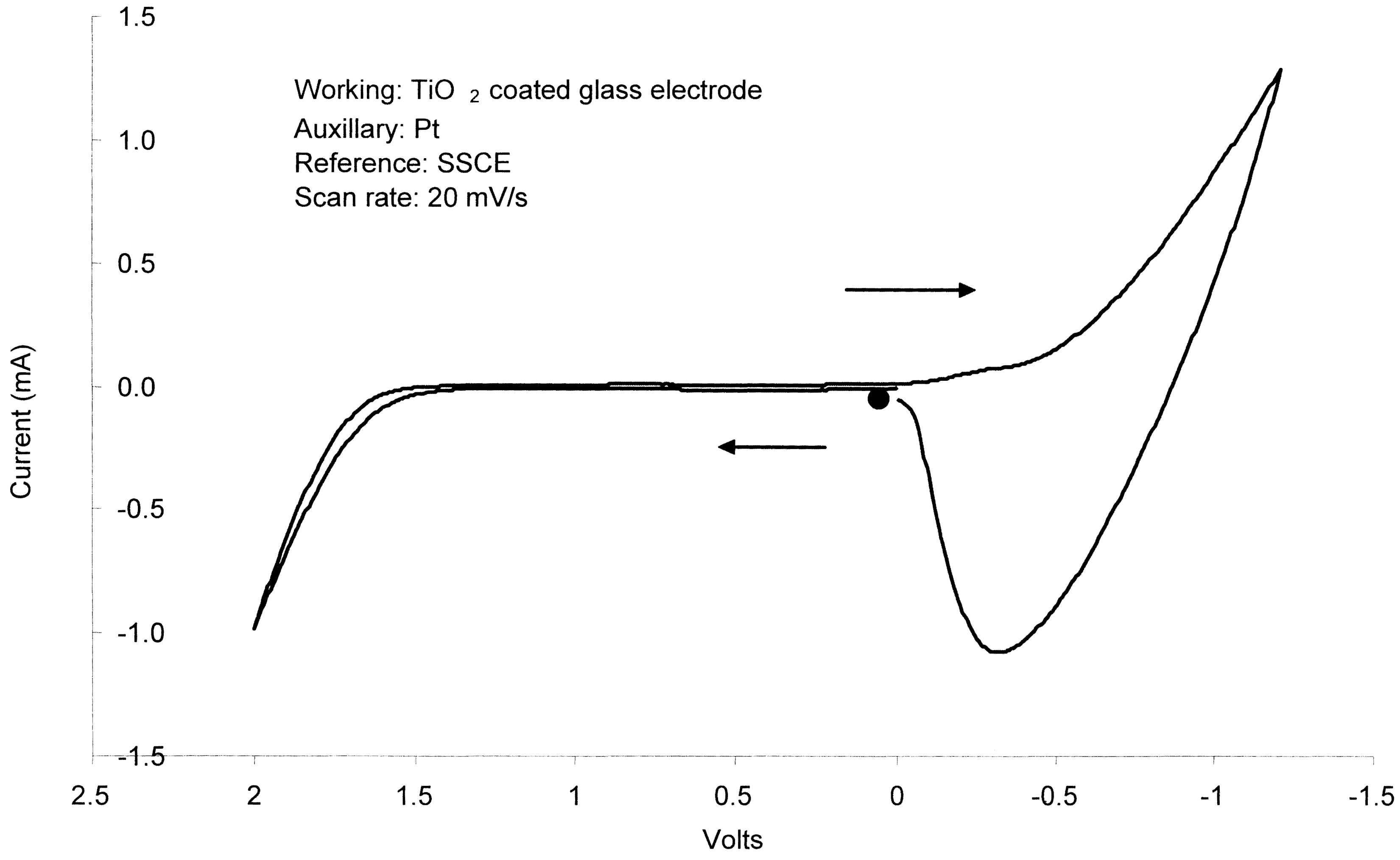

Figure 52b: CV of bare TiO_2 after bubbling with Ar in pH 3.5 acetate buffer

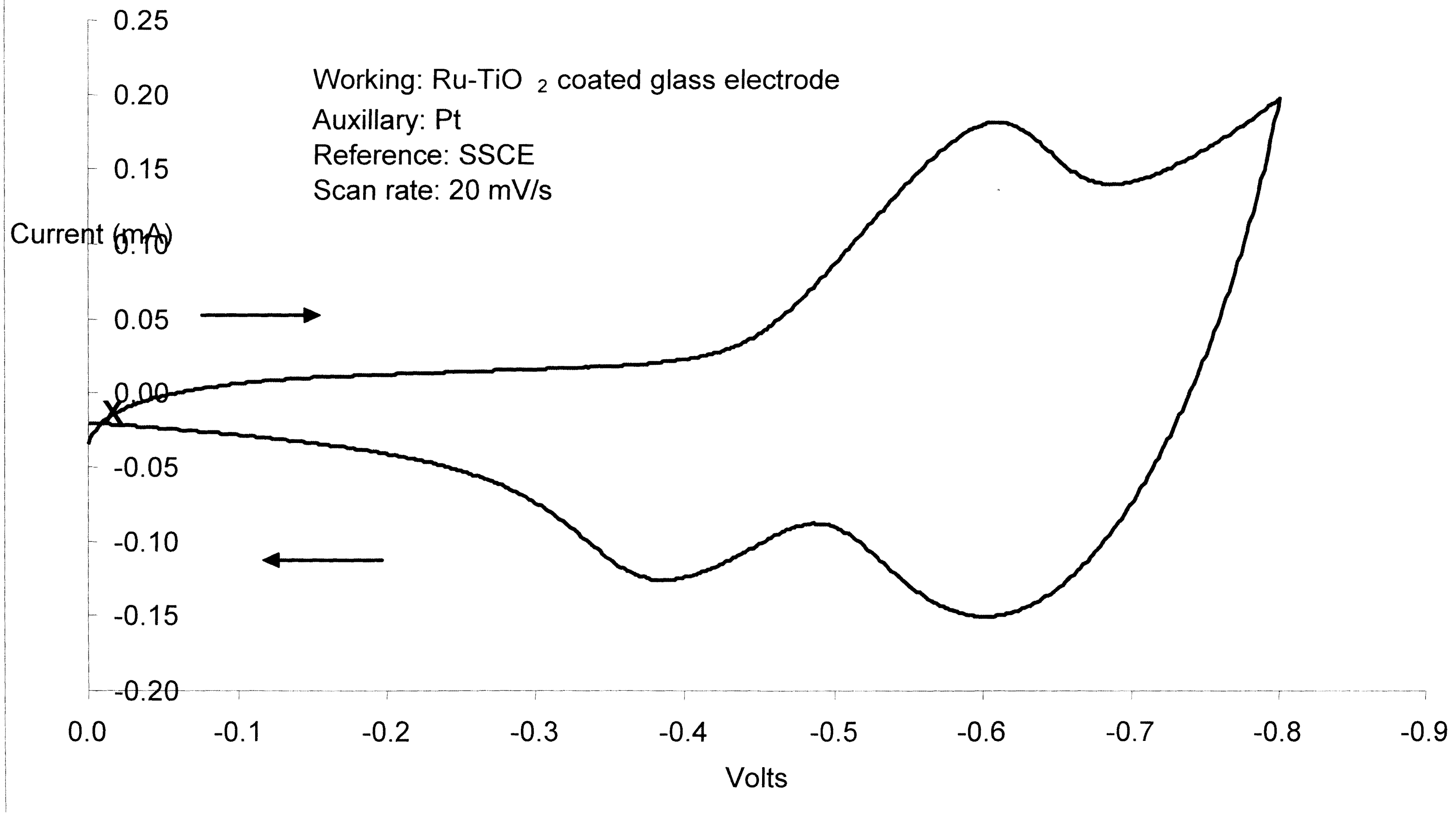

Figure 52c: CV of Ru-TiO_2 electrode in pH 3.5 acetate buffer

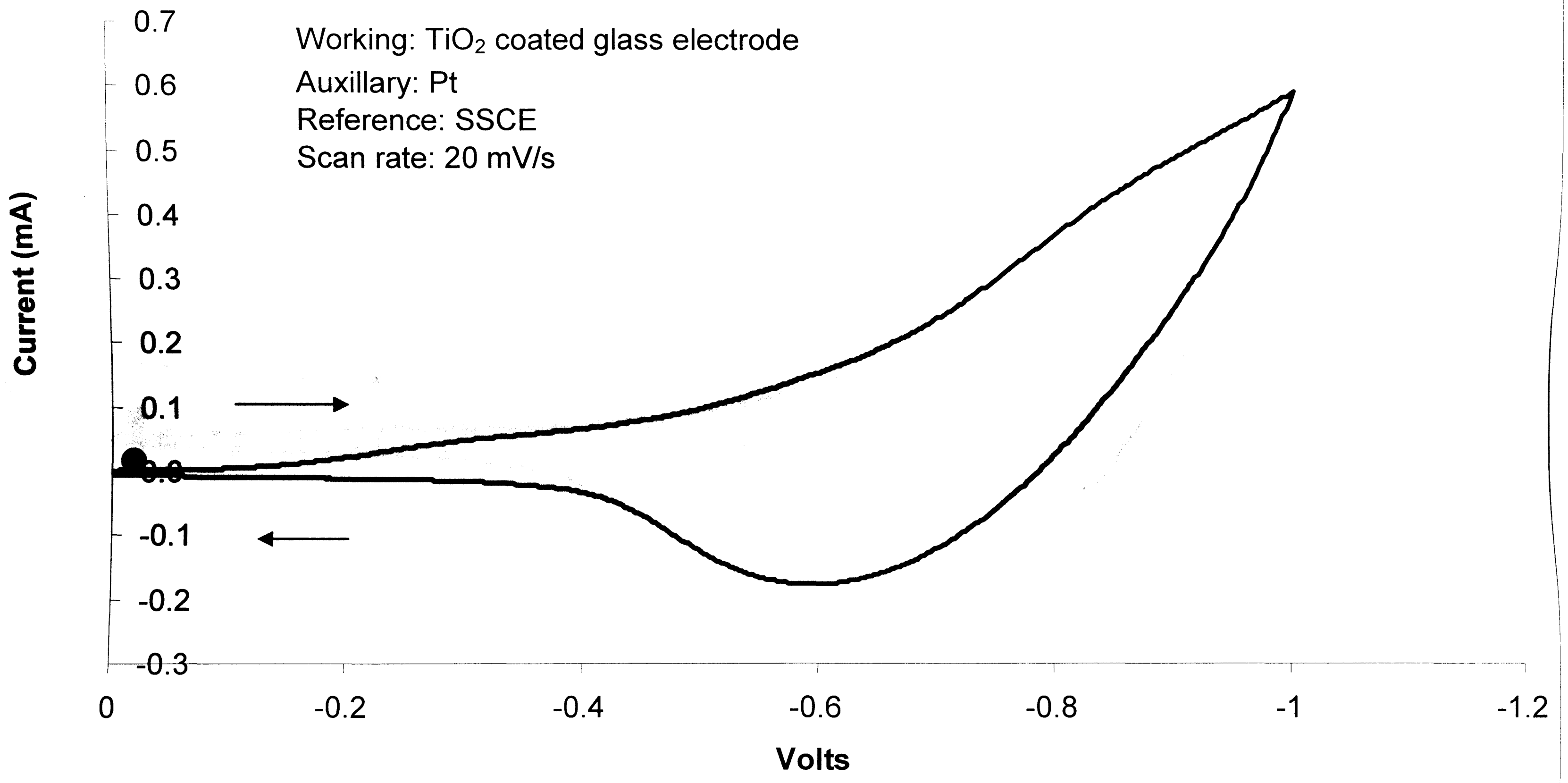

Figure 53a: CV of bare TiO_2 electrode in pH 4.0 acetate buffer with O_2 present

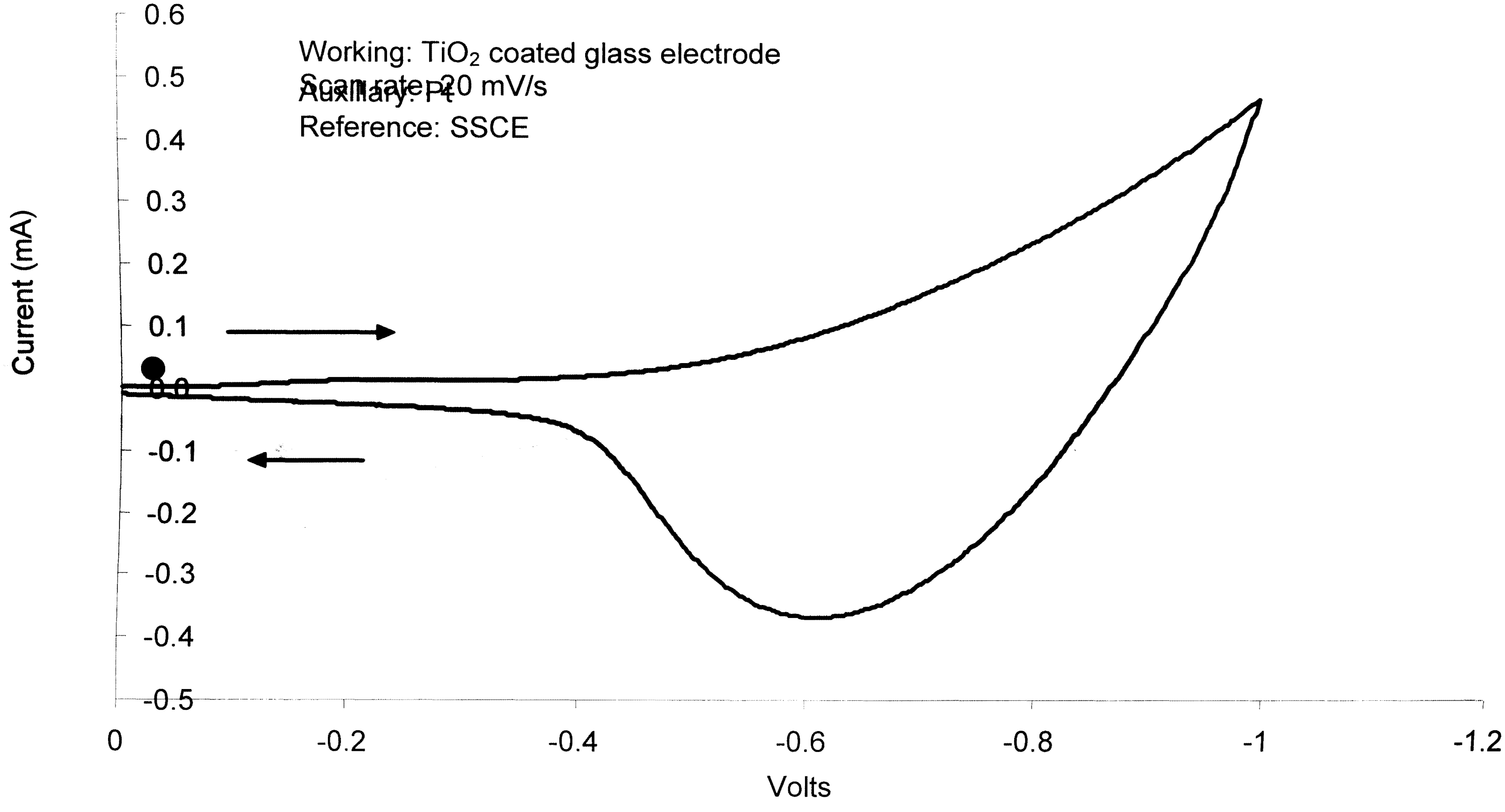

Figure 53b: CV of bare TiO_2 in pH 4.0 acetate buffer after bubbling with Ar

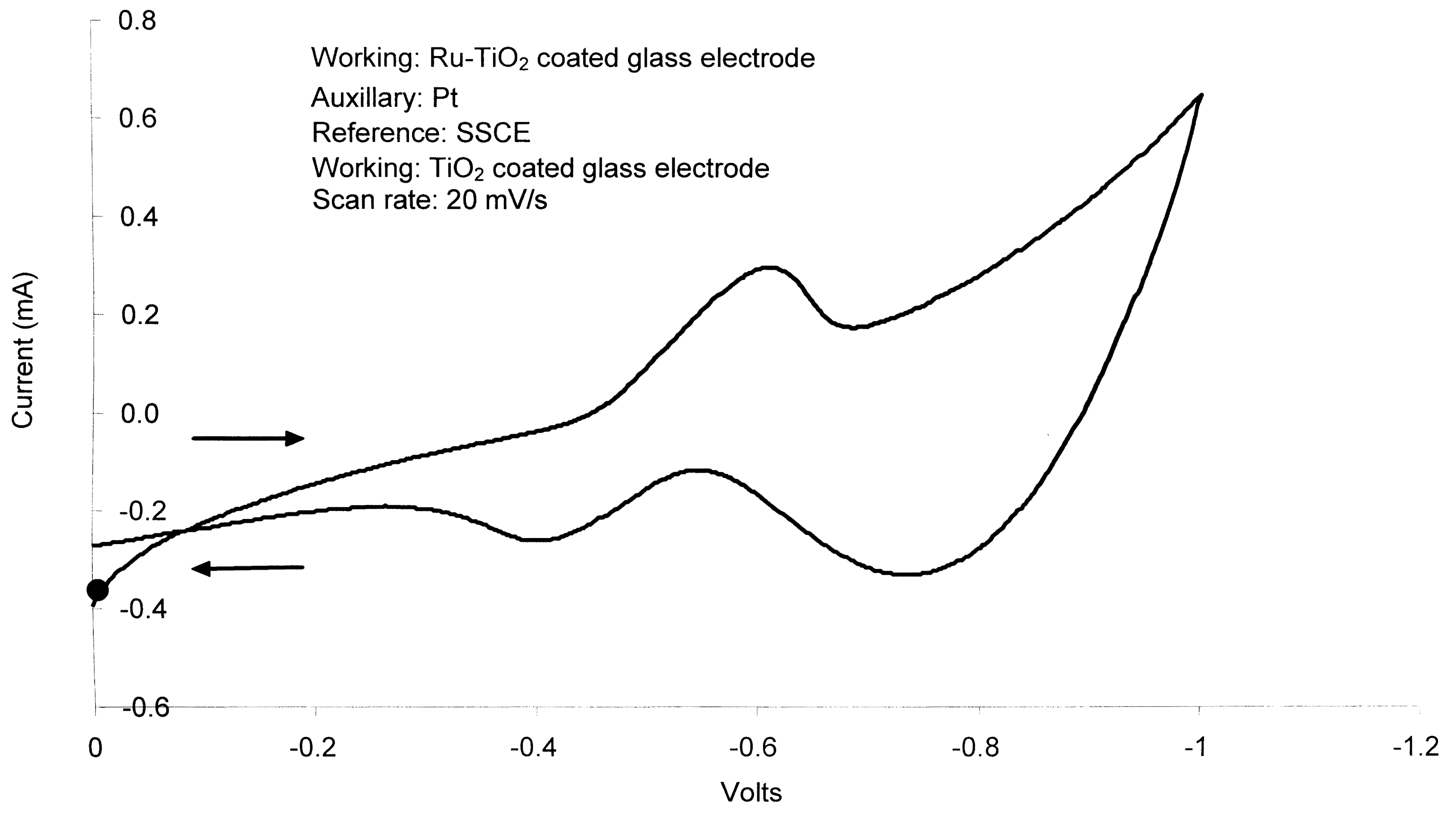

Figure 53c: CV of TiO_2-Ru complex in pH 4.0 acetate buffer

Table 1: Electrochemical Data for Complexes in DMF solution[a]

Complex[b]	Figure #	$E_{1/2}{}^{c}$(V) (ΔE_p (mV))
[Ru^{II}(bpy)$_2$(phen)](PF$_6$)$_2$	45d-e	+0.83 V (30 mV)
	45c	-1.74 V (94 mV)
		-1.91 V (94 mV)
		-2.18 V (93 mV)
[Ru^{II}(bpy)$_2$(pptd)](PF$_6$)$_2$	46c	+0.86 V (150 mV)
	46a-b	-1.27 V (61 mV)
		-1.47 V (50 mV)
		-1.80 V (83 mV)
		-2.00 V (116 mV)
		-2.34 V (94 mV)
[Ru^{II}(H$_2$dcbpy)$_2$(phen)](PF$_6$)$_2$	47d	+0.58 V (38 mV)
	47a-b	-1.4 V[d]
		-1.6 V[d]
		-2.1 V[d]
[Ru^{II}(H$_2$dcbpy)$_2$(pptd)](PF$_6$)$_2$	48d	+ 0.84 V (100 mV)
	48b/c	-1.29 V (100 mV)
		-2.00 V (180 mV)
		-2.19 V (100 mV)
		-2.44V (60 mV)

[a] CV data obtained using glass carbon (GC) working electrode; Pt auxiliary electrode; Ag wire reference electrode; ferrocene (Fc) added as an internal standard and scan rate of 100 mV/s

[b] $E_{1/2}$ of O_2 / O_2^{-} couple measured to be at –1.34 V.

[c] All potentials reported vs. measured $E_{1/2}$ of the Fc^+/Fc couple in each run.

[d] E_{pc}

Table 2: Electrochemical Data for $[Ru^{II}(H_2dcbpy)_2(pptd)](PF_6)_2$ in pH 4.0 and pH 7.0 acetate buffer[a, b]

Complex	Figure #	$E_{1/2}$[b](V) (ΔE_p (mV))
$[Ru^{II}(H_2dcbpy)_2(pptd)](PF_6)_2$	49c (pH 4.0)	-0.50 V (132 mV)
	49d (pH 4.0)	+1.16 V (125 mV)
	50c (pH 7.0)	-0.67 V (61 mV)

[a] CV data obtained using glass carbon (GC) working electrode; Pt auxiliary electrode; SSCE reference electrode; scan rate of 100 mV/s

[b] All potentials reported vs. SSCE

Table 3: Electrochemical Data for TiO_2-$[Ru^{II}(H_2dcbpy)_2(pptd)](PF_6)_2$ in pH 3.5 and pH 4.0 acetate buffer[a]

Complex	Figure #	$E_{1/2}$[b](V) (ΔE_p (mV))
$[Ru^{II}(H_2dcbpy)_2(pptd)](PF_6)_2$	52c (pH 3.5)	-0.61 V (~0 mV)
	52c (pH 4.0)	-0.62 V (E_{pc})

[a] CV data obtained using TiO_2-Ru complex working electrode; Pt auxiliary electrode; SSCE reference electrode; scan rate of 20 mV/s

[b] All potentials reported vs. SSCE

APPENDIX A

The change in electrochemical potential with pH can be related by the Nernst Equation

$[Ru^{II}(H_2dcbpy)_2(pptd)]^{2+} = A$

$[Ru^{II}(H_2dcbpy)_2(pptdH_2)]^{2+} = AH_2$

$A + 2\bar{e} + 2H^+ \rightarrow AH_2$

$$E_{1/2} = E_{1/2}^{\circ} - \frac{0.0592\ V}{2} \log\left[\frac{[AH_2]}{[A][H^+]^2}\right]$$

$$E_{1/2} = E_{1/2}^{\circ} - \frac{0.0592\ V}{2}\left[\log[AH_2] - \log[A][H^+]^2\right]$$

$$E_{1/2} = E_{1/2}^{\circ} - \frac{0.0592\ V}{2}\left[\log[AH_2] - \log[A] - 2\log[H^+]\right]$$

$$E_{1/2} = E_{1/2}^{\circ} - \left[\frac{0.0592\ V}{\cancel{2}}\right]\left[-\cancel{2}\log[H^+]\right] - \frac{0.0592V}{2}\left[\log\frac{[AH_2]}{[A]}\right]$$

$$E_{1/2} = E_{1/2}^{\circ} - \left[0.0592\ V\right]\left[-\log[H^+]\right] - \frac{0.0592V}{2}\left[\log\frac{[AH_2]}{[A]}\right]$$

$$E_{1/2} = E_{1/2}^{\circ} - \left[0.0592\ V\right]\left[pH\right] \underbrace{- \frac{0.0592V}{2}\left[\log\frac{[AH_2]}{[A]}\right]}$$

so this changes 0.0592 V per pH unit. Therefore, a change from pH 4.0 to 7.0 would result in a change of 0.1776 V [3 x 0.0592]

Assume ratio of $[AH_2]$ and $[A]$ constant during the reduction